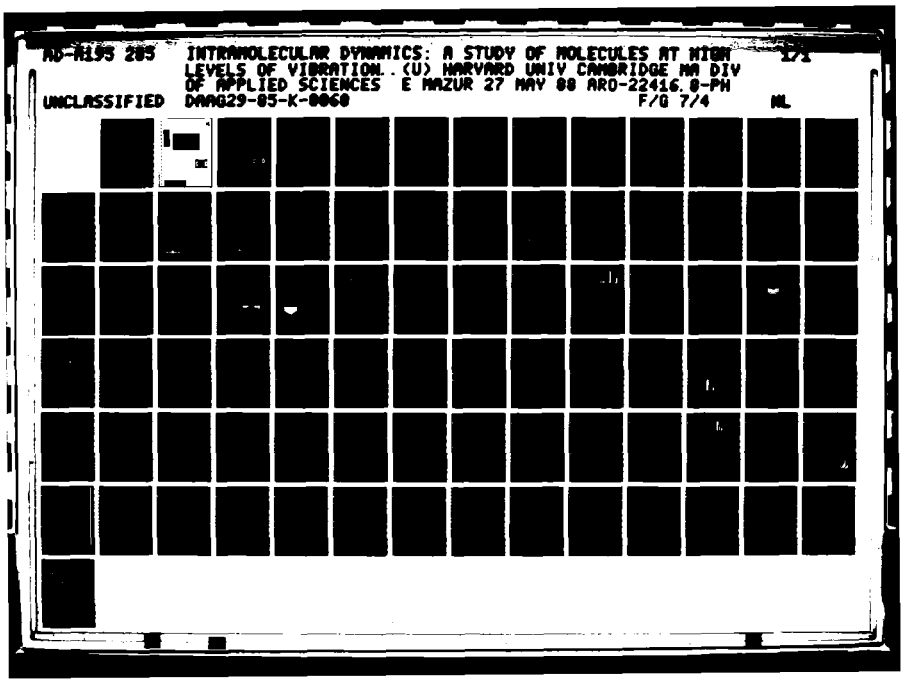
AD-A195 285
INTRAMOLECULAR DYNAMICS: A STUDY OF MOLECULES AT HIGH
LEVELS OF VIBRATIONAL.(U) HARVARD UNIV CAMBRIDGE MA DIV
OF APPLIED SCIENCES E MAZUR 27 MAY 88 ARO-22416.8-PH
UNCLASSIFIED
DAAG29-85-K-0060
F/G 7/4
NL

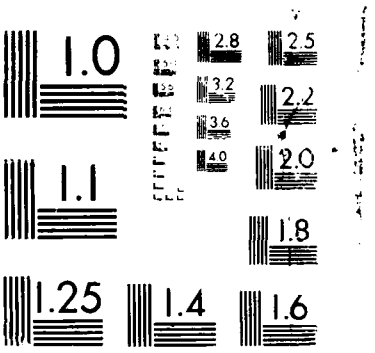

Intramolecular Dynamics: A Study of Molecules at High Levels of Vibrational Excitation

FINAL REPORT ARO DAAG29-85-K-0060

Eric Mazur

22416-PH

Intramolecular Dynamics: A Study of Molecules at High Levels of Vibrational Excitation

FINAL REPORT ARO DAAG29-85-K-0060

Eric Mazur

UNCLASSIFIED
SECURITY CLASSIFICATION OF THIS PAGE *(When Data Entered)*

REPORT DOCUMENTATION PAGE		READ INSTRUCTIONS BEFORE COMPLETING FORM
1. REPORT NUMBER ARO 22416.8-PH	2. GOVT ACCESSION NO. N/A	3. RECIPIENT'S CATALOG NUMBER N/A
4. TITLE *(and Subtitle)* Intermolecular Dynamics: A Study of Molecules at High Levels of Vibrational Excitation		5. TYPE OF REPORT & PERIOD COVERED Final Report 1 Mar. 1985 - 29 Feb. 1988
		6. PERFORMING ORG. REPORT NUMBER
7. AUTHOR(s) Professor Eric Mazur		8. CONTRACT OR GRANT NUMBER(s) DAAG29-85-K-0060
9. PERFORMING ORGANIZATION NAME AND ADDRESS Harvard University 1350 Massachusetts Ave., Rm. 440 Cambridge, MA 02138		10. PROGRAM ELEMENT, PROJECT, TASK AREA & WORK UNIT NUMBERS
11. CONTROLLING OFFICE NAME AND ADDRESS U. S. Army Research Office Post Office Box 12211 Research Triangle Park, NC 27709		12. REPORT DATE 4/27/88 13. NUMBER OF PAGES 79
14. MONITORING AGENCY NAME & ADDRESS*(if different from Controlling Office)*		15. SECURITY CLASS. *(of this report)* Unclassified 15a. DECLASSIFICATION/DOWNGRADING SCHEDULE

16. DISTRIBUTION STATEMENT *(of this Report)*

Approved for public release; distribution unlimited.

17. DISTRIBUTION STATEMENT *(of the abstract entered in Block 20, if different from Report)*

NA

18. SUPPLEMENTARY NOTES

The view, opinions, and/or findings contained in this report are those of the author(s) and should not be construed as an official Department of the Army position, policy, or decision, unless so designated by other documentation.

19. KEY WORDS *(Continue on reverse side if necessary and identify by block number)*

Lasers Infared Multiphoton Excitation Dissociation Selectivity Raman Spectroscopy

20. ABSTRACT *(Continue on reverse side if necessary and identify by block number)*

The intramolecular vibrational energy distribution of infared multiphoton-excited molecules is studied with time-resolved spontaneous Raman spectroscopy. For several molecules highly nonthermal energy distributions are observed, indicating high selectivity below the dissociation threshold.

DD FORM 1 JAN 73 1473 EDITION OF 1 NOV 65 IS OBSOLETE

UNCLASSIFIED
SECURITY CLASSIFICATION OF THIS PAGE *(When Data Entered)*

Intramolecular Dynamics:

A Study of Molecules at High Levels of Vibrational Excitation

FINAL REPORT

Eric Mazur

April 24, 1988

U.S. ARMY RESEARCH OFFICE

DAAG29-85-K-0060

Harvard University

1. Foreword

A fundamental understanding of the intramolecular dynamics of highly excited molecules is of central importance in molecular physics and has great chemical and physical implications: Selectivity at high levels of excitation may eventually lead to the realization of laser-controlled photochemistry, with broad applications in such diverse areas as laser-assisted chemical vapor deposition, isotope separation, and photosynthesis. Equilibration of vibrational energy among the molecular modes, which occurs in molecules that are excited above the dissociation threshold, however, causes the course and rate of laser-induced unimolecular reactions to depend only on total energy. This intramolecular flow of vibrational energy seriously impairs the prospect for developing a novel 'mode-selective' or 'bond-specific' photochemistry, despite the high selectivity of infrared excitation.

Whereas the equilibration of energy for molecules excited close to or above the dissociation threshold is well understood, there is no agreement in the community as to the validity of theoretical models that presuppose equipartitioning of energy in the region *below* the dissociation threshold. Under ARO contract DAAG29-85-K-0060 our laboratory has obtained direct information on the intramolecular vibrational energy distributions of highly vibrationally excited molecules below the dissociation threshold. The experiments carried out under this contract, which involve *spontaneous* Raman spectroscopy of infrared multiphoton excited molecules, for the first time clearly show that the present theoretical descriptions of infrared multiphoton excitation are indeed not generally valid.

The results of this research are summarized in this final report. For a more detailed description the reader is referred to the Appendices. The research findings were published in nine publications in scientific journals, and presented at various international conferences. Two Harvard graduate students will earn their Ph.D. degrees on work performed under this contract. This year also, the National Science Foundation awarded a Presidential Young Investigator Award to the principal investigator in recognition of the work done under the Army Research Office contract.

2. Table of Contents

3. List of Appendices

A1. *Computer-controlled Raman spectrometer for time-resolved measurements in low pressure gaseous samples*
Eric Mazur, Rev. Sci. Instrum. 57 (1986) 2507

A2. *Time-resolved spontaneous Raman spectroscopy of collisionless infrared multiphoton excited SF_6*
Jyhpyng Wang, Kuei-Hsien Chen and Eric Mazur, Phys. Rev. A 34 (1986) 3892

A3. *Raman spectroscopy of infrared multiphoton excited molecules*
Kuei-Hsien Chen, Jyhpyng Wang and Eric Mazur, Technical Digest, Int. Quantum Electronics Conf., San Francisco, June 1986

A4. *The interaction of infrared radiation with isolated molecules: intramolecular nonequilibrium*
Eric Mazur, Kuei-Hsien Chen and Jyhpyng Wang, Proc. Int. Conf. on Lasers '86, Orlando, November 1986, p. 359

A5. *Raman spectroscopy of infrared multiphoton excited molecules*
Jyhpyng Wang, Kuei-Hsien Chen and Eric Mazur, Laser Chemistry, January 1988

A6. *Highly nonthermal intramolecular energy distribution in isolated infrared multiphoton excited CF_2Cl_2 molecules*
Eric Mazur, Kuei-Hsien Chen and Jyhpyng Wang, in *Laser Spectroscopy*, Ed. S. Svanberg (Springer, 1987) 236

A7. *Nonthermal intramolecular vibrational energy distribution in infrared-multiphoton-excited CF_2Cl_2*
Kuei-Hsien Chen , Jyhpyng Wang and Eric Mazur, Phys. Rev. Lett. 59, 2728 (1987)

A8. *The interaction of intense picosecond infrared pulses with isolated molecules*
Eric Mazur, in *Atomic and Molecular Processes with short intense laser pulses*, Ed. A. Bandrauk, (Plenum, in press)

A9. *Energy localization in infrared multiphoton excited CF_2Cl_2 studied by time resolved Raman spectroscopy*
Jyhpyng Wang, Kuei-Hsien Chen and Eric Mazur, Int. Conf. Quantum Electronics 1988, Tokyo Japan, submitted

4. Final Report

A. Statement of problems studied

The major objective of the present contract was to provide detailed information on the molecular excitation dynamics below the dissociation threshold by means of time-resolved spontaneous Raman scattering. Specifically, the following questions were addressed:

- What is the intramolecular distribution of energy after infrared multiphoton excitation?
- Are there differences in the distribution for different pulse duration?
- What is the fluence dependence?
- Is there a certain trend with molecular size?
- Are there certain molecules for which the intramolecular distribution is highly non-equilibrium?

B. Summary of most important results

Under ARO sponsorship we have obtained detailed quantitative information on the intramolecular vibrational energy distributions of highly vibrationally excited molecules below the dissociation threshold by time-resolved Raman spectroscopy. We have collected a large number of data on infrared multiphoton excited molecules ranging in size from 5 to 8 atoms. Most of these molecules have more than one Raman active mode and thus allow direct observation of the intramolecular distribution of vibrational energy among these modes after the infrared multiphoton excitation. Two significant new observations were made: (1) the final distribution of energy—*i.e.* after excitation, but before collisional relaxation—does not necessarily correspond to an equilibrium distribution, and apparently some form of localization of vibrational energy is possible even at high excitation, and (2) direct transfer of energy to modes with a higher energy step than the pumped mode is seen to occur. If part of the energy remains localized in a small set of modes it may be possible to induce reactions that are not thermodynamically favored. Some of the more important findings are summarized below.

1. The experimental setup was completely overhauled in the beginning of the contract period[1]. By repeating previously reported measurements on SF_6 [2], the reproducibility of the measurements was confirmed. In addition we carried out more detailed measurements on SF_6

[3], and we extended our study to other molecular systems (see below).

2. For CF_2HCl preliminary tests in the old apparatus had shown that five Raman active modes of widely different energy can be observed at densities low enough to ensure a collisionless excitation. This molecule, however, absorbs on the edge of the CO_2-laser bandwidth at the 9.4 μm R(32) line. At the maximum fluence we could achieve, photoacoustic measurements show that the molecules absorb less than one photon per molecule. At those fluences and excitation levels, no measurable change in the Raman spectrum could be observed [4–5].

3. For $C_2H_4F_2$ we were able to cover the entire excitation range from the ground state up to the dissociation limit. At high fluence, just below the dissociation threshold, one of the four accessible Raman active modes shows a very small change, but it is clear that the intramolecular vibrational energy distribution for this molecule is not in equilibrium (like CF_2Cl_2, unlike SF_6). Apparently the energy remains *partly localized*. This measurement consituted the first indication that a 'statistical description' of the ensemble of modes in infrared multiphoton excited molecules —which has been proposed by several authors— is not justified in general [6]. Unfortunately the pump mode (C—F stretch; for the cis-configuration of this molecule this is a highly asymmetric vibration) is not accessible in our spontaneous Raman spectroscopy apparatus.

4. Most of the measurements have centered around the five-atom CF_2Cl_2 molecule [7-10]. This molecule can be pumped on two infrared modes (ν_8 and ν_1), and it has four Raman active modes—of which we have observed three after infrared multiphoton excitation. In contrast to the well established equilibrium intramolecular vibrational energy distribution in molecules excited above dissociation threshold), it was found that excitation of the ν_1 and ν_8 mode below the dissociation threshold give rise to different, highly nonequilibrium vibrational energy distributions, which tend toward equilibrium when buffer gas is added. In both cases the pumped mode reaches the highest excitation, while the energy of the ν_2 mode remains almost an order of magnitude smaller. The measurements thus show a surprising amount of 'localization' of excitation energy up to levels of excitations ($E_{int} > 21{,}000$ cm^{-1}) quite close to the dissociation threshold ($E_{diss} \approx 27{,}000$ cm^{-1}). The data also show an asymmetry in the intramolecular vibrational energy relaxation between the various modes.

   After excitation of the ν_8 mode, it was found that this mode contains an excess of energy up to *at least* 10,000 cm^{-1} of excitation energy. Although this is at variance with observations made

in the Soviet Union, that claim complete equilibration above about 7,000 cm^{-1}, it agrees with recent theoretical studies of the intramolecular dynamics of model systems, which shows that for some molecules equilibration occurs only for energies close to the dissociation limit.

After excitation of the ν_1 mode, again a distinct nonequilibrium is observed, this time with an excess of energy in the ν_1 mode up to levels of excitation as high as 21,000 cm^{-1} [10].

If N_2 buffer gas is added, collisional relaxation of energy takes place, and a clear trend toward equilibrium is observed. The behavior of the Raman signal intensities with increasing laser fluence show that complete randomization of vibrational energy does not occur even at the highest fluence at which Raman signals were measured.

5. At very high fluence both $C_2H_4F_2$ and $CF_2C'_2$ dissociate and the Raman probe laser induces a broadband fluorescence from the dissociation fragments. For CF_2Cl_2 we studied this fluorescence in detail and found that (*a*) the dissociation fragments carry a considerable amount of energy (up to 5000 cm^{-1}), and (*b*) the unimolecular dissociation rate of infrared multiphoton excited CF_2Cl_2 must be much smaller than the excitation rate.

6. During the present contract we also received an award under ARO-URIP Grant No. DAAL03-86-G-70098 for the purchase of equipment for coherent anti-Stokes Raman spectroscopy. We have meanwhile completed the construction of a coherent anti-Stokes Raman spectrometer. The new setup is capable of performing measurements at pressures below 1000 Pa. Preliminary measurements of the depletion of the ground vibrational state of SF_6 after infrared multiphoton excitation have been performed. The first measurements will be presented at the International Laser Spectroscopy Conference in Shanghai, China this summer.

7. A three-year renewal proposal to further extend the work started in the current contract period has been submitted to the Army Research Office. In the proposed research we plan to work on several fronts: First, the spontaneous Raman experiment will be replaced by the above mentioned *coherent* anti-Stokes Raman spectroscopy, which is more sensitive and which has a higher spectral resolution. During the transition period the time-resolved spontaneous Raman work will be continued. Second, part of the proposed effort will be directed toward developing new sources for picosecond infrared pulses, *viz.* a picosecond mode-locked CO_2 laser, and possibly also a continuously tunable, transversely pumped high pressure CO_2 laser. Finally, in the final stage of the proposed research, several new research possibilities (above

threshold dissociation of diatomic molecules; spectroscopy of the transition region below the quasicontinuum; determination of the onset of energy randomization) will be explored. These topics can then form the basis for future research.

C. List of publications

1. *Computer-controlled Raman spectrometer for time-resolved measurements in low pressure gaseous samples*
   Eric Mazur, Rev. Sci. Instrum. 57 (1986) 2507

2. *Time-resolved spontaneous Raman spectroscopy of collisionless infrared multiphoton excited SF_6*
   Jyhpyng Wang, Kuei-Hsien Chen and Eric Mazur, Phys. Rev. A 34 (1986) 3892

3. *Raman spectroscopy of infrared multiphoton excited molecules*
   Kuei-Hsien Chen, Jyhpyng Wang and Eric Mazur, Technical Digest, Int. Quantum Electronics Conf., San Francisco, June 1986

4. *The interaction of infrared radiation with isolated molecules: intramolecular nonequilibrium*
   Eric Mazur, Kuei-Hsien Chen and Jyhpyng Wang, Proc. Int. Conf. on Lasers '86, Orlando, November 1986, p. 359

5. *Raman spectroscopy of infrared multiphoton excited molecules*
   Jyhpyng Wang, Kuei-Hsien Chen and Eric Mazur, Laser Chemistry, January 1988

6. *Highly nonthermal intramolecular energy distribution in isolated infrared multiphoton excited CF_2Cl_2 molecules*
   Eric Mazur, Kuei-Hsien Chen and Jyhpyng Wang, in *Laser Spectroscopy*, Ed. S. Svanberg (Springer, 1987)

7. *Nonthermal intramolecular vibrational energy distribution in infrared-multiphoton-excited CF_2Cl_2*
   Kuei-Hsien Chen , Jyhpyng Wang and Eric Mazur, Phys. Rev. Lett. 59, 2728 (1987)

8. *The interaction of intense picosecond infrared pulses with isolated molecules*
   Eric Mazur, in *Atomic and Molecular Processes with short intense laser pulses*, Ed. A. Bandrauk, (Plenum, in press)

9. *Energy localization in infrared multiphoton excited CF_2Cl_2 studied by time resolved Raman spectroscopy*
   Jyhpyng Wang, Kuei-Hsien Chen and Eric Mazur, Int. Conf. Quantum Electronics 1988, Tokyo Japan, submitted

D. List of participating scientific personnel and awards:

Prof. Eric Mazur	—	Presidential Young Investigator
Mr. K.H. Chen	—	Ph. D. end 1988
Mr. D.S. Chung		
Mr. J. Wang	—	Ph. D. summer 1988

5. Bibliography

[1] E. Mazur, *Rev. Sci. Instrum.* 57 (1986) 2507

[2] E. Mazur, I. Burak and N. Bloembergen, *Chem. Phys. Lett.*, 105, 258 (1984).

[3] J. Wang, K.H. Chen and E. Mazur, *Phys. Rev.* A 34 (1986) 3892

[4] E. Mazur, K.H. Chen and J. Wang, Proc. Int. Conf. on Lasers '86 (1986), p. 359

[5] J. Wang, K.H. Chen and E. Mazur, Laser Chemistry, January 1988

[6] K.H. Chen, J. Wang and E. Mazur, Int. Quantum Electronics Conf., (1986)

[7] E. Mazur, K.H. Chen and J. Wang, in *Laser Spectroscopy*, Ed. S. Svanberg (Springer, 1987) 236

[8] K.H. Chen , J. Wang and E. Mazur, Phys. Rev. Lett. 59, 2728 (1987)

[9] E. Mazur, in *Atomic and Molecular Processes with short intense laser pulses*, Ed. A. Bandrauk, (Plenum, in press)

[10] J. Wang, K.H. Chen and E. Mazur, Int. Conf. Quantum Electronics 1988, submitted

Computer-controlled Raman spectrometer for time-resolved measurements in low-pressure gaseous samples

Eric Mazur

Department of Physics and Division of Applied Sciences, Harvard University, Cambridge, Massachusetts 02138

(Received 10 March 1986; accepted for publication 30 June 1986)

A spectrometer for measuring spontaneous Raman scattering in gaseous samples at pressures below 100 Pa (0.75 Torr) with nanosecond time resolution is presented. The apparatus was developed for studying intramolecular vibrational energy distributions in infrared multiphoton excited molecules and makes it possible to study the anti-Stokes Raman scattering from isolated molecules at pressures down to 14 Pa (110 mTorr). To achieve high sensitivity and time resolution simultaneously, spectral resolution (1 nm) is sacrificed. Because of the low level of the signals, the measurements are completely computer controlled. A detailed description of the apparatus, including the multichannel data-acquisition hardware and computer interface, is given.

INTRODUCTION

Since the cross sections for spontaneous Raman transitions are extremely small,[1] experiments on spontaneous Raman scattering are normally performed at high pressure. There are circumstances, however, under which a high pressure is not desirable. One example is the study of collisionless infrared multiphoton excitation.[2] Since the aim of this study is to observe vibrational energy distributions in *isolated* molecules, the observation time has to be several orders of magnitude smaller than the average time between molecular collisions, which puts an upper limit on the sample pressure. For times of the order of magnitude of nanoseconds this means a pressure below 100 Pa (0.75 Torr), at least three orders of magnitude lower than usual for Raman spectroscopy.

This paper presents the details of an apparatus that has allowed measurements of spontaneous Raman scattering on a nanosecond time scale at pressures down to 14 Pa, i.e., from virtually isolated molecules. The apparatus has a large collection efficiency and effectively reduces stray light, which forms the major obstacle when measuring Raman scattering at low pressures. Because the signals are in the photon counting regime and extensive averaging is required, the measurements are completely automated.

Apart from the detection method presented here, there are several other possibilities for measuring Raman scattering from isolated molecules. For example, one can use a molecular beam or jet,[3] or one can resort to more sensitive spectroscopy techniques, such as coherent anti-Stokes Raman spectroscopy.[4] Both methods, however, require additional equipment and may have certain disadvantages. The first method requires a molecular beam apparatus and extensive vacuum equipment. Moreover, measurements are carried out in a nonequilibrium situation. Coherent anti-Stokes Raman spectroscopy, on the other hand, requires a much more elaborate laser setup, but has a higher sensitivity and higher spectral resolution. Moreover, at very low densities spontaneous Raman scattering is more efficient than coherent anti-Stokes Raman spectroscopy, which is proportional to the density squared. For certain research projects, such as the one discussed here, the research goal can be accomplished with a careful design of the scattering cell, and a convenient and flexible multichannel data-acquisition system.

The design of the scattering cell may also be useful in other light scattering experiments that require maximum collection efficiency and minimum stray light. A detailed description of the setup is given below, and representative experimental results obtained with the apparatus are presented.

I. GENERAL LAYOUT

The design of the scattering cell is based on the following experimental approach. A sample of low-pressure gas (typically 100 Pa or lower) is excited by an infrared pulse from a high-power picosecond CO_2 laser (100 mJ in 500 ps or less). After a short controlled time delay the excited molecules are probed by an ultraviolet pulse (30 mJ in 18 ns) from a frequency-doubled ruby laser.

For a strong Stokes Raman transition at a sample pressure of 100 Pa, one can expect a Raman signal of about 20 photons/sr per mJ input power of the probing pulse. For a fixed pressure the signal can only be increased by either increasing the collection angle or the input power. At the same time one has to minimize the effect of unwanted, elastically scattered light. The two main contributions to elastically scattered light are Rayleigh scattering and stray light scattered from the windows and walls of the cell. Typically, the Rayleigh scattering is about four orders of magnitude more intense than the Stokes Raman signal. Stray light, which is independent of sample pressure, quickly becomes the dominant source of scattered light at low pressures. A scattering of only one in 10^9 photons into the detection angle already results in 1.6×10^6 photons/sr, per mJ of input power. Therefore, to be able to measure Raman scattering at low pressures, one has to optimize collection efficiency and mini-

 0034-6748/86/102507-05$01.30

mize stray light in the design of the scattering cell on one hand, and simultaneously maximize the rejection of unwanted signal in the detection.

A. Scattering cell

The cell, in which the exciting and probing laser beams cross at right angles, is shown in Figs. 1 and 2. It consists of a cube-shaped aluminum body with two pairs of arms of circular cross section. The arms for the exciting infrared beam are 0.15 m long, the ones for the probing ultraviolet beam 0.3 m. In order to minimize stray light from the windows the long arms have quartz windows at Brewster angle. In addition, each of these arms contains six pairs of straight [see Fig. 2(a), D1] and conical (D2) baffles. The straight baffles collimate and restrict the probe beam, while the conical baffles trap any light scattered along the path of the beam.[5] The baffles are made separately from the arms and are installed by sliding them into the arms, so that they can be arranged in various configurations. The best results were obtained with apertures increasing from 2 mm nearest to the windows to 4 mm nearest to the center of the cell. In the center part of the cell a vertical stray-light jacket (J) of circular cross section prevents any light scattered from the last baffle from reaching the detection aperture directly. It has two 6-mm holes for the probe beam and two 15-mm holes for the infrared beam. Light scattered at the intersection of the two beams is collected over a solid angle of $\pi/16$ sr and collimated by a quartz lens (L) that serves as a window. The focus of this lens coincides with the intersection of the two beams. All parts of the cell are vapor blasted and black anodized to absorb as much stray light as possible. A gas inlet on the bottom plate connects the cell to a gas-handling and vacuum system.

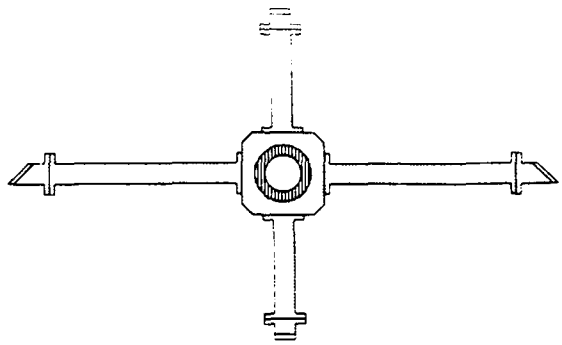

FIG. 1. Top view of the low-pressure Raman cell. The CO_2-laser beam (pump) enters through the short arms, while the probing UV beam enters through the long arms. Scattered light exits through a collimating lens at the top.

To simplify the alignment of the laser beams, the cell is mounted on four tightly fitting posts (P) shown in Fig. 2(b). It can easily be removed and put back accurately by lifting a black nylon shaft (S) through which the collimated scattered light reaches the detection. Alignment of the beams is achieved as follows. First, a He-Ne laser beam is aligned through the probe arms. Then the cell is removed and two diaphragms are centered on the beam, one in front of and one behind the cell. Finally, the pulsed probe beam is aligned through the two diaphragms and subsequently optimized through the cell. To overlap the two beams, the cell is again removed after the alignment of the probe beam, and the infrared beam is adjusted until the two beams produce overlapping burn spots on a piece of thermo-fax infrared copy paper. Final adjustments are made by optimizing the signal.

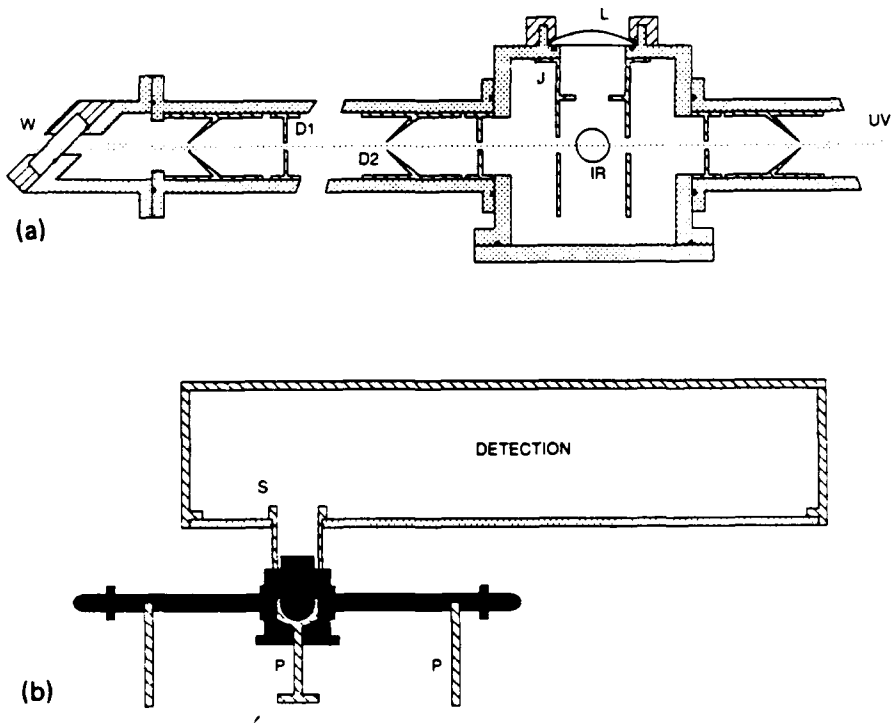

FIG. 2. Cross-sectional (a) and side view (b) of the Raman cell. W = quartz window, D1, D2 = straight and conical baffles, J = stray light jacket, IR = position of IR pump beam, UV = probing UV beam, L = collimating lens. The cell is mounted on four posts, P, from which it can easily be removed by lifting the light shaft, S, through which the scattered light reaches the detection hardware. The window holder in the upper drawing has been rotated by 90° to show the Brewster angle mounting.

B. Detection

The scattered light is analyzed in a light-tight enclosure on a raised platform above the scattering cell [see Figs. 2(b) and 3]. The scattered light that exits the cell consists of Stokes and anti-Stokes Raman signals, Rayleigh scattering, and stray light. A dichroic mirror and a quartz lens image the scattering region onto the entrance slit of a double monochromator. The imaging ratio of the detection lenses is 2 : 1, so that the 6 × 2-mm entrance slit of the monochromator corresponds to a 3 × 1 mm area of the scattering region. Additional spatial filtering between the two monochromators further reduces stray light. Since high spectral resolution is not a requirement for the present study, two small 0.25 m $f/3.5$ monochromators were employed. Apart from their high throughput, small monochromators have a high rejection ratio (typically 10^9), which is needed to eliminate the elastically scattered light. The total throughput of the two monochromators is about 4%. A photomultiplier is mounted directly onto the exit slit of the monochromator in a thermoelectrically cooled housing.

C. Specifications

The overall signal-to-noise ratio of cell and detection is excellent: Even though single photons are registered for each laser pulse, the measurements can be performed in daylight or with room lights on. The amount of ambient light that reaches the photomultiplier after the spatial and spectral filtering is well below the 1.5-kHz dark count rate of the photomultiplier tube and therefore entirely negligible. The amount of stray light detected just behind the entrance slit of the monochromator after evacuating the cell is less than 10^{-10} of the probe beam and around 10^{-6} at the position of the lens. The overall detection efficiency, including the quantum efficiency of the photomultiplier is 3×10^{-4}.

II. HARDWARE DESCRIPTION

The general layout of the setup for measuring the Raman scattering from infrared multiphoton excitation is shown in Fig. 3. A description of the high-power picosecond CO_2-laser facility can be found in Ref. 6. The infrared pulse power is monitored by a pyroelectric detector (P2) and focused into the cell with a cylindrical ZnSe lens. The full width at half-maximum (FWHM) beam size at the intersection of the two laser beams is 0.35×6 mm. The output of the Q-switched ruby laser (300 mJ in 20 ns) is monitored by a fast silicon photodiode (FND) and frequency doubled with a temperature tuned RDA crystal. The resulting ultraviolet radiation at 347 nm is split off with a harmonic beam splitter, its polarization rotated in the plane of the two laser beams with a half-wave plate, and focused into the cell. The FWHM beam waist at the focus is 180 μm. The power of the ultraviolet pulse (30 mJ in 18 ns) is monitored with a Hamamatsu phototube. The scattered light is focused onto the entrance slit of a tandem Jarrel-Ash 0.25-m Ebert-type monochromator with 2400 grooves/mm gratings. The linear dispersion of the system is 1.65 nm/mm. Most measurements were carried out at a resolution of 3 nm, enough to prevent elastically scattered light from reaching the detector. The output of the monochromator is detected with a Amperex XP2020Q photomultiplier tube (1-ns time resolution, 1.5-kHz dark count rate, 25% quantum efficiency). A mechanical shutter (S) protects the tube when the detection box is opened.

Since the power of the CO_2 laser and the time delay between the two laser pulses are fluctuating considerably, and since the observed signals are in the photon counting regime, many thousands of laser shots (typically 10^4) are needed for a single experimental run. The data are sorted out after measurement, and the random fluctuations in power (and to a certain degree those in timing) provide the variation needed to obtain results as a function of these param-

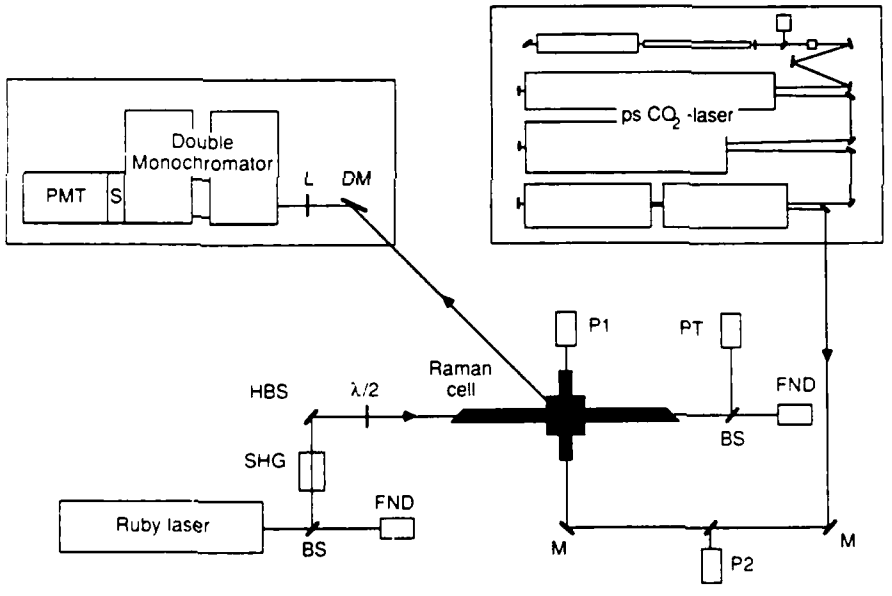

FIG. 3. Setup for measuring the spontaneous Raman scattering from infrared multiphoton excited molecules at low densities. Molecules excited by a CO_2 laser are probed by the second harmonic of a Ruby laser. BS = beam splitter, SHG = second-harmonic generator, HBS = harmonic beam splitter, $\lambda/2$ = half-wave plate, FND = fast photodiode, PT = phototube, P1, P2 = pyroelectric detector, M = mirror, DM = dichroic mirror, L = quartz lens, S = shutter, and PMT = photomultiplier tube. The detection (monochromator, photomultiplier, etc.) is located in a light-tight enclosure located directly above the Raman cell. Drawing not to scale.

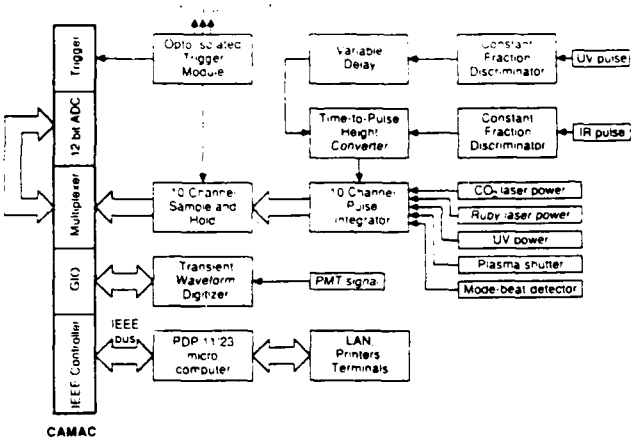

FIG. 4. Schematic view of the data-acquisition electronics.

eters. The long duration of the measurements and the large amount of data collected made it necessary to automate the data acquisition. Figure 4 shows a diagram of the data-acquisition electronics. The CO_2 laser is located in a rf shielded room to prevent interference with the data-acquisition electronics. Furthermore, all trigger connections with the two lasers are opto-isolated to prevent any feedback of noise via the trigger cables. The electronics are mounted in NIM (nuclear instrumentation module) racks and a CAMAC (computer automated measurement and control) crate.

A home-built master trigger module provides the trigger pulses for the ruby laser, Q switch, CO_2-laser and laser amplifiers, and the data acquisition. Even though the trigger pulses can be set with nanosecond accuracy, the inherent jitter of the lasers prevents synchronization better than 100 ns. Therefore, the time delay between pump and probe is measured for each pair of laser pulses. A fast pyroelectric detector (Fig. 3, P1) and a fast photodiode (FND), both with subnanosecond resolution, provide the start and stop pulses for an EG&G Ortec model 457 time to pulse-height converter. A variable delay for the start pulse allows both negative and positive time delays between the two pulses to be registered. To make the timing measurement independent of the fluctuations in intensity, the two pulses are first processed by an EG&G Ortec model 934 constant fraction discriminator. The overall accuracy of the time-delay measurement is better than 1-ns. The overall time resolution of the measurements, however, is limited by the 18-ns duration of the probe pulse.

The incoming data pulses (see Fig. 4) are integrated and sampled twice in each data-acquisition cycle, once 160 ms before and once immediately after the lasers fire. Thus one can correct for possible base-line drift during long measurements. A Kinetic Systems model 3531 multiplexer sequentially scans the incoming pulses to a Kinetic Systems model 3553-Z1C 12-bit analog-to-digital converter. The output from the photomultiplier tube is recorded by a Gould Biomation 8100 transient waveform digitizer and then read out to the CAMAC crate with a Standard Engineering model GIO-816 input/output register and interface. All data, i.e., the base-line data and signals from the integrators and the digitized waveform, are transferred to a microcomputer by a Kinetic Systems model 3988-G2A GPIB CAMAC crate controller. The computer analyzes the output from the photomultiplier tube, corrects for the tail of darkcounts that occurred just before the probe pulse, displays the resulting data, and stores them on a Winchester disk. Data analysis and display can be done on line at any point during the measurement. The computer is connected to a local area network of computing facilities for backups and further data handling.

The software is all written in C language. Up to 19 different channels can be measured and analyzed. The measurement program also allows manual input on one data channel. This is particularly useful when a signal needs to be measured as a function of a parameter that cannot be controlled or measured directly by computer, e.g., the alignment of certain optics, the optimization of the timing of the laser amplifiers, or calibrations. This feature has proven to be of great help during the development of the setup, and effectively means that *any* measurement, even in the photon counting regime, can be carried out with the same data-acquisition and analysis software.

The analysis programs allow the display of any combination of the datachannels on two axes. The data can also be calibrated, transformed, and averaged. Finally, theoretical curves can be fitted to the points obtained.

III. EXPERIMENTAL RESULTS

The apparatus is used to study the intramolecular vibrational distribution of energy in various infrared multiphoton excited molecules.[7] The scope of this research project is to determine whether the intramolecular vibrational energy distribution after multiphoton excitation corresponds to a common equilibrium among the various vibrational degrees of freedom of the molecules. This can be determined by measuring the intensity of different Raman lines.

Figure 5 shows the Stokes and anti-Stokes signals from the ν_1 mode of SF_6 as a function of the time delay between the pump (tuned to the ν_3 mode of SF_6) and probe pulses. A clear increase in the signals can be seen immediately after the multiphoton excitation at $t = 0$. This measurement was car-

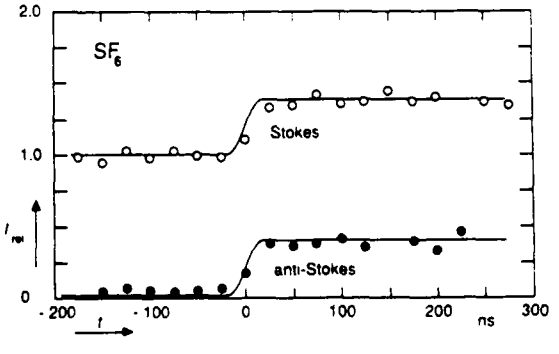

FIG. 5. Intensity of Stokes and anti-Stokes signals for SF_6 at a pressure of 133 Pa as a function of the time delay between pump and probe pulses. A negative delay means that the molecules are probed before they are excited. The signals are normalized to the thermal Stokes signals. The rise time in the curves reflects the 18-ns FWHM duration of the probe pulse.

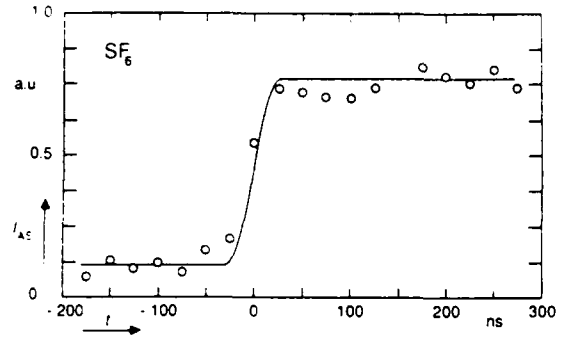

FIG. 6. Normalized intensity of the anti-Stokes signals for SF_6 at a pressure of 14 Pa as a function of the time delay between pump and probe pulses. The rise time in the curve reflects the 18-ns FWHM duration of the probe pulse.

ried out at a cell pressure of 140 Pa. The data were accumulated over a period of 10 h, or 6×10^3 laser pulses. Figure 6 shows that even at a pressure of 14 Pa good data can be obtained. The data in these two graphs have been averaged in 20-ns intervals. The same signal-to-noise ratio can be obtained with 5-ns intervals. It should be recalled, however, that in the present experimental setup the time resolution is limited by the 18-ns duration of the probe pulse. For full details of the measurements and a discussion of the results the reader is referred to Ref. 7.

Figure 7 shows two spectra obtained with the present apparatus at a cell pressure of 150 Pa. The spectral resolution, which is determined by the exit slit of the monochromator, is 3 nm. These graphs clearly show the capabilities of the

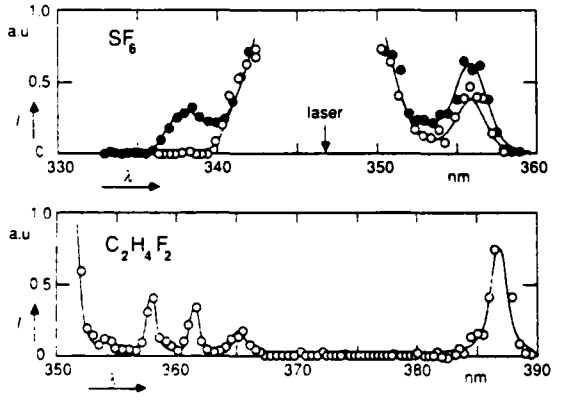

FIG. 7. Raman spectra for SF_6 (top) and $C_2H_4F_2$ (bottom) obtained at 150 Pa with (closed symbols) and without (open symbols) infrared excitation. The small vertical arrow shows the position of the probe pulse at 347.15 nm.

present setup and the feasibility of measuring spontaneous Raman scattering at these low pressures. There is no measurable contribution of stray light at the position of the Raman lines—at a shift of about 2 times the resolution of the spectrometer.

IV. DISCUSSION

The apparatus described above has been in use for well over a year now and has proven to be a valuable tool in the study of intramolecular dynamics. This apparatus has made it possible to carry out time-resolved spontaneous Raman spectroscopy in samples at pressures down to 14 Pa. The main features of the apparatus are the reduction of stray light, the high collection efficiency, the automated multichannel data acquisition, and integrated data handling, as well as proven reliability.

ACKNOWLEDGMENTS

I would like to thank Emil Sefner of the Gordon McKay Scientific Instrumentation Shop for his valuable advice in designing and building the Raman cell. This research was supported by the U.S. Army Research Office and the Joint Services Electronics Program under Contracts No. DAAG29-85-K-0600 and No. N00014-84-K-0465 with Harvard University.

[1] G. Herzberg, *Molecular Spectra and Molecular Structure* (van Nostrand, New York, 1950).

[2] See, e.g., W. Fuss and K. L. Kompa, Prog. Quantum Electron. **7**, 117 (1981); D. S. King, in *Dynamics of the Excited State*, edited by K. P. Lawley (Wiley, New York, 1982); V. S. Lethokov, *Nonlinear Laser Chemistry*, Chemical Physics Series, Vol. 22 (Springer, Berlin, 1983); V. N. Bagratashvili, V. S. Lethokov, A. A. Makarov, and E. A. Ryabov, *Multiple Photon Infrared Laser Photophysics and Photochemistry* (Harwood, New York, 1984), and references therein.

[3] See, e.g., K. Bergmann, W. Demtröder, and P. Hering, Appl. Phys. **8**, 65 (1975); D. H. Levy, L. Wharton, and R. E. Smalley, in *Chemical and Biochemical Applications of Lasers*, edited by C. Bradley Moore (Academic, New York, 1977).

[4] J. W. Nibler and G. V. Knighten, in *Raman Spectroscopy of Gases and Liquids*, edited by A. Weber (Springer, Berlin, 1979).

[5] The use of baffles is common practice in the design of scattering cells; see, e.g., K. D. van den Hout, P. W. Hermans, E. Mazur, and H. F. P. Knaap, Physica **104A**, 509 (1980); D. M. Brenner, J. Chem. Phys. **74**, 494 (1981).

[6] H. S. Kwok and E. Yablonovitch, Rev. Sci. Instrum. **46**, 814 (1975); J. G. Black, P. Kolodner, M. J. Schultz, E. Yablonovitch, and N. Bloembergen, Phys. Rev. A **19**, 704 (1979).

[7] E. Mazur, I. Burak, and N. Bloembergen, Chem. Phys. Lett. **105**, 258 (1984); Jyhpyng Wang, Kuei-Hsien Chen, and Eric Mazur, Phys. Rev. A (to be published).

PHYSICAL REVIEW A VOLUME 34, NUMBER 5 NOVEMBER 1986

Time-resolved spontaneous Raman spectroscopy of infrared-multiphoton-excited SF_6

Jyhpyng Wang, Kuei-Hsien Chen, and Eric Mazur
Department of Physics and Division of Applied Sciences, Harvard University, Cambridge, Massachusetts 02138
(Received 22 May 1986)

Spontaneous Raman spectroscopy is used as a tool for studying the vibrational energy distribution of collisionless infrared-multiphoton-excited SF_6. A collisionless increase in Stokes and anti-Stokes signals from the strong Raman-active ν_1 mode is observed after infrared-multiphoton excitation by a high-power 500-ps CO_2-laser pulse tuned to the infrared active ν_3 mode. Results are presented over a pressure range from 13 Pa (100 mTorr) to 270 Pa (2 Torr). The pressure dependence clearly proves that the increase does not depend on collisions. The effects are studied as a function of time and of the infrared energy fluence, infrared wavelength, and infrared pulse duration. The experimental data show that an intramolecular equilibrium of vibrational energy is established within the 20-ns time resolution of the experimental setup. The multiphoton excitation shows a red shift and intensity broadening. A comparison with results from photoacoustic measurements is made.

I. INTRODUCTION

In 1973 it was discovered that isolated molecules in the ground electronic state can be dissociated by a short, intense pulse from a CO_2-laser.[1] During the last decade the absorption of many monochromatic infrared photons by isolated molecules, called infrared multiphoton excitation, has been studied extensively by many groups.[2] It was found that this is a general property of polyatomic molecules that have an infrared active mode resonant with the laser field. The dependence of multiphoton excitation on infrared intensity, fluence, frequency and molecular size, as well as spectra of infrared multiphoton excited molecules have been reported. Technological applications of infrared multiphoton excitation have also been developed: Examples are isotope separation,[3–6] unimolecular reactions,[7,8] and molecular synthesis.[9] At the same time several theoretical approaches have been proposed to describe this phenomenon.[10–15] Because the spectrum of vibrational and rotational transitions between excited vibrational states is not well known, multiphoton excitation has proven difficult to describe quantitatively. Although most of the conceptual ideas of the theory have been verified experimentally, many open questions remain.

One question that has been receiving recent attention concerns the intramolecular distribution of energy in infrared multiphoton excited molecules.[16] As is well-known, collisions with other molecules rapidly equilibrate vibrational energy among the different molecular degrees of freedom. In the absence of collisions, however, the energy distribution mechanisms in highly vibrationally excited molecules are not yet well understood. At high excitation the spacing between vibrational levels becomes increasingly smaller and many quasi-isoenergetic combinations of states exist. In this regime molecular excitation occurs mostly through incoherent one-photon transitions between states that are defined by total energy content. Since the number of states involved is large — and often not even known — the problem is inherently complicated, even for a modest size molecule. Moreover, the lack of spectroscopic data of highly excited states renders a complete quantum mechanical treatment of the excitation dynamics nearly impossible. So it is in general not possible to determine the intramolecular distribution of energy in infrared multiphoton excited molecules *a priori*.

A statistical description of the ensemble of modes within a single molecule has therefore been proposed as an alternative.[17,18] Nonlinear dynamics studies have shown that energy can swing back and forth between two coupled oscillators in such a way that — in the sense of a time-average — energy is equipartitioned.[19] This conclusion agrees with recent experiments,[20] where transfer of energy between two closely spaced, isolated, modes has been demonstrated by observing the beating fluorescence signal from these modes. For a system consisting of many coupled oscillators, such as a highly vibrationally excited polyatomic molecule, there are many channels for transferring excitation energy. Since the period of Poincaré cycles is an exponential function of the dimension of phase space,[21] it exceeds the mean free time between collisions even for a modest size molecule at pressures above 10 Pa. Therefore intramolecular vibrational energy transfer in a highly excited polyatomic molecule can be considered irreversible for all practical purposes. A statistical description implies an intramolecular equilibrium distribution of energy among the various modes of an infrared multiphoton excited molecule on collisionless time scales. The aim of our present research effort is to establish experimentally whether such an approach is justified.

Direct experimental information on both intramolecular and intermolecular energy distribution after infrared multiphoton excitation has been obtained by spontaneous Raman spectroscopy[22–27] and from infrared double resonance experiments.[28–30] In this paper we elaborate on a previously reported experiment,[31] in which internal energy leakage from an infrared active mode to a Raman active mode is observed by monitoring the evolution of the anti-Stokes Raman

signal. Both collisional and collisionless aspects will be discussed.

II. THEORY

In this section we present a brief treatment of spontaneous Raman scattering, in order to derive a simple expression for the total intensity of the light scattered from a Raman active mode. Both radiation field and molecular system are treated quantum mechanically. To describe the mechanism of Raman scattering we consider the interaction of the field with the induced polarization P of the molecule,

$$P = \mu_0 + \alpha \cdot E, \tag{1}$$

where μ_0 is the permanent dipole moment of the molecule, α a tensor representing the molecular polarizability, and $\alpha \cdot E$ the induced dipole moment. The physical system is described by the Hamiltonian operator, which contains terms describing the molecular system and the electromagnetic radiation field, and a term representing the interaction between the molecular polarization and the field. This last term, the interaction Hamiltonian H_{int}, is responsible for the light scattering. In the electric-dipole approximation one has

$$H_{\text{int}} = E \cdot \alpha \cdot E . \tag{2}$$

Following Placzek[32] one expands the molecular polarizability α as a Taylor series of the generalized coordinate q of the molecular vibrational mode being considered

$$\alpha = \alpha_0 + \left(\frac{\partial \alpha}{\partial q}\right)_0 q + \frac{1}{2}\left(\frac{\partial^2 \alpha}{\partial q^2}\right)_0 q^2 + \ldots . \tag{3}$$

Substituting α into H_{int} we obtain,

$$H_{\text{int}} = E \cdot \alpha \cdot E + E \cdot \left(\frac{\partial \alpha}{\partial q}\right)_0 \cdot E\, q + \frac{1}{2} E \cdot \left(\frac{\partial^2 \alpha}{\partial q^2}\right)_0 \cdot E\, q^2 + \ldots . \tag{4}$$

The first term represents the Rayleigh scattering, the remaining terms first and higher order Raman scattering. Since higher order scattering is rejected in our experiment, we need only consider the term linear in q. In simple harmonic approximation we have

$$q = (h/8\pi^2 \mu \nu_R)^{1/2} [\, b^\dagger + b \,] \tag{5}$$

where $b^\dagger$ and b are the creation and annihilation operator for the vibrational quanta respectively, and ν_R the frequency of the harmonic oscillator. The field is quantized similarly:

$$E_\lambda = (2\pi h \nu_R / \varepsilon V)^{1/2} \sum \mathbf{e}_\lambda [\, a_\lambda^\dagger + a_\lambda \,] \tag{6}$$

with $a^\dagger$ and a the creation and annihilation operators for the field, ε the relative permittivity, V the mode volume, and $\mathbf{e}_\lambda$ a unit vector representing the polarization of the light of wavelength λ. The linear term in the interaction Hamiltonian can therefore be written in the following form,

$$H_{\text{int}} \sim \left(\frac{\partial \alpha}{\partial q}\right)_0 [\, a_L b^\dagger a_{AS}^\dagger + a_L b\, a_S^\dagger \,] (\mathbf{e}_L \cdot \mathbf{e}_R) , \tag{7}$$

where the indices L, AS, S and R stand for laser, anti-Stokes, Stokes and Raman respectively. The first term in this expression annihilates a vibrational quantum and therefore corresponds to the anti-Stokes branch. The second term corresponds to the Stokes branch. The transition probability from an initial state $|\, i \,\rangle$ to a final state $|\, f \,\rangle$, is given by

$$W_{i \to f} = |\langle f | H_{\text{int}} | i \rangle|^2 . \tag{8}$$

For the eigenstates $|n\rangle$ of the harmonic oscillator one has

$$b^\dagger |\, n \,\rangle = (n+1)^{1/2} |\, n+1 \,\rangle , \tag{9}$$

and

$$b |\, n \,\rangle = n^{1/2} |\, n-1 \,\rangle , \tag{10}$$

with n the vibrational quantum number corresponding to state $|n\rangle$.

From eqs. (7) through (10) it can now immediately be seen that the transition probabilities for Stokes and anti-Stokes transitions depend on $n+1$ and n, respectively

$$W_{n \to n+1} \sim n+1, \quad W_{n \to n-1} \sim n. \tag{11}$$

Hence the *total* intensity of the spontaneous Stokes and anti-Stokes Raman signals (summed over *all* vibrational levels of the particular vibrational mode considered), I_S and I_{AS}, are given by

$$I_S \sim \sum_{n=0}^{\infty} W_{n \to n+1} N(n) \sim \sum_{n=0}^{\infty} (n+1) N(n) = 1 + \sum_{n=1}^{\infty} n N(n) , \tag{12}$$

$$I_{AS} \sim \sum_{n=0}^{\infty} W_{n \to n-1} N(n) \sim \sum_{n=1}^{\infty} n N(n) ,$$

with $N(n)$ the population of level n. Substituting the average energy in the mode per molecule, $E_R = h\nu_R \sum n N(n)$, we find for the summations in eq. (12)

$$I_S \sim 1 + \frac{E_R}{h\nu_R} , \qquad I_{AS} \sim \frac{E_R}{h\nu_R} . \tag{13}$$

It is important to note that in the harmonic approximation the result obtained does not depend on the energy distribution $N(n)$, but only on the *average* energy E_R.

Thus, the intensity of a Raman active mode is a measure for the average energy content of the mode. This can then be compared with the energy content of other modes and with the total energy deposited into the sample. Such a comparison will tell how the absorbed energy is distributed in the absence of collisions.

III. EXPERIMENTAL METHOD AND APPARATUS

A schematic view of the setup is shown in Fig. 1. An infrared exciting beam and an ultraviolet probing beam cross inside a scattering cell[33]. The spontaneous Raman signal of the SF_6 molecules is detected along the direction perpendicular to the incident beams. The scattering cell consists of two orthogonal arms, that contain a series of black anodized baffles, arranged to trap scattered or diffracted light, see Fig. 2. Light scattered in the interaction region is collected over a solid angle of $\pi/16$ sr, and focused onto the entrance slit of a double monochromator of 3 nm resolution. The output from the monochromator is detected by a fast ultraviolet-sensitive photomultiplier. Since the number of photons that reach the photomultiplier per laser pulse is less than ten, the signal has to be averaged over a large number of shots, typically 10^4.

The short-pulse CO_2-oscillator-amplifier system is shown in Fig. 3. The laser pulse originates in the 241 cm long cavity of a hybrid CO_2-laser, with a 62 MHz longitudinal mode spacing. The cavity consists of a transversely excited atmospheric-pressure (TEA) section and a low pressure (500 Pa) continuous wave (CW) discharge cell. Since the TEA section, a Taschisto Model 215 CO_2-laser head, has a bandwidth of 3.6 GHz, the laser can oscillate on many modes simultaneously. The low pressure section, which has a 55 MHz bandwidth, however, acts as an active filter and allows only one longitudinal mode in the cavity.[34] To prevent the laser from occasionally lasing on two adjacent modes, each laser pulse is monitored by a fast detector. When lasing on two modes occurs, the detector signal has a beat frequency of 62 MHz. An electronic circuit then adjusts the length of the laser cavity with a piezoelectric transducer to restore single mode operation.

The single mode output pulses from this hybrid laser, which have a 100 ns full-width at half maximum duration, are truncated by a self-triggered plasma shutter.[35,36] The truncated pulses have a slow rise time — identical to the rise time of the 100 ns pulses — and an ultra-short fall time of about 10 ps. The pulses are further shortened by optical free induction decay (OFID) in a 4 m long low-pressure CO_2-cell.[37] The output pulse duration can be varied continuously from 30 to 250 ps by adjusting the pressure in the cell from 30 kPa to 4 kPa. The peak power of the short pulse

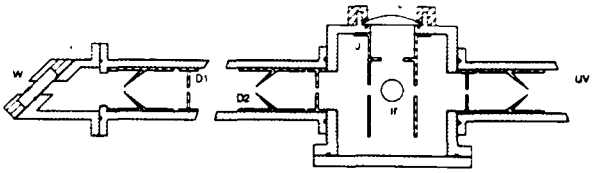

FIG. 2. Cross-sectional view of the Raman cell. W = quartz window, D1, D2 = straight and conical baffles, J = stray light jacket, IR = position of ir pump beam, UV = probing uv beam, L = collimating lens. The window holder has been rotated by 90° to show the Brewster angle mounting.

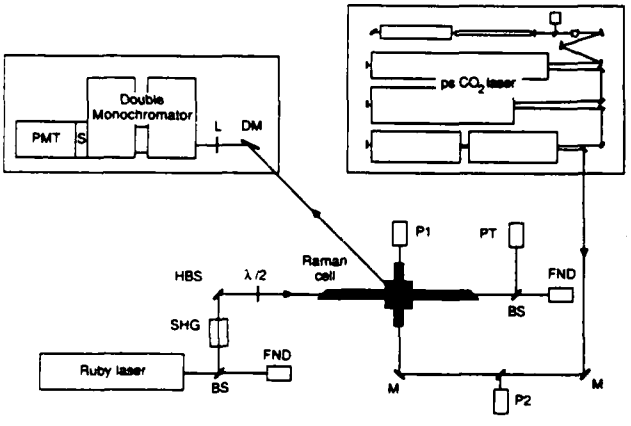

FIG. 1. Setup for measuring the spontaneous Raman scattering from infrared multiphoton excited molecules at low densities. Molecules excited by a CO_2-laser are probed by the second harmonic of a Ruby laser. BS = beam splitter, SHG = second harmonic generator, HBS = harmonic beam splitter, $\lambda/2$ = half-wave plate, FND = fast photodiode, PT = photo-tube, P1, P2 = pyroelectric detector, M = mirror, DM = dichroic mirror, L = quartz lens, S = shutter, PMT = photomultiplier tube. The detection (monochromator, photomultiplier, etc.) is located in a light-tight enclosure located directly above the Raman cell. Drawing not to scale.

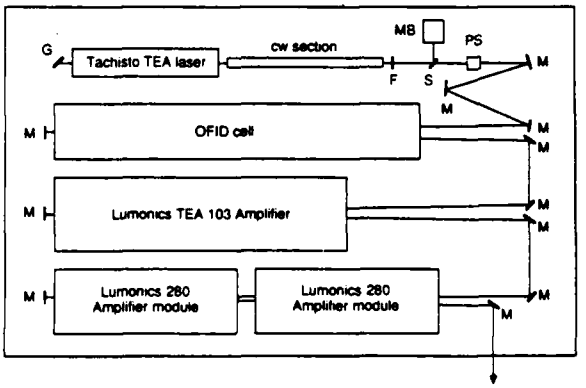

FIG. 3. The short-pulse CO_2-oscillator-amplifier system used for the infrared multiphoton excitation of the SF_6 (see text for explanation). G = grating, F = output coupler, S = beam splitter, MB = mode-beat detector, PS = plasma shutter, M = mirror.

generated is equal to that of the input pulse, while the total energy is decreased by a factor that is the ratio of the duration of output and input pulses.

One Lumonics model 103 laser amplifier operating at atmospheric pressure and two 10 atm Lumonics model 280 amplifiers are used to boost the energy of the short laser pulse. The atmospheric pressure amplifier, which has the smallest bandwidth, limits the pulse duration to 500 ps. With the high pressure amplifiers, which have a much larger bandwidth, pulses shorter than 50 ps can be amplified without significant stretching. The output beam is focused into the scattering cell by a cylindrical lens. Depending on the optical arrangement used, the beam waist is 2.2×0.18 mm or 6×0.35 mm. The average output energy is 100 mJ.

The probe beam is generated by a Raytheon model SS-420 Q-switched ruby laser that is frequency-doubled with a RDA-crystal second harmonic generator. The second harmonic at 347.15 nm is vertically polarized, i.e. in the direction of detection. A half-wave plate rotates the polarization by 90° into the plane of the two laser beams to obtain a maximum cross-section for Raman scattering, see Eq. (7). The beam is focused into the scattering region, where it crosses the infrared laser beam. The beam waist at the focal point is 500 mm, and the average probing pulse energy is 5 mJ.

A 0.3 Hz pulse generator controls the timing of the lasers and the data-acquisition system. The trigger pulses are optically isolated to prevent feedback of radio-frequency noise from the lasers. The synchronization of lasers and amplifiers is controlled electronically. The accuracy is limited by the 100 ns jitter of the lasers. Since this is inadequate for our measurements, the time-delay between infrared and ultraviolet pulses is measured for each pair of pulses. Two fast detectors provide start and stop pulses for an EG&G model 457 time to pulse-height converter, which measures the time delay between the two laser pulses. Although the resolution of the time to pulse-height converter is better than 100 ps, the time resolution of the setup is limited by the 18 ns duration of the probe beam, which we plan to improve in the near future. The energy of pump and probe pulses are measured by a pyroelectric detector and a phototube, respectively. Two electrodes, placed around the focal point of the plasma shutter, allow monitoring of the plasma breakdown. A small electronic circuit can thus determine if the infrared pulses are truncated correctly. All signals are collected by a data-acquisition system that is controlled by a Digital PRO 350 microcomputer.

The 19-channel data-acquisition system is shown in Fig. 4. It consists of home-made pulse sampling electronics, and a computer automated measurement and control (CAMAC) crate, containing a multiplexer, analog-to-digital converter, general input/output interface, and a general purpose interface bus (GPIB) crate controller. For every laser pulse, the pulse generator provides two trigger pulses to the data-acquisition system, one 100 ms before and one immediately after the lasers fire. This makes it possible to correct for a baseline-offset each time the signals are sampled. All data from the sample and hold circuits are converted to digital signals by the multiplexer and analog-to-digital converter. To correct for dark counts, the photomultiplier tube signal is recorded by a Biomation model 8100 transient waveform digitizer with 10 ns sampling intervals. The crate controller provides the interface to the computer, which in addition to reading and storing data, also monitors the values and rejects invalid data. A more detailed description of the experimental setup can be found in Ref. 33.

For the measurements presented in this paper, the following signals were recorded: Raman signal intensity, input energy and time-delay of ultraviolet and infrared pulses, ruby laser energy, and plasma breakdown. For every measurement the various signals are calibrated. The pyroelectric detector, which monitors the infrared pumping energy, is calibrated with a Scientech Joule meter, and the ultraviolet phototube, which monitors the ultraviolet probing pulse energy, with a Molectron pyroelectric detector. The photomultiplier signal is calibrated by measuring the room temperature Stokes sig-

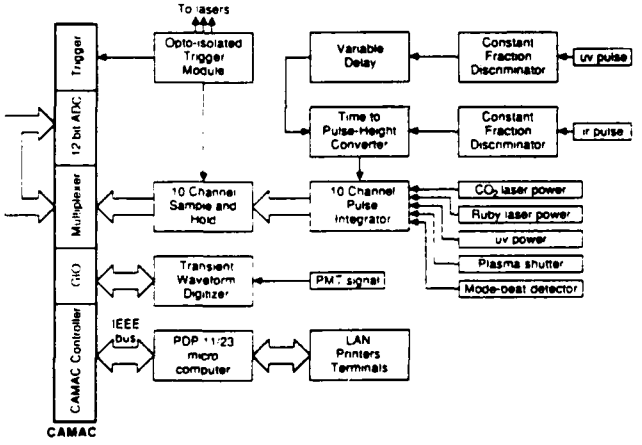

FIG. 4. Schematic diagram of the multichannel data-acquisition system.

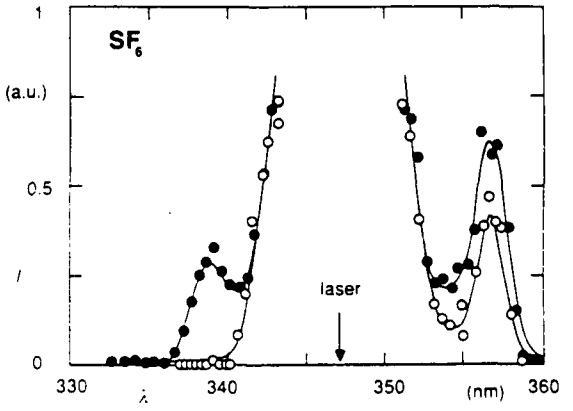

FIG. 5. Raman spectrum of SF_6, with (closed symbols) and without (open symbols) infrared multiphoton excitation. Infrared excitation: 10.6 μm P(20) line, 0.5 ns pulse duration, and average fluence 0.6×10^4 J/m^2. The small arrow shows the position of the laser radiation at 347.15 nm.

nal without infrared multiphoton excitation, henceforth referred to as "thermal Stokes," as a reference.

As we are dealing with small signals, several consistency checks were performed to ensure that no systematic errors occur. It was verified that there are no signals without ultraviolet probing pulse, or without gas in the scattering cell, and no anti-Stokes signal for negative time-delay. Reproducibility of the measurements was checked routinely during each measurement and from measurement to measurement.

Data analysis starts with a histogram of the infrared energy values. Then, the datapoints within the optimal range of infrared energy are further analyzed. The data are further restricted to include only valid data and subsequently calibrated and plotted. All Raman signals are normalized with the ultraviolet pumping intensity and the thermal Stokes signal so that the results from different measurements can be compared. Each individual measurement carried out at a fixed pressure contains enough datapoints to obtain the time and fluence dependence of the Raman signals. The pressure dependence was obtained separately by varying the pressure within one experimental run.

IV. RESULTS

Experiments have been performed at room temperature on SF_6 at sample pressures ranging from 13 Pa to 270 Pa. The SF_6 gas, obtained commercially, had a purity of 99.995%. Data were obtained for the CO_2-laser frequencies between the P(12) and P(28) lines of the 10.6 μm branch, which are resonant with the triply degenerate infrared active ν_3-mode (F_{1u}) of SF_6. Two different pulse durations were employed: short 0.5 ns and truncated 15 ns full-width at half-maximum pulses with fluences up to 7×10^4 J/m^2. The 15 ns truncated pulses are obtained with an optical free induction decay cell pressure of 1.3 kPa. At these low pressures, the pulses have an asymmetric shape, with a 10-90% rise time of 10 ns and a short subnanosecond fall time. The Raman signals are obtained at a shift of 775 cm^{-1} from the frequency-doubled ruby laser, corresponding to the totally symmetric breathing ν_1-mode (A_{1g}) of SF_6. Results are shown in Figs. 5 through 12. The vibrational modes of SF_6 are given in Table I.[38]

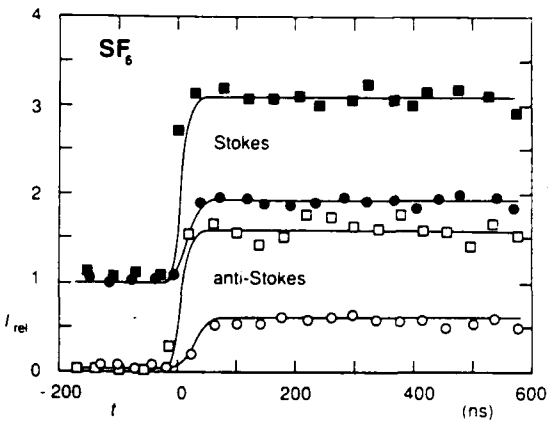

FIG. 6. Intensity of Stokes (closed symbols) and anti-Stokes (open symbols) signal as a function of the time delay between pump and probe pulses at a pressure of 67 Pa. The data are normalized to the thermal Stokes signal. Negative time delay means that the signals are measured before the infrared multiphoton excitation. The rise time in the curves reflects the 18 ns FWHM duration of the probe pulse. Results are shown for two different durations, 0.5 ns (squares) and 15 ns (circles). Infrared excitation at the 10.6 μm P(20) line, with an average fluence of 0.8×10^4 J/m^2.

The points shown in the figures are obtained by dividing the x-axis into a number of intervals (usually twenty), and averaging the data that lie within each of the intervals. Since our experiment is done in the photon counting regime, the standard deviation of the photomultiplier signal is comparable to its average value, even when the data is restricted to those data points where the fluctuation in the pump laser intensity is no more than 20%. According to the central limit theorem, the standard deviation in average value for a certain interval is inversely proportional to the square root of the number of data within that interval.[39] Typically, at 100 Pa, about 200 laser pulses are needed to obtain a 10% standard deviation. Since the experiment is carried out at a repetition rate of 0.3 Hz, the stability of the alignment limits the total number of shots to 10^4 for a single experimental run. This means that there is a trade-off between the number of points in one figure and

TABLE I. Vibrational modes of SF_6, taken from Ref. 38 (s = strong, w = weak).

Mode	k (cm^{-1})	ν (THz)	symmetry	degeneracy	activity
ν_1	775	23.25	A_{1g}	1	Raman (s)
ν_2	644	19.32	E_g	2	Raman (w)
ν_3	965	28.95	F_{1u}	3	infrared
ν_4	617	18.51	F_{1u}	3	infrared
ν_5	524	15.72	F_{2g}	3	Raman (w)
ν_6	363	10.89	F_{2u}	3	inactive

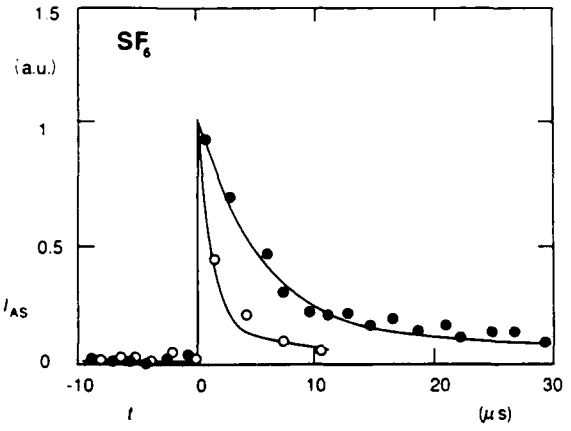

FIG. 7. Long time behavior of the anti-Stokes signal for two pressures: p = 70 Pa (open symbols) and p = 270 Pa (closed symbols). The signal is normalized to one at $t = 20$ ns. Infrared excitation: 10.6 μm P(20) line, 0.5 ns pulse duration, and average fluence 10^4 J/m^2. The decay of the curves, which is due to diffusion of the excited molecules out of the interaction region, scales with pressure (see text for details).

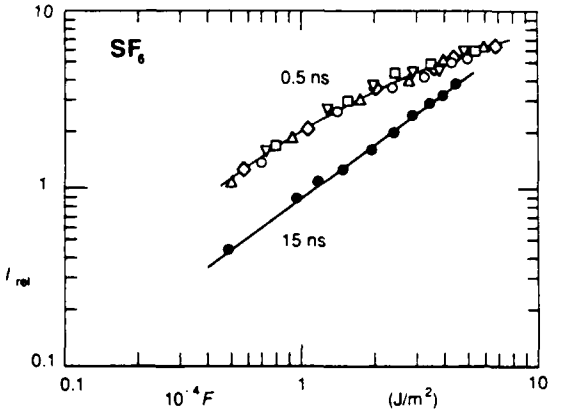

FIG. 9. Relative anti-Stokes signal as a function of the infrared pumping fluence for various pressures and two infrared pulse durations at the 10.6 μm P(20) line: 0.5 ns (open symbols) and 15 ns (closed symbols). This graph shows the reproducibility of the data from measurement to measurement.
□: 33 Pa; ○: 67 Pa; △: 133 Pa; ▽: 200 Pa;
◇: 267 Pa; ●: 133 Pa.

the length of the error bars. In all measurements presented here the error bars are about 10% of the absolute value of the data points.

Fig. 5 shows the Raman spectrum of SF_6 with and without infrared pumping. The central peak is due to elastically scattered light — mainly Rayleigh scattering. The spectral resolution, which is determined by the slit of the monochromator, is 3 nm. Without the infrared pumping only a Stokes shifted peak is observed. This is because at room temperature less than 3% of the molecules are in excited states of the Raman active mode. With infrared pumping it is seen that both Stokes and anti-Stokes signals increase. Since the ν_3 and ν_1 modes have opposite symmetry, they do not couple at low excitation. This figure, however, clearly shows that under infrared multiphoton excitation the energy distribution of the Raman active mode is changed. It also shows that there is no contribution from elastically scattered light at the position of the Raman lines. The remainder of the experimental results are obtained at fixed frequencies, 356.7 nm and 338 nm for the Stokes and anti-Stokes lines, respectively.

Fig. 6 shows the increase of both Stokes and anti-Stokes signals as a function of the time delay between the infrared pump and the probe pulse for two infrared pulse durations, 0.5 ns and 15 ns at a pressure of 67 Pa and an average infrared fluence of 0.8×10^4 J/m^2. Negative time delay, $t < 0$, means that the molecules are probed before the

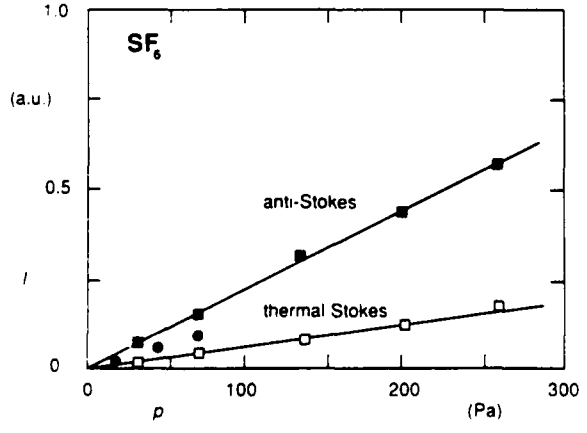

Fig. 8. Pressure dependence of anti-Stokes (closed symbols) and thermal Stokes (open symbols) signal. Infrared excitation for anti-Stokes data: 10.6 μm P(20) line, 0.5 ns (squares) and 15 ns (circles) pulse duration, and average fluence 2×10^4 J/m^2.

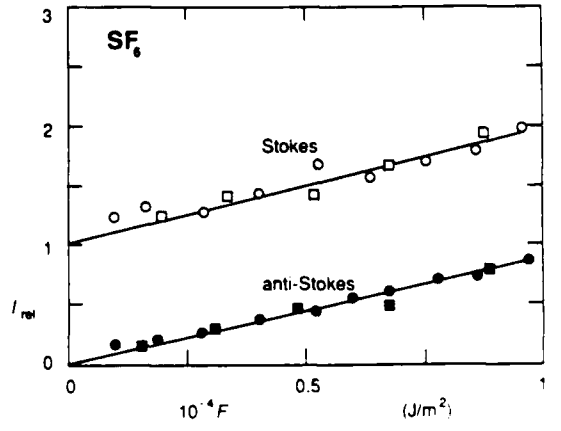

FIG. 10. Relative Stokes (open symbols) and anti-Stokes (closed symbols) signal as a function of the infrared pumping fluence at the 10.6 μm P(20) line for 15 ns pulses at two different pressures. $p = 27$ Pa (squares), and $p = 133$ Pa (circles).

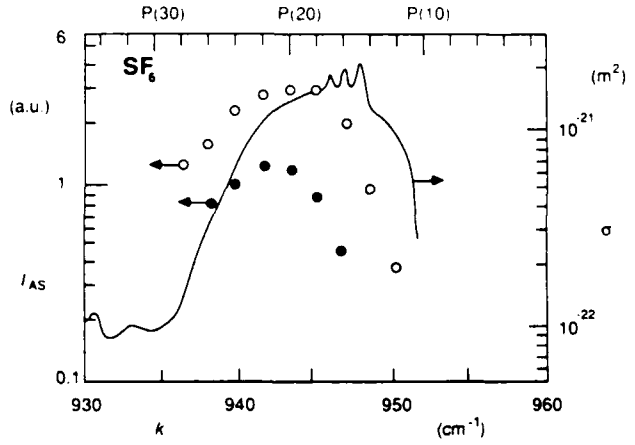

FIG. 11. Anti-Stokes signal for excitations at different CO_2-lines. The curve shows the one photon absorption cross section (see scale on the right). A clear red-shift can be observed. Data for two different pulse durations at an average fluence of 10^4 J/m^2 are shown: 0.5 ns (open symbols) and 15 ns (closed symbols). The position of the data points with respect to the right hand vertical scale is arbitrary.

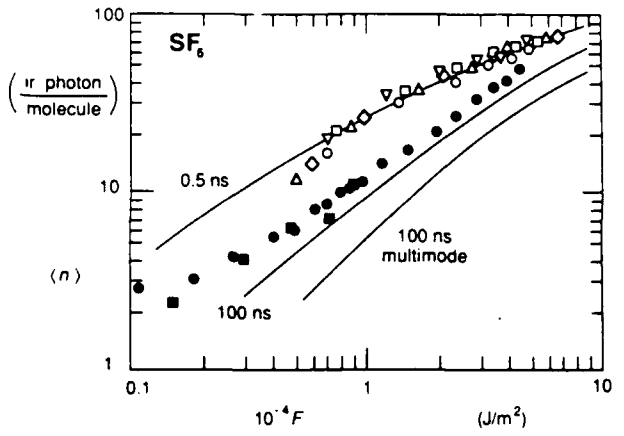

FIG. 12. Average number of infrared photons absorbed per molecule as a function of infrared fluence. The data points shown were obtained from the ones shown in Figs. 9 and 10, assuming thermal equilibrium between all vibrational modes immediately after the infrared multiphoton excitation. See those figures for an explanation of the symbols. The solid lines are the average number of infrared photons obtained from the photoacoustic measurements reported in Ref. 43. The results show a remarkable agreement.

infrared multiphoton excitation, i.e. the molecules are at thermal room temperature equilibrium. The Raman signals are normalized with the equilibrium room temperature (thermal) Stokes signal. Within the 20 ns time resolution of the experiment, determined by the duration of the ultraviolet pulse, a *collisionless* (see discussion) increase of both Stokes and anti-Stokes signals is observed. The increase is consistent with the result obtained in Eq. (13), i.e. for each pulse duration both Stokes and anti-Stokes signal increase by the same amount. After the initial increase the signals remain constant, even on a time scale on which collisional vibrational energy relaxation starts to play a role (the vibrational relaxation time constant, $\tau_{1\to}$, is given by $p\tau_{1\to} \approx 70\,\mu$s Pa).[40] Clearly, collisions do not affect the total intensity of the anti-Stokes signal. This shows that intramolecular equilibrium is reached on a time scale shorter than the time resolution. Since the intensity of the signal is determined by the average energy in the mode only, intermolecular vibrational-vibrational energy transfer will not affect the Raman signals once intramolecular equilibrium is reached.

The long time evolution of the anti-Stokes signal, measured at two different gas pressures, 70 and 270 Pa is shown in Fig. 7. The observed decay in the signals is about ten times faster than the relaxation time reported for collisional transfer of vibrational energy to translational degrees of freedom ($p\tau_{1\to} \approx 16$ ms Pa).[41] Moreover, the low pressure signal decays faster than the high pressure signal, showing the decay is not caused by collisional energy relaxation, but by diffusion of the excited molecules out of the interaction region — a process inversely proportional to pressure. Indeed, data points obtained at the higher pressure can be made to overlap the low pressure points by scaling the horizontal axis with pressure (see curves in Fig. 7).

Fig. 8 shows the pressure dependence of the signal, obtained by varying the pressure in a single experimental run. Both the anti-Stokes signal from infrared multiphoton excited molecules as well as the thermal Stokes signal from unexcited molecules are shown. The points lie on straight lines, which account for the trivial dependence of the signals on particle density. This figure excludes the possibility that the observed changes in Raman signal are caused by a collisional process, in which case one would expect to see a p^2-dependence.

The infrared fluence dependence of the Stokes and anti-Stokes signal is shown in Figs. 9 and 10 for different pressures and pulse durations. The results shown were obtained in different runs, each one calibrated individually. The spread in data therefore shows the absolute accuracy and the reproducibility of the experimental data. Fig. 10 shows once again that both Stokes and anti-Stokes signals increase by the same amount, in agreement with Eq. (13).

Fig. 11 shows the anti-Stokes signal for excitations at different CO_2-lines. Each point shown represents a separate experimental run in which the anti-Stokes signal was measured at a particular laser line. From each of these measurements, carried out with two different pulse durations, the infrared fluence dependence was obtained, yielding graphs similar to Fig. 10. One point from each of these fluence dependencies (at a fluence of 10^4 J/m^2) is shown here. As a reference the low signal absorption cross-section for SF_6 is also plotted.[42] The relation between the two vertical scales is arbitrary. Because of the anharmonicity of the mode the energy level spacing decreases with increasing excitation. Therefore a red shift from the center of the one photon absorption band is observed. Because of the low spectral resolution of 3 nm (250 cm^{-1}) of the present setup, a previously reported red shift of the Raman displacement,[25] could not be observed.

V. DISCUSSION

Within the 20 ns time-resolution of the experiment, an instantaneous collisionless increase of the anti-Stokes signal or, alternatively, the average energy stored in the Raman-active mode, is observed. If the energy distribution among the different vibrational modes is not in equilibrium, collisions would alter the energy in the Raman active mode, and consequently change the Raman signal intensity. Since the Raman signals remain constant (within the 10% experimental accuracy) for 1 μs after infrared multiphoton excitation, an intramolecular vibrational energy equilibrium must be established within the time-resolution of the experiment.

Further evidence of an intramolecular equilibrium is obtained by comparing the present results with the results obtained from photoacoustic measurements.[43] Since the Raman signals are proportional to the energy stored in the Raman active mode, the energy can be obtained from the relative increase in anti-Stokes signal

$$E_R = h\nu_R I_{rel}/[1 - \exp(-h\nu_R/kT_0)], \quad (14)$$

where I_{rel} is the ratio between the anti-Stokes signal and the thermal Stokes signal, k the Boltzmann factor, and T_0 room temperature. This equation is obtained from Eq. (13) and the Boltzmann value of the energy in the mode at room temperature. If one assumes intramolecular equilibrium among the different vibrational modes, the energy distribution of the different modes should correspond to a common temperature. The total increase in vibrational energy of the molecule can thus be calculated from this temperature, and compared to the total absorbed energy, obtained from the photoacoustic measurements. The result of this comparison is shown in Fig. 12. The average total energy absorbed per molecule in units of pumping infrared photons is plotted as a function of infrared fluence. The data points are obtained from the current experiments, while the curves show the results of the photoacoustic measurements from Ref. 43. The agreement between the two measurements is remarkable, providing strong evidence for an intramolecular equilibrium.

It should be pointed out that the photoacoustic measurements monitor all molecules absorbing one or more infrared photons, while the Raman measurements only involve the fraction of molecules absorbing enough photons to reach the region where the infrared and Raman active mode couple to each other, a region frequently referred to as the quasicontinuum.[17] Consequently the curve for the Raman experiment should fall off more rapidly for low fluences than the one for the photoacoustic experiment, since the fraction of excited molecules is smaller. This is indeed observed for fluences below 10^4 J/m^2.

Another remarkable feature is that a collisionless increase in anti-Stokes signal within 20 ns can still be observed at infrared fluences as low as 3×10^2 J/m^2,[31] where the average infrared absorption of SF_6 is reported to be below 1 photon per molecule.[43] At these fluences the *inter*molecular vibrational energy distribution — in contrast to the *intra*molecular distribution — is not in equilibrium. Apparently even at low infrared fluence a small yet measurable fraction of molecules is excited high enough to show a change in Raman spectrum, while most molecules remain unexcited. Such a bimodal distribution, consisting of some highly excited molecules and the others unexcited, is consistent with a recent observation of two or three photon transitions in a pulse jet of SF_6 at infrared fluences below 2×10^3 J/m^2.[44] At higher fluences direct experimental evidence for a bimodal distribution was obtained from high resolution Raman experiments.[25]

The fluence dependence in Fig. 9 shows that the ratio of the anti-Stokes signals obtained for the 0.5 and 15 ns pulses decreases as the fluence increases. This observation, which is in agreement with the photoacoustic results,[43] shows that in the low fluence range intensity plays a more important role in the infrared multiphoton excitation of SF_6 than in the high fluence range. At low excitation high intensity is needed to over-come the anharmonic shift of the energy levels.[45] In this regime the fraction of molecules excited high enough to show a change in Raman spectrum depends more on intensity than it does the in high fluence range. Once the molecules are excited to a regime where the many intramolecular couplings help excitation, only fluence plays a role. Therefore the increase in anti-Stokes signal, which is a direct consequence of intramolecular couplings, depends also somewhat on intensity in the low fluence regime.

In Fig. 11 the dependence of the anti-Stokes signals on the infrared pumping wavelength is shown for both 15 ns and 0.5 ns multiphoton excitation. Because of the anharmonic shift of the levels at high excitation, the signals shift toward the red by about 5 cm^{-1} from the center of the one photon absorption band. The present data matches the absorption profiles for SF_6 at a temperature of 450 K,[46] much lower than the 2800 K final temperature corresponding to the average absorption of 25 infrared photons per molecule at 10^4 J/m^2. The width of the multiphoton excitation profiles also shows some intensity broadening.

The results shown in Fig. 11 agree with the infrared multiphoton absorption profile[47] and the frequency dependence of the infrared multiphoton dissociation probability[48] for SF_6 reported in the literature. This implies that the anti-Stokes Raman signal is proportional to the total vibrational energy stored in the molecule for all the CO_2-lines within the absorption profile, and not only for the center frequency. Therefore a rapid intramolecular vibrational energy equilibrium appears to be established for collisionless infrared multiphoton excitation at all frequencies that lie within the absorption profile of SF_6.

VI. CONCLUSIONS

This paper presents detailed measurements on collisionless infrared multiphoton excited SF_6. Spontaneous Raman spectroscopy is used as a tool to monitor the energy in the strong Raman active ν_1-mode. The pressure dependence of the observed signals clearly proves that one is dealing with a

collisionless process. Furthermore, the results present strong evidence that an intramolecular equilibrium among the various vibrational modes is achieved within the 20 ns time-resolution of the experiment.

We have observed a red shift and intensity broadening of the pump-frequency dependence and determined the fluence dependence of the increase in Raman signal. The observations are in excellent agreement with the results obtained by other techniques, such as dissociation and photoacoustic measurements. These techniques, however, monitor the total vibrational energy in the molecules, whereas the present experimental technique is only sensitive to the energy in one single mode.

For SF_6 in the gas phase, one is limited to probing one single Raman active mode. Experiments on molecules that have more than one accessible Raman active mode are in progress. These experiments should provide further information on the intramolecular energy distribution in collisionless infrared multiphoton excited molecules. Even more detail will be provided by forthcoming picosecond coherent anti-Stokes Raman spectroscopy experiments on infrared multiphoton excited molecules.

ACKNOWLEDGMENTS

The authors gratefully acknowledge helpful comments and stimulating discussions with Prof. N. Bloembergen. This research was supported by the U.S. Army Research Office and the Joint Services Electronics Program under contracts no. DAAG29-85-K-0600 and N00014-84-K-0465, respectively, with Harvard University.

[1]N. R. Isenor, V. Merchant, R. S. Hallsworth, and M. C. Richardson, Can. J. Phys. **51**, 1281 (1973).

[2]See, e.g, the following publications and references therein. V. N. Bagratashvili, V. S. Letokhov, A. A. Makarov, and E. A. Ryabov, *Multiple Photon Infrared Laser Photophysics and Photochemistry* (Harwood Academic, New York, 1985); N. Bloembergen and E. Yablonovitch, Phys. Today **5**, 23 (1978); W. Fuss and K. L. Kompa, Prog. Quantum Electron. **7**, 117 (1981); D. S. King, *Dynamics of the Excited State*, edited by K. P. Lawley (Wiley, New York, 1982).

[3]R. V. Ambartsumian, V. S. Letokhov, E. A. Ryabov, and N. V. Chekalin, JETP Lett. **20**, 273 (1974).

[4]V. S. Letokhov, Phys. Today **5**, 25 (1977).

[5]M. Drouin, M. Gauthier, R. Pilon, P. A. Hackett, and C. Willis, Chem. Phys. Lett. **60**, 16 (1978).

[6]J. B. Marling and I. P. Herman, J. Chem. Phys. **72**, 5603 (1980).

[7]Aa. S. Sudbø, P. A. Schulz, E. R. Grant, Y. R. Shen, and Y. T. Lee, J. Chem. Phys. **68**, 1306 (1978); **70**, 912 (1979).

[8]C. R. Quick, Jr. and C. Wittig, J. Chem. Phys **72**, 1694 (1980).

[9]V. N. Bagratashvili, M. V. Kuzmin, and V. S. Letokhov, J. Chem. Phys. **88**, 5780 (1984).

[10]M. Quack, J. Chem. Phys. **69**, 1282 (1978).

[11]C. D. Cantrell, S. M. Freund, and J. L. Lyman, *Laser Handbook*, edited by M. L. Stitch (North-Holland, Amsterdam, 1979), Vol. 3.

[12]S. Mukamel, Adv. Chem. Phys. **47**, 509 (1981).

[13]J. R. Ackerhalt, H. W. Galbraith, and P. W. Milonni, Phys. Rev. Lett. **51**, 1259 (1983).

[14]G. Hose and H. S. Taylor, Chem. Phys. **84**, 375 (1984); G. Hose, H. S. Taylor, and Y. Bai, J. Chem. Phys. **80**, 4363 (1984).

[15]I. Schek and R. E. Wyatt, J. Chem. Phys. **83**, 4650 (1985).

[16]N. Bloembergen and A. H. Zewail, J. Phys. Chem. **88**, 5459 (1984).

[17]N. Bloembergen and E. Yablonovitch, Phys. Today **5**, 23 (1978).

[18]H. W. Galbraith and J. R. Ackerhalt, in *Laser Induced Chemical Processes*, edited by J. I. Steinfeld (Plenum, New York, 1981).

[19]D. W. Noid, M. L. Koszykowski and R. A. Marcus, Annu. Rev. Phys. Chem. **32**, 267 (1981).

[20]P. M. Felker and A. H. Zewail, Chem. Phys. Lett. **102**, 113 (1983); **108**, 303 (1984); see also, Phys. Rev. Lett. **53**, 501 (1984).

[21]P. Mazur and E. W. Montroll, J. Math. Phys. **1**, 70 (1960).

[22]V. N. Bagratashvili, Yu. G. Vainer, V. S. Doljikov, S. F. Koliakov, A. A. Makarov, L. P. Malyavkin, E. A. Ryabov, E. G. Silkis, and V. D. Titov, Appl. Phys. **22**, 101 (1980).

[23]V. N. Bagratashvili, Yu. G. Vainer, V. S. Dolzhikov, S. F. Kol'yakov, V. S Letokhov, A. A. Makarov, L. P. Malyavkin, E. A. Ryabov, E. G. Sil'kis, and V. D. Titov, Sov. Phys.—JETP **53**, 512 (1981).

[24]V. N. Bagratashvili, V. S. Doljikov, V. S. Letokhov, A. A. Makarov, L. P. Maljavkin, E. A. Ryabov, E. G. Silkis, and Yu. G. Vainer, Opt. Commun. **38**, 31 (1981).

[25]V. N. Bagratashvili, Yu. G. Vainer, V. S. Doljikov, V. S. Letokhov, A. A. Makarov, L. P. Malyavkin, E. A. Ryabov, and E. G. Sil'kis, Opt. Lett. **6**, 148 (1981).

[26]Yu. S. Doljikov, V. S. Letokhov, A. A. Makarov, A. L. Malinovsky, and E. A. Ryabov, Chem. Phys. Lett. **124**, 304 (1986).

[27]V. S. Doljikov, Yu. S. Doljikov, V. S. Letokhov, A. A. Makarov, A. L. Malinovsky, and E. A. Ryabov, Chem. Phys. **102**, 155 (1986).

[28]D. S. Frankel and T. J. Manuccia, Chem. Phys. Lett. **54**, 451 (1978).

[29]R. C. Sharp, E. Yablonovitch, and N. Bloembergen, J. Chem. Phys. **74**, 5357 (1981).

[30]P. Mukherjee and H. S. Kwok, J. Chem. Phys. **84**, 1285 (1986).

[31]E. Mazur, I. Burak, and N. Bloembergen, Chem. Phys. Lett. **105**, 258 (1984).

[32]G. Placzek, *Marx Handbuch der Radiologie*, 2nd ed. (Academische Verlagsgesellschaft, Leipzig, 1934), Vol. VI, p. 206.

[33]Eric Mazur, Rev. Sci. Instrum. **57**, 2507 (1986).

[34]A. Gondhalekar, N. R. Heckenberg, and E. Holzhauer, IEEE J. Quantum Electron. **QE-11**, 103 (1975).

[35]H. S. Kwok and E. Yablonovitch, Appl. Phys. Lett. **27**, 583 (1975).

[36]H. S. Kwok and E. Yablonovitch, Opt. Commun. **21**, 252 (1977).

[37]E. Yablonovitch and J. Goldhar, Appl. Phys. Lett. **25**, 580 (1974).

Raman spectroscopy of infrared multiphoton excited molecules

Kuei-Hsien Chen, Jyhpyng Wang and Eric Mazur

Department of Physics and Division of Applied Sciences, Harvard University, Cambridge MA 02138

Anti-Stokes signals from various modes of isolated, infrared multiphoton excited SF_6 and $C_2H_4F_2$ molecules are measured as a function of pressure, infrared fluence and wavelength. This allows to verify whether intramolecular equilibrium of vibrational energy is established after infrared multiphoton excitation in isolated molecules.

A question in the field of infrared multiphoton excitation on which much effort has been focusing recently is how, under collisionless conditions, vibrational energy is distributed among the different modes of isolated infrared multiphoton excited molecules.[1] In recent experiments we have been using time-resolved spontaneous Raman spectroscopy in low pressure samples as a tool to study the intramolecular vibrational energy distribution in isolated infrared multiphoton excited molecules. Several authors have proposed that the ensemble of modes in highly vibrationally excited molecules can be described statistically.[2-3] A statistical description implies an equipartitioning of energy among the various molecular modes. The aim of our current research is to determine experimentally whether such an approach is justified.

Measurements were carried out on SF_6 and $C_2H_4F_2$. In both cases it is observed that part of the excitation energy is distributed to Raman active modes. The total amount of energy in the Raman active mode can be determined by measuring the intensity of the Raman signals. Quantitative measurements of the Raman signals have been carried out as a function of time, gas pressure, infrared excitation energy, pulse duration and frequency.

Fig. 1 shows the increase in anti-Stokes Raman intensity for one of the four accessible Raman active lines of $C_2H_4F_2$. Whithout excitation no anti-Stokes signal could be observed. This is due to the fact that at room temperature less than 2% of the molecules are in excited states. After multiphoton excitation the energy in the Raman mode is changed as can be seen from the increase in anti-Stokes intensity. At a fluence of 1.5 J/cm^2 all of a sudden broadband fluorescence obscures the Raman scattering. This broadband fluorescence is due to electronic excitation by the probing ultraviolet pulse of either highly excited $C_2H_4F_2$ or its dissociation fragments.

After measuring the energy in the Raman modes, one can compare this energy with the energy in other Raman active modes and with the total energy absorbed by the molecule as a whole (known from photoacoustic measurements).[4] In Fig. 2 the energy in the Raman active mode of multiphoton excited SF_6 is compared to the average energy (in units of infrared photons) absorbed per molecule, assuming equipartitioning of energy among the different modes. The results show a remarkable agreement. For $C_2H_4F_2$, on the other hand, the energy stored in the various Raman active modes after the infrared multiphoton excitation does not correspond to a 'common temperature.' The energy in one mode (at a Raman shift of 3000 cm^{-1}), namely, does not change within the experimental accuracy, while the other modes do exhibit changes.

In conclusion, we report here on detailed quantitative measurements of the intramolecular vibrational energy

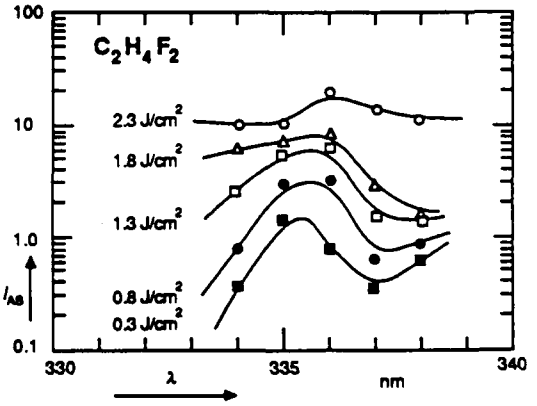

Fig. 1. Anti-Stokes spectrum for one of the Raman active lines of $C_2H_4F_2$ at a shift of 863 cm^{-1} for different infrared excitation fluences. The increase in intensity at the right is due to Rayleigh scattering. Above 1.5 J/cm^2 broadband fluorescence obscures the Raman scattering.

distributions in infrared multiphoton excited molecules. It is found that although intramolecular equilibrium is reached in infrared multiphoton excited SF_6, this is not necessarily true for infrared multiphoton excited molecules in general.

1 See *e.g.* the following publications and references therein: V.N. Bagratashvili, V.S. Letokhov, A.A. Makarov, E.A. Ryabov, *Multiple Photon Infrared Laser Photophysics and Photochemistry* (Harwood Academic Publishers, New York, 1985); W. Fuss and K. L. Kompa, *Prog. Quant. Electr.* 7, 117 (1981); D.S. King, *Dynamics of the Excited State*, Ed. K. P. Lawley (Wiley, New York, 1982);

2 N. Bloembergen and E. Yablonovitch, *Physics Today* 5, 23 (1978)

3 H.W. Galbraith and J.R. Ackerhalt, in *Laser induced Chemical Processes*, Ed. J.I. Steinfeld (Plenum, New York, 1981)

4 J.G. Black, P. Kolodner, M.J. Schultz, E. Yablonovitch, and N. Bloembergen, *Phys. Rev.* A19, 704 (1979)

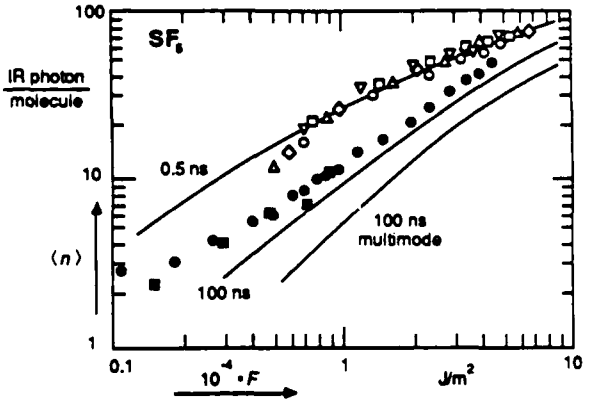

Fig. 2. Average number of infrared photons absorbed per molecule as a function of infrared fluence. The data points shown were obtained from the present Raman measurements, assuming thermal equilibrium between all vibrational modes immediately after the infrared multiphoton excitation. The solid lines are the average number of infrared photons obtained from previously reported photoacoustic measurements. The results show a remarkable agreement.

REPRINTED FROM PROCEEDINGS OF THE INTERNATIONAL CONFERENCE ON LASERS '86, NOVEMBER 3–7, 1986

The interaction of infrared radiation with isolated molecules: intramolecular nonequilibrium

Eric Mazur, Kuei-Hsien Chen and Jyhpyng Wang

Department of Physics and Division of Applied Sciences, Harvard University, Cambridge, MA 01238

Anti-Stokes signals from various modes of isolated, infrared multiple photon excited molecules are measured to determine the intramolecular distribution of vibrational energy. This paper presents results for CF_2HCl, CF_2Cl_2, SF_6 and *1,1*-$C_2H_4F_2$. All but CF_2HCl exhibit collisionless changes in Raman spectrum after infrared multiphoton excitation. This shows that the excitation modifies the population of these modes. Even though the symmetric SF_6 molecule reaches an intramolecular equilibrium within the 20 ns time resolution of the experiment, the other molecules exhibit a distinct nonequilibrium intramolecular distribution of vibrational excitation energy.

Introduction

The rather surprising discovery, that isolated polyatomic molecules in the ground electronic state can absorb a large number of photons from a resonant high-power infrared laser,[1] has led to extensive experimental and theoretical studies of this phenomenon during the last decade.[2] Since the vibrational modes of a molecule are generally anharmonic,[3] one would expect the molecules to become out of resonance with an initially resonant laser field after the absorption of one or two photons (see Fig. 1a). The number of photons absorbed per molecule, however, can be as large as 30, and the increase in internal energy comparable to electronic excitation energies. Often the excitation results in collisionless dissociation of the molecules. Experiments showed that the absorption is a stepwise process and not a simultaneous absorption of many photons. The list of molecules that exhibit this behavior grows continuously,[4] and infrared multiphoton excitation evidently is a general property of all but the smallest polyatomic molecules.

Clearly, stepwise absorption of infrared laser photons up a single anharmonic vibrational manifold is not possible. This precludes the infrared multiple photon excitation of diatomic molecules. For a polyatomic molecule, consisting of N atoms, however, 3N–6 coupled anharmonic vibrational modes can participate in the process. In short the excitation mechanism can be explained as follows. At a certain level of excitation the density of states becomes very large and many quasi-isoenergetic (combinations of) states exist. In this high density of states region molecular excitation occurs through incoherent one-photon transitions. The high density of states and the anharmonic coupling of molecular modes provide a way for the molecules to continue to absorb photons. Fig. 1b schematically shows the absorption of one photon in this regime: a resonant mode absorbs a photon, and immediately 'dissipates' the energy to an intramolecular heat-bath formed by other nonresonant modes of the molecule.

Immediately the question arises how the absorbed energy is distributed among the various modes during this process. Do all modes participate, or are some excluded from the process? This question has received much attention because the excitation of only a few modes inside a molecule might lead to interesting new techniques for controlling chemical reactions. The large, and often not even known, number of states renders the problem inherently complicated from a theoretical point of view. Several authors have

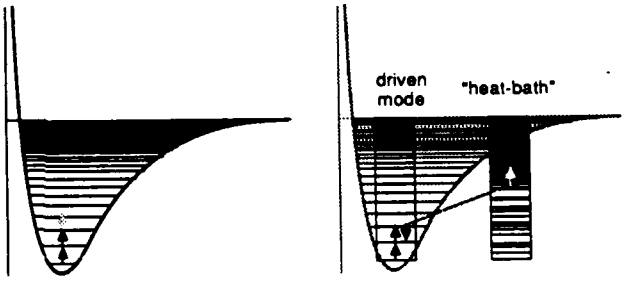

Fig. 1. Infrared excitation in a diatomic molecule (a) and multiple photon excitation in a polyatomic molecule (b). The diatomic molecule becomes out of resonance with the laser field after the absorption of one or two photons, even for very intense pulses when considerable power broadening occurs. Polyatomic molecules, however, have many vibrational modes which are coupled by cross-anharmonicities. Multiple photon excitation can then take place through stepwise incoherent excitation between combinations of states. Because other modes participate in the process, energy slowly 'leaks' into these modes. The figure shows one possible intramolecular energy exchange.

proposed a statistical description of the ensemble of modes,[5,6] suggesting an intramolecular equilibrium distribution of vibrational energy among the various modes of an isolated infrared multiphoton excited molecule.

Direct information on the intramolecular energy distribution in highly excited molecules was obtained experimentally with pump-probe type experiments, such as infrared double resonance experiments[7-9] and spontaneous[10-17] and coherent[18,19] Raman experiments. Raman spectroscopy was first employed by Bagratashvili and coworkers[10] and later by our group[16] as a tool for studying infrared multiple photon excitation. Fig. 2 schematically shows the general concept of these experiments. First, an intense infrared laser pulse, resonant with a particular infrared active mode (shown at the right), excites an isolated molecule. The figure shows one possible excitation pathway: after the (coherent) absorption of a few photons at the bottom of the resonant vibrational ladder, the molecule reaches the high density of states region known as the quasicontinuum (shown in the figure as an overlap of the various modes), and energy starts to 'leak' to other modes. After the excitation a second laser pulse probes one Raman-active mode from the intramolecular 'heat-bath' of modes (shown at the left). At room temperature the population of excited states of the Raman active modes is only a few percent, so that without infrared excitation only a Stokes signal is observed (Fig. 2, transition 1). If some high lying states of the Raman active mode participate in the excitation process they may become populated. Because of the anharmonicity of the Raman active mode, a shift in Stokes signal is then observed[13] (Fig. 2, transition 2), and an anti-Stokes signal appears (Fig. 2, transition 3). Anti-Stokes scattering is a particularly sensitive probe for the population of excited levels in the Raman active mode, because of the absence of signal without excitation.

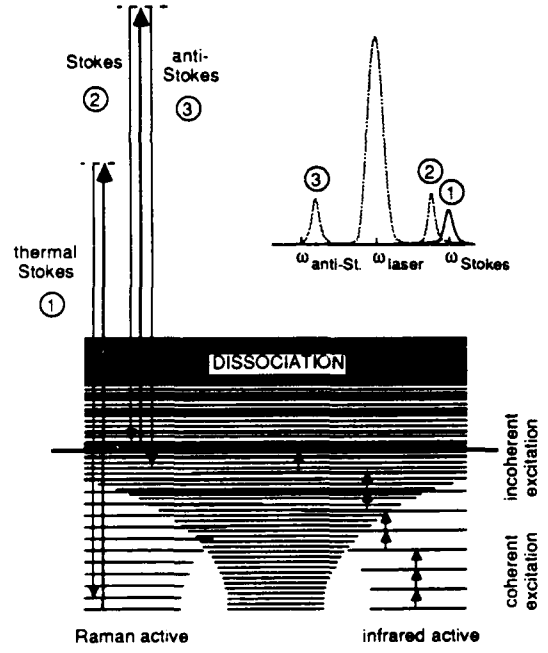

Fig. 2. Spontaneous Raman spectroscopy of infrared multiple photon excited molecules. After irradiation with an intense infrared pulse the molecules reach a region of high density of states known as the 'quasicontinuum'. Molecules that remain in the lower vibrational states (cold molecules) show only Stokes scattering (1), while the highly excited ones (hot molecules) show both a shifted Stokes (2) and an anti-Stokes signal (3).

In simple harmonic approximation one can readily show that the transition probabilities $W_{n\to n+1}$ and $W_{n\to n-1}$, for Stokes and anti-Stokes transition respectively, are proportional to the quantum number n.[17] Therefore the intensity of the Stokes and anti-Stokes signals are proportional to the average total energy in the mode, $E_R = h\nu_R \sum n N(n)$, with ν_R the frequency of the Raman active mode, and $N(n)$ the population of level n.

$$I_S \sim \sum_{n=0}^{\infty} W_{n\to n+1} N(n) \sim \sum_{n=0}^{\infty} (n+1) N(n) = \frac{E_R}{h\nu_R} + 1, \quad (1)$$

$$I_{AS} \sim \sum_{n=0}^{\infty} W_{n\to n-1} N(n) \sim \sum_{n=0}^{\infty} n\, N(n) = \frac{E_R}{h\nu_R}. \quad (2)$$

From these equations it follows that if the infrared multiphoton excitation alters the population of the levels in the Raman active mode, the Stokes and anti-Stokes signal intensities will change. Thus, spontaneous Raman spectroscopy allows one to determine experimentally the role of various modes in the infrared multiple photon excitation process.

Experimental setup

The experimental setup, shown schematically in Fig. 3, is discussed in detail in a previous paper.[16,17] Basically, molecules excited by a pulse of either 0.5 or 15 ns duration from a high power tunable CO_2-laser are probed by frequency-doubled ruby laser pulse of 20 ns duration. The two laser beams cross in a low pressure cell and scattered light from the interaction region is detected in a direction perpendicular to the two beams. A low resolution monochromator (1-2 nm) separates the Raman light from elastically scattered light. Spectral resolution is sacrificed for nanosecond time resolution and signal intensity (to enable measurement at low density).[20] For each pulse the infrared pulse energy and the time delay between the pump and the probe pulse is measured.

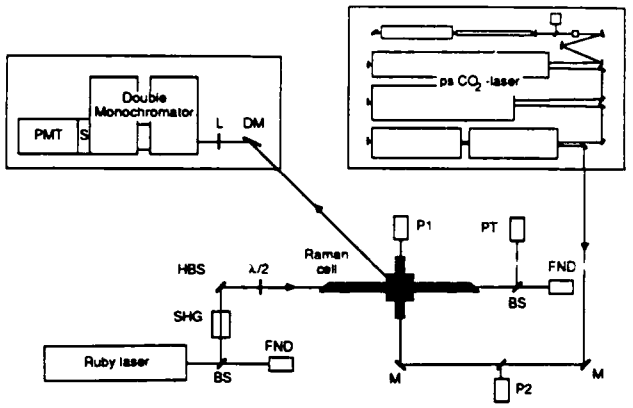

Fig. 3. Setup for the measurement of spontaneous Raman scattering from infrared multiphoton excited molecules at low densities. BS = beam splitter, SHG = second harmonic generator, HBS = harmonic beam splitter, $\lambda/2$ = half-wave plate, FND = fast photodiode, PT = phototube, P1, P2 = pyroelectric detector, M = mirror, DM = dichroic mirror, L = quartz lens, S = shutter, PMT = photomultiplier tube.

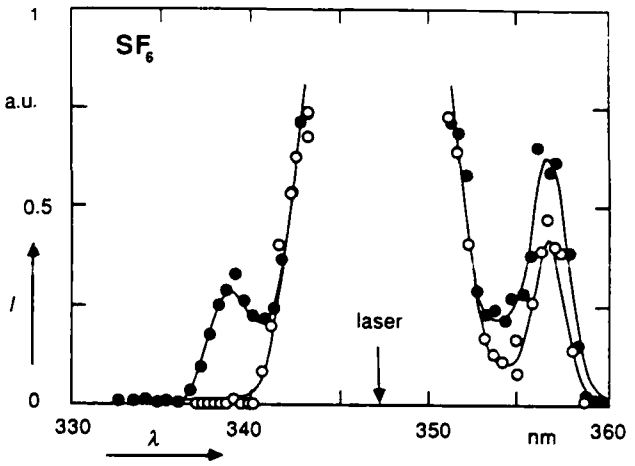

Fig. 4. Raman spectrum of SF_6, with (closed symbols) and without (open symbols) infrared multiphoton excitation. Infrared excitation: 10.6 μm P(20) line, 0.5 ns (squares) and 15 ns (circles) pulse duration, both at an average fluence of 0.6×10^4 J/m^2. The small arrow shows the position of the laser radiation at 347.15 nm.

To isolate intramolecular from (collisional) intermolecular effects the signals are measured at pressures low enough to ensure that no significant collisional relaxation of vibrational energy occurs on the time scale of the experiment. Since the gas-kinetic mean-free time τ_{mf} is roughly given by $p\tau_{mf} \approx 10^4$ ns Pa, and the probe pulse limits the time resolution of the experiment to 20 ns, one has to work at pressures of 400 Pa (3 torr) or lower. The Raman signals then correspond to single photon counts, and therefore the data must be averaged over at least 10^4 pulses to obtain a satisfactory signal-to-noise ratio. At the end of a measurement the data points are sorted out according to infrared pump intensity and time-delay between pump and probe, and averaged.

Experimental results and discussion

Four different molecules, CF_2HCl, CF_2Cl_2, SF_6 and *1,1*-$C_2H_4F_2$, varying in size from five to eight atoms, were studied with the present apparatus. Figs. 3 through 9 show some of the experimental results. Table I presents some relevant molecular data as well as an overview of the experimental results. All measurements were carried out at room temperature, with gas pressures ranging from 14 to 500 Pa and with infrared fluences up to 8×10^4 J/m^2. The commercially obtained gases have a reported purity better than 99.9%.

1. *SF_6*: Measurements on this symmetric molecule have been reported in detail previously.[17] This molecule has only one accessible Raman active mode, ν_1, with a Raman shift of 775 cm^{-1}. Data were obtained for CO_2-laser frequencies between the P(12) and the P(28) lines of the 10.6 μm branch, which are resonant with the triply degenerate infrared active ν_3-mode (944 cm^{-1}). Two different pulse durations were employed: 0.5 and 15 ns full-width at half-maximum pulses.

Fig. 4 shows the (low resolution) Raman spectrum with and without infrared pumping. As expected, the molecules show only a Stokes signal at room temperature. After excitation, however, an anti-Stokes signal appears, and at the same time the Stokes signal increases in accordance with Eqs. (1) and (2). These changes occur on time scales several orders of magnitude shorter than the average time between collisions.

Fig. 5 shows the increase in Stokes and anti-Stokes signals, measured at 356.7 and 338 nm respectively, as a function of the time delay between the pump and the probe pulse for two infrared pulse durations. The signals for negative time delay ($t < 0$, room temperature equilibrium) serve as calibration for the Raman signals. At $t = 0$ infrared excitation takes place and the Raman signals increase. Within the experimental accuracy both Stokes and anti-Stokes signal increase by the same amount, in accordance with Eqs. (1) and (2). The rise time of the signals is determined by the 20 ns pulse duration of the second harmonic of the probe laser. However, even though not resolved in these measurements, the increase in signal

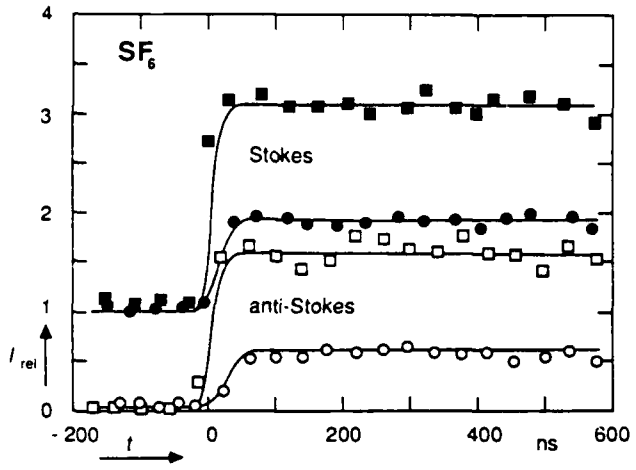

Fig. 5. Intensity of Stokes (closed symbols) and anti-Stokes (open symbols) signals of SF_6 as a function of the time delay between pump and probe pulses at a pressure of 67 Pa. The data are normalized to the thermal Stokes signal. Negative time delay means that the signals are measured before the infrared multiphoton excitation. The rise time in the curves reflects the 20 ns FWHM duration of the probe pulse. These results were obtained for 0.5 ns infrared excitation at the 10.6 μm P(20) line, with an average fluence of 0.8×10^4 J/m^2.

clearly occurs on a time-scale much shorter than the mean free time between collisions (about 200 ns at a pressure of 67 Pa). The pressure dependence of the signals, which is not presented here, shows that the increase in signal is not due to collisions, but is truly a *collisionless* phenomenon.[17] Interestingly enough the signals remain constant, even on a time scale on which collisional vibrational energy relaxation occurs.[21] For longer delay times ($t > 2$ μs), diffusion of the excited molecules out of the probing region causes the signals to revert to their original values.[17]

The dependence of the anti-Stokes signal intensity on the infrared laser fluence (energy per unit area) is shown in Fig. 6 for different pressures and pulse durations. These results were obtained in separate experimental runs, as indicated by the different symbols. The data obtained for the two pulse durations show that at low fluence the signals depend on the exciting laser pulse intensity: a larger increase in Raman signal occurs at the shorter, higher intensity, pulses. At low excitation one needs a high intensity for *coherent* multiphoton excitation through the lower part of the vibrational ladder. At the higher fluences, once the molecules are highly excited, the curves for the 0.5 and 15 ns pulse durations approach each other, and the dependence of the signal intensity on laser pulse intensity vanishes. This is consistent with the concept of a quasicontinuum[5] at high excitation, and agrees with the behavior observed in photoacoustic measurements, which determine the total amount of energy absorbed per molecule.[22]

The main purpose of this research is to obtain information on the role of nonresonant modes in the multiphoton excitation of polyatomic molecules. The observed collisionless changes in Raman signals provide clear and direct evidence that some of the nonresonant modes do indeed participate in the excitation process. Since the intensity of the signals is proportional to the average energy in the mode, one can determine E_R from the ratio of the anti-Stokes intensity to the thermal room temperature value of the Stokes signal, I_S^o. From Eqs. (1) and (2), one obtains

Table I. Overview of molecular data and experimental results.

Molecule	Number of atoms	Symmetric	Pump mode (cm^{-1})	CO_2-line (cm^{-1})	Raman lines (cm^{-1})	Equilibrium
CF_2HCl	5	no	1108	9.4 μm R(32); 1086	587,[2] 800,[2] 1134,[2] 1325,[2] 3029 [2]	no?
CF_2Cl_2	5	no	919	10.6 μm P(32); 933	664,[1] 919,[1] 1082,[1] 1147[3]	no
SF_6	7	yes	944	10.6 μm P(20); 944	775 [1]	yes
$C_2H_4F_2$	8	no	942	10.6 μm P(20); 944	870 [1], 1141,[2] 1457,[2] 2978[2]	no

[1] Measured in this experiment: exhibits change in intensity after infrared excitation
[2] Measured in this experiment: no measurable change in intensity
[3] Not measured; very weak

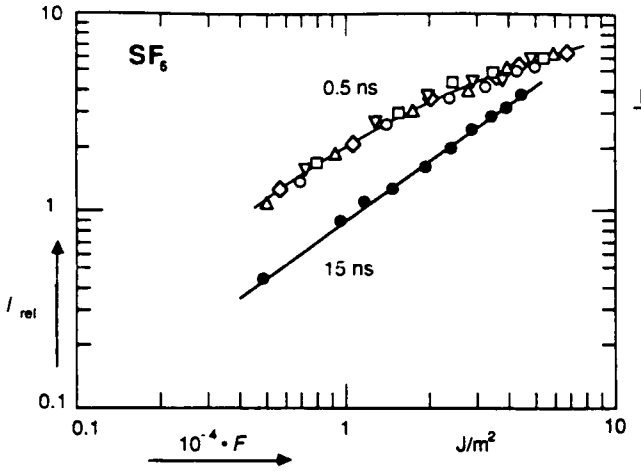

Fig. 6. Fluence dependence of anti-Stokes signal for SF_6. Relative anti-Stokes signal as a function of the infrared pump fluence for various pressures and two infrared pulse durations, at the 10.6 μm P(20) line: 0.5 ns (open symbols) and 15 ns (closed symbols). This graph shows the reproducibility of the data from measurement to measurement.
□: 33 Pa; ○: 67 Pa; Δ: 133 Pa; ▽: 200 Pa;
◇: 267 Pa; ●: 133 Pa.

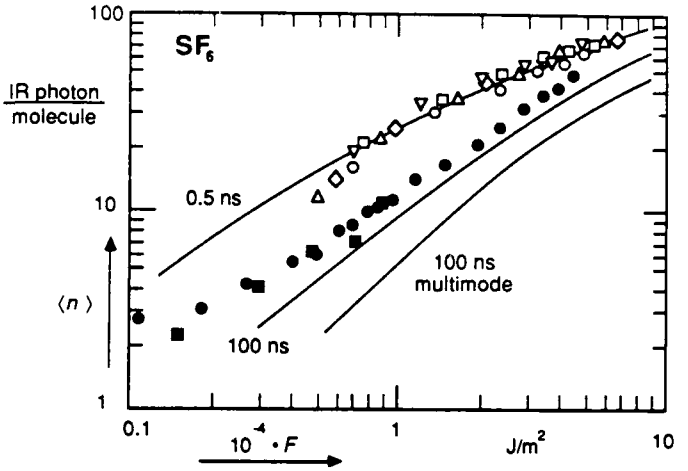

Fig. 7. Comparison with photoacoustic measurements for SF_6. The average number of infrared photons absorbed per molecule is plotted as a function of infrared fluence. The data points shown were obtained from the ones shown in Fig. 6, assuming thermal equilibrium between all vibrational modes immediately after the infrared multiphoton excitation. The solid lines show the average number of infrared photons obtained from photoacoustic measurements. The results show a remarkable agreement.

$$I_{rel} \equiv \frac{I_{AS}}{I_S^o} = \frac{E_R}{h\nu_R + E_R^o}, \qquad (3)$$

with E_R^o the room temperature equilibrium value of E_R.

Unfortunately the lack of more than one accessible Raman active mode for SF_6 makes it impossible to compare the energy in different modes. This limits us therefore to a comparison of E_R with the average total energy absorbed per molecule, $\langle E \rangle$, known from photoacoustic measurements. One may also write

$$\langle E \rangle = \langle n \rangle h\nu_R, \qquad (4)$$

with $\langle n \rangle$ the average number of infrared photons absorbed per molecule. If the intramolecular distribution of energy has reached equilibrium, $\langle E \rangle$ may be obtained from E_R and compared to the value of $\langle n \rangle$ determined in photoacoustic measurements. This is done in Fig. 7, which shows $\langle n \rangle$ as a function of fluence. The data points correspond to the data points in Fig. 6 (assuming intramolecular equilibrium), and the curves show the results obtained from photoacoustic measurement. The data agree remarkably well, suggesting that for SF_6 the intramolecular energy distribution indeed equilibrates. The absence of a decay of the Raman signals in Fig. 4 further supports this suggestion. Even though the initially nonequilibrium *intermolecular* distribution of energy equilibrates,[13] E_R remains constant once intramolecular equilibrium is achieved. In the absence of intramolecular equilibrium, one would expect E_R, and consequently the signal intensities, to change on a much shorter time scale because of a rearrangement of energy over the various vibrational modes.

2. *CF_2HCl*: This molecule has five accessible Raman active modes of widely different energy (600—3000 cm^{-1}). The peak absorption of this molecule coincides with the 9.4 μm R(32) CO_2 laser line at 1086 cm^{-1}. Even at the maximum fluence at this line (2×10^4 J/m^2), none of the five Raman lines show any detectable change in intensity. Photoacoustic studies[23] of the infrared multiphoton excitation of this molecule have shown that at such a fluence the molecules absorb about ten infrared photons. The absence of anti-Stokes scattering from low lying levels, such as the Raman active mode at 587 cm^{-1}, suggests that not all modes participate in the excitation process. This leads to the conclusion that the energy distribution for this molecule does not equilibrate without collisions.

3. *1,1-$C_2H_4F_2$*: This asymmetric isomer has four accessible Raman modes. Data were obtained for 0.5 ns long pulses at the P(20) line of the 10.6 μm branch, which is resonant with the infrared active C—F stretch mode at 942 cm^{-1}. At fluences above 1.5×10^4 J/m^2, an intense broadband fluorescence appears. At those fluences the molecules apparently dissociate, and the probe laser induces a

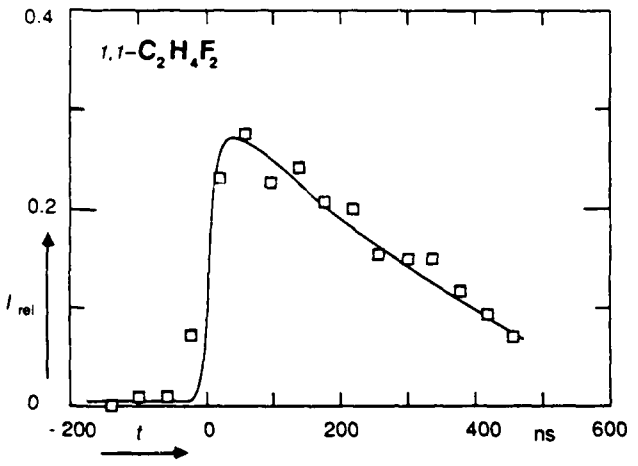

Fig. 8. Intensity of anti-Stokes signal for the 870 cm^{-1} mode of *1,1*-$C_2H_4F_2$ as a function of the time delay between pump and probe pulses at a pressure of 660 Pa. The data show a behavior distinctly different from the one for SF_6. These results were obtained for 0.5 ns infrared excitation at the 10.6 μm P(20) line, with an average fluence of 1.5×10^4 J/m^2.

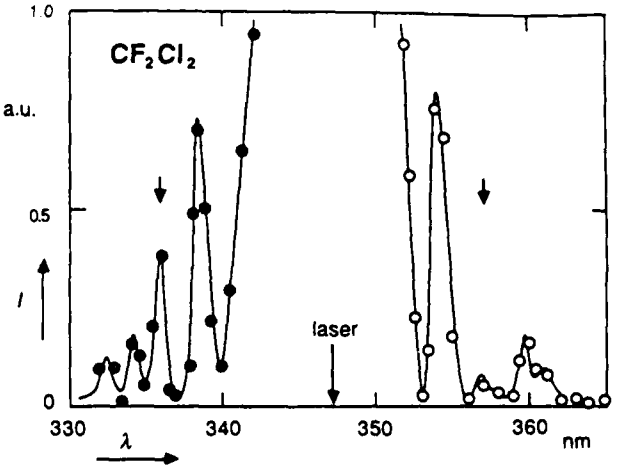

Fig. 9. Stokes spectrum of CF_2Cl_2 without infrared multiple photon excitation (open symbols) and anti-Stokes spectrum with infrared multiphoton excitation (closed symbols). Infrared excitation: 10.6 μm P(32) line, and 15 ns pulse duration. The arrows mark the positions of the laser radiation at 347.15 nm, and the pumped mode at 919 cm^{-1}. The ratio of anti-Stokes to (corresponding) Stokes peak intensities clearly show that the pump mode is the 'hottest' mode after the infrared multiphoton excitation.

fluorescence from the dissociation fragments. This laser induced fluorescence extends far (at least 3000 cm^{-1}) into the anti-Stokes side of the spectrum, which indicates that the dissociation fragments carry a considerable amount of excitation energy. One can discriminate the fluorescence from Raman scattering either spectrally or temporally. The fluorescence has a broad continuous spectrum and a long decay (μs), while the spectrally discrete Raman signals (see Figs. 4 and 9) coincide with the 20 ns probe pulse. Since the present measurements are carried out at fixed wavelengths, only temporal discrimination can be applied. A fast electronic circuit therefore monitors the coincidence of the signals with the probe pulse, and flags the data point if any signal appears after the probe.[24] The analysis is then limited to either fluorescence or Raman signals. We restrict ourselves here to a discussion of the Raman signals. Up to the dissociation threshold, only one of the Raman active lines, at 870 cm^{-1}, shows a small but measurable amount of anti-Stokes signal after excitation.

Fig. 8 shows the time-dependence of the anti-Stokes signal for the mode at 870 cm^{-1} at a pressure of 660 Pa and a fluence of 1.5×10^4 J/m^2. Again a short collisionless increase in signal occurs. In contrast to SF_6, however, the anti-Stokes signal shows a decay on a time scale of the same order of magnitude as collisional vibrational relaxation. This, combined with the fact that no other Raman active mode exhibits any change up to the dissociation of the molecule, indicates that for this particular molecule too, the vibrational energy does not reach equilibrium.

The pumped C—F stretch of *1,1*-$C_2H_4F_2$ is a highly asymmetric vibrational mode. It is consequently not surprising that almost no coupling to the (symmetric) Raman active modes takes place. Measurements on the other isomer, *1,2*-$C_2H_4F_2$, with a much more symmetric C—F stretch, might therefore lead to a better insight of the role of symmetry in the coupling of vibrational modes.

4. *CF_2Cl_2*: This five atom molecule has four accessible Raman active modes, three of which, at a shift of 664, 919, and 1082 cm^{-1} respectively, were measured after infrared multiphoton excitation. The C—Cl stretch mode at 919 cm^{-1} is both infrared and Raman active and can be pumped with the P(32) line of the 10.6 μm branch of the CO_2 laser. This allows to directly observe the energy in the pump mode and compare it with the energy in other modes. The measurements presented here were all carried out at a gas pressure of 400 Pa. For this molecule too, broadband laser induced fluorescence appears at fluences above 1.8×10^4 J/m^2.[25]

Fig. 9 shows the Raman spectrum of CF_2Cl_2 with and without infrared multiphoton excitation. At 400 Pa and room temperature, the equilibrium anti-Stokes signal cannot be detected because of the small population of excited levels. The anti-Stokes part of the spectrum therefore shows the increase in energy in the four vibrational modes. The pump mode, indicated in the graph with small arrows, clearly contains the largest amount of energy (see the anti-Stokes—Stokes intensity ratio). Surprisingly enough, the mode at 664 cm^{-1} remains relatively 'cold'. Changes in

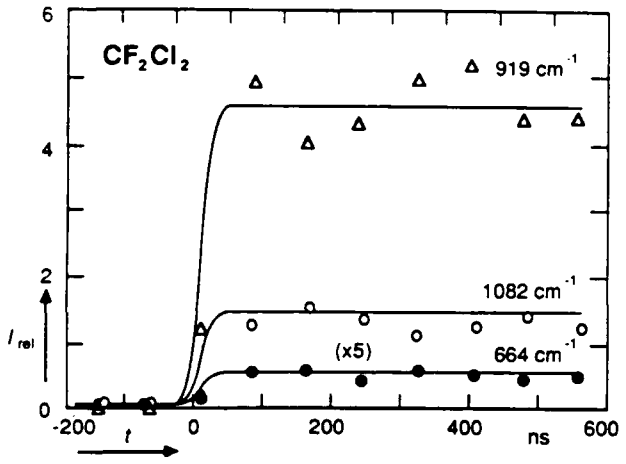

Fig. 10. Intensity of normalized anti-Stokes signals for three modes of CF_2Cl_2 as a function of the time delay between pump and probe pulses at a pressure of 400 Pa. The data points for the mode at 664 cm^{-1} are multiplied by 5. These results were obtained for 15 ns infrared excitation at the 10.6 μm P(32) line, with an average fluence of 1×10^4 J/m^2.

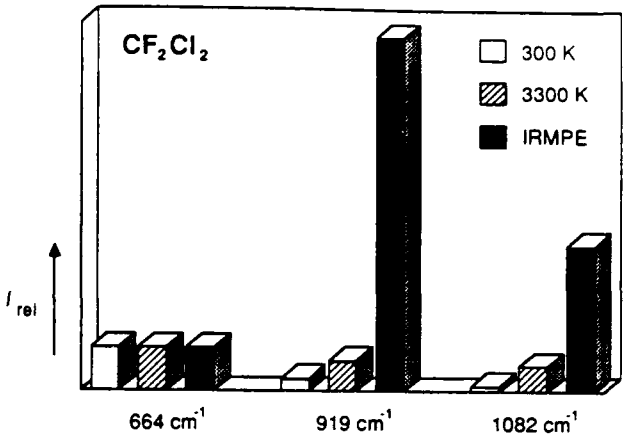

Fig. 11. Comparison of the anti-Stokes to Stokes intensity ratios for 3 modes of CF_2Cl_2. The grey bars are calculated from the equilibrium intensities at 300 K and 3300 K. The black bars show ratios obtained after infrared multiple photon excitation. For clarity the intensities for 300 K and 3300 K have been multiplied by 6.2 and 0.1, respectively.

energy of modes with a larger energy step than the energy of the infrared photons (1082 and 1147 *vs.* 933 cm^{-1}) also occur.

In Fig. 10 the anti-Stokes signals of three modes, normalized with the corresponding room temperature Stokes signal, are plotted as a function of time. Again the signals rise in 20 ns and remain constant up to 600 ns. We can now assess the distribution of energy over these three modes. From the ratio of anti-Stokes to room temperature Stokes signal in Figs. 9 and 10 one can immediately deduce that the distribution has not reached equilibrium. Fig. 11 compares these ratios for the three modes in equilibrium at both 300 K and 3300 K with the ratio obtained in the present experiment. A temperature of 3300 K equals an increase in internal vibrational energy corresponding to 19 infrared laser photons. The graph clearly shows that the intramolecular distribution of energy of CF_2Cl_2 is not in equilibrium, and that the pump mode is much more highly excited than the other Raman active modes.

Conclusion

This paper presents the results of measurements of various collisionless infrared multiphoton excited molecules. The amount of energy in various modes of these molecules is determined from the spontaneous Raman scattering of each of these modes. After infrared multiphoton excitation a collisionless change in energy distribution takes place within the 20 ns time resolution. Whereas the distribution of vibrational energy over the different modes is in equilibrium for the symmetric SF_6, the other (not symmetric) molecules show a distinct nonequilibrium distribution.

Acknowledgments

The research for this paper is supported by the Army Research Office and the Joint Services Electronics Program under contracts with Harvard University.[26]

[1] N.R. Isenor, V. Merchant, R.S. Hallsworth and M.C. Richardson, Can. J. Phys. 51, 1281 (1973).

[2] See e.g. the following publications and references therein: V.N. Bagratashvili, V.S. Letokhov, A.A. Makarov, E.A. Ryabov, Multiple Photon Infrared Laser Photophysics and Photochemistry (Harwood Academic Publishers, New York, 1985); N. Bloembergen and E. Yablonovitch, Physics Today 5, 23 (1978) W. Fuss and K. L. Kompa, Prog. Quant. Electr. 7, 117 (1981); D.S. King, Dynamics of the Excited State, Ed. K. P. Lawley (Wiley, New York, 1982).

[3] G. Herzberg, Molecular spectra and molecular structure, Vol. 2 (Van Nostrand Reinhold, New York, 1979).

[4] See almost any issue of J. Chem. Phys.
[5] N. Bloembergen and E. Yablonovitch, Physics Today 5, 23 (1978).
[6] H.W. Galbraith and J.R. Ackerhalt, in Laser induced Chemical Processes, Ed. J.I. Steinfeld (Plenum, New York, 1981).
[7] D.S. Frankel and T.J. Manuccia, Chem. Phys. Lett. 54, 451 (1978).
[8] R.C. Sharp, E. Yablonovitch and N. Bloembergen, J. Chem. Phys. 74, 5357 (1981).
[9] P. Mukherjee and H.S. Kwok, J. Chem. Phys. 84, 1285 (1986).
[10] V.N. Bagratashvili, Yu.G. Vainer, V.S. Doljikov, S.F. Koliakov, A.A. Makarov, L.P. Malyavkin, E.A. Ryabov, E.G. Silkis, and V.D. Titov, Appl. Phys. 22, 101 (1980).
[11] V.N. Bagratashvili, Yu.G. Vainer, V.S. Dolzhikov, S.F. Kol'yakov, V.S. Letokhov, A.A. Makarov, L.P. Malyavkin, E.A. Ryabov, E.G. Sil'kis, and V.D. Titov, Sov. Phys. JETP 53, 512 (1981).
[12] V.N. Bagratashvili, V.S. Doljikov, V.S. Letokhov, A.A. Makarov, L.P. Maljavkin, E.A. Ryabov, E.G. Silkis, and Yu.G. Vainer, Opt. Comm. 38, 31 (1981).
[13] V.N. Bagratashvili, Yu.G. Vainer, V.S. Doljikov, V.S. Letokhov, A.A. Makarov, L.P. Malyavkin, E.A. Ryabov, and E.G. Sil'kis, Opt. Lett. 6, 148 (1981).
[14] Yu.S. Doljikov, V.S. Letokhov, A.A. Makarov, A.L. Malinovsky and E.A. Ryabov, Chem. Phys. Lett. 124, 304 (1986).
[15] V.S. Doljikov, Yu.S. Doljikov, V.S. Letokhov, A.A. Makarov, A.L. Malinovsky and E.A. Ryabov, Chem. Phys. 102, 155 (1986).
[16] E. Mazur, I. Burak, and N. Bloembergen, Chem. Phys. Lett. 105, 258 (1984).
[17] Jyhpyng Wang, Kuei-Hsien Chen and Eric Mazur, Phys. Rev. A **34**, 3892 (1986).
[18] R.V. Ambartsumyan, S.A. Akhmanov, A.M. Brodnikovskii, S.M. Gladkov, A.V. Evseev, V.N. Zadkov, M.G. Karimov, N.I. Koroteev, and A.A. Puretskii, JETP Lett. **35**, 210 (1982).
[19] S.S. Alimpiev, S.I. Valyanskii, S.M. Nikiforov, V.V. Smirnov, B.G. Sartakov, V.I. Fabelinskii, and A.L. Shtarkov, JETP Letters, **35**, 360 (1982).
[20] Eric Mazur, Rev. Sci. Instrum. **57**, 2507 (1986).
[21] R.D. Bates Jr., J.T. Knudtson, G.W. Flynn and A.M. Ronn, Chem. Phys. Lett. 8, 103 (1971)
[22] J.G. Black, P. Kolodner, M.J. Schultz, E. Yablonovitch, and N. Bloembergen, Phys. Rev. A **19**, 704 (1979).
[23] T.B. Simpson, J.G. Black, I. Burak, E. Yablonovitch and N. Bloembergen, J. Chem. Phys. 83, 628 (1985)
[24] Jyhpyng Wang and Eric Mazur, Rev. Sci. Instrum. to be published.
[25] Kuei-Hsien Chen, Jyhpyng Wang and Eric Mazur, to be published.
[26] Contract numbers: DAAG29-85-K-0600 and N00014-84-K-0465 , respectively.

Raman spectroscopy of infrared multiphoton excited molecules

Jyhpyng Wang, Kuei-Hsien Chen and Eric Mazur
Division of Applied Sciences and Department of Physics
Harvard University, Cambridge, MA 02138, USA

This paper presents an overview of data obtained on the intramolecular vibrational energy distribution in infrared multiphoton excited CF_2HCl, CF_2Cl_2, SF_6 and CH_3CHF_2. All but CF_2HCl show collisionless changes in the intensity of the spontaneous Raman signals after excitation, indicating that the excitation alters the population in the Raman active modes. A comparison of the spectrally integrated intensities of the Raman signals yields information on the distribution of vibrational energy over the modes of the molecule. The results for CF_2Cl_2 show a nonthermal distribution of energy after the excitation.

1. Introduction

Most polyatomic molecules with a strong vibrational absorption band can absorb many (10 to 40) infrared photons when irradiated with an intense resonant infrared laser pulse. At high excitation many dissociate without interacting with other molecules. The early work in this field was motivated by the hope of driving chemical reactions in either a bond-specific or isotopically selective fashion.[1] This could be achieved if some of the initial energy deposition were 'localized' in a small subset of modes. In the past decade much work[2-7] has been directed toward gaining a better understanding of the infrared multiphoton excitation and dissociation of polyatomic molecules and the intramolecular dynamics of highly vibrationally excited molecules in general.

Many experimental techniques have been applied to study infrared multiphoton excitation. Photoacoustic measurements were applied to deter-

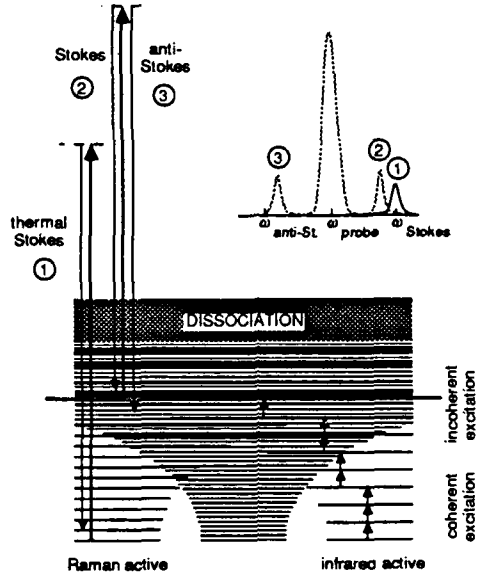

Fig. 1. Spontaneous Raman spectroscopy of infrared multiphoton excited molecules. Molecules that remain in the lower vibrational states (cold molecules) show only Stokes scattering (1), while the highly excited ones (hot molecules) show both a shifted Stokes (2) and an anti-Stokes signal (3).

mine the energy absorbed by the molecules,[8] and to study the excitation as a function of various parameters, such as pumping fluence, intensity, and wavelength, pressure, etc. Photoacoustic spectroscopy was also used at high intensities to study dissociation yields as a function of absorbed energy. More detailed information on infrared multiphoton dissociation, such as the species of the dissociation fragments, branching ratios of different dissociation channels, and the translational energy distribution of the fragments, was obtained by mass and time-of-flight spectrometry.[9] Pump-and-probe experiments have also provided more detailed knowledge of the infrared multiphoton excitation and dissociation. For example, laser induced fluorescence[10,11] was used to measure the vibrational energy distribution of the infrared multiphoton dissociation fragments. Infrared double-resonance experiments[12–14] were done to determine the rotational relaxation rate and the population depletion of the vibrational ground state. Spontaneous and coherent anti-Stokes Raman scattering were used to probe the distribution of vibrational energy over the different modes of infrared multiphoton excited molecules.[15–21]

In this paper we report on results obtained by time-resolved spontaneous Raman spectroscopy. The principle of the experiments, which were pioneered in the Soviet Union,[15–20] is illustrated in Fig. 1. First, the molecules are pumped into the high vibrational excitation region by a short, intense CO_2 laser pulse resonant with a vibrational mode. Then the Raman signals from the different Raman active modes accessible to the apparatus are measured with a second, ultraviolet laser pulse. While unexcited molecules show only a Stokes signal (Fig. 1, 1), highly excited ones show both a shifted Stokes signal (Fig. 1, 2) as well as an anti-Stokes (Fig. 1, 3) signal. Since the total, spectrally integrated signal from a Raman active mode is a measure of the amount of energy in the mode (see discussion), the intramolecular vibrational energy distribution after the excitation can be determined by comparing the Raman signals from different modes. Time-resolved information is obtained by varying the time delay between pump and probe.

2. Experimental

The experimental procedure is described in detail in previous publications.[22,23] Briefly, molecules contained within a low pressure gas cell are excited by an infrared laser pulse and probed by an ultraviolet laser pulse. To isolate intramolecular from (collisional) intermolecular effects, the signals are measured at pressures low enough to ensure that no significant collisional relaxation of vibrational energy occurs on the time scale of the experiment.

A schematic view of the setup is shown in Fig. 2. The infrared radiation is generated by a high power short-pulse tunable CO_2 laser with 0.5 to 15 ns pulse duration and a maximum energy of 200 mJ. A 20 ns frequency-doubled ruby laser pulse of 3 mJ serves as Raman probe. The infrared exciting beam and an ultraviolet probing beam are focused inside the scattering cell[23] where they cross at right angles. The spontaneous Raman signals from the interaction region are detected perpendicular to the incident beams with a double monochromator and a high gain fast photomultiplier tube. The spectral resolution is 1.5 nm, which is high enough to resolve the different Raman active modes, and low enough to integrate the signals over the states within one mode. A complete description of the experimental setup can be found in previous papers.[22,23]

Time resolution is obtained by varying the time delay between pump and probe. The synchronization of lasers, which is controlled electronically, is

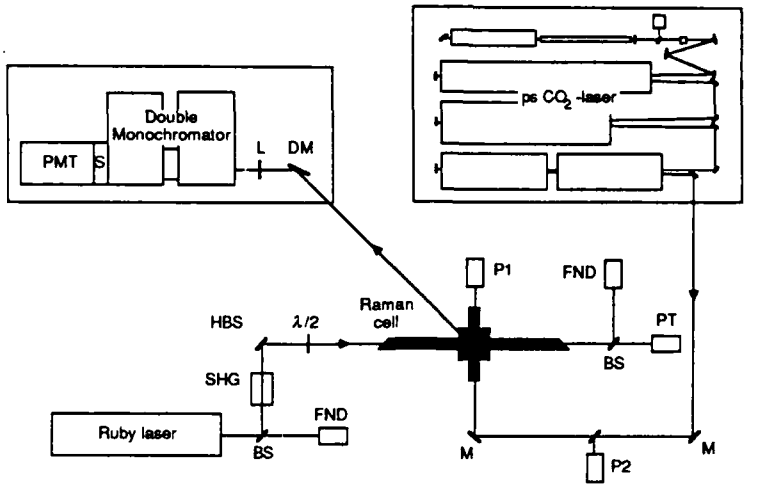

Fig. 2. Experimental setup. BS = beam splitter, SHG = second harmonic generator, HBS = harmonic beam splitter, $\lambda/2$ = half-wave plate, FND = fast photodiode, PT = phototube, P1, P2 = pyroelectric detector, M = mirror, DM = dichroic mirror, L = quartz lens, S = shutter, PMT = photomultiplier tube.

limited by the 100 ns trigger jitter of the lasers. To obtain time-resolved data on a shorter time scale, the actual time delay between infrared and ultraviolet pulses is measured for each pair of laser pulses with two fast detectors and a time-to-pulse-height converter. The time resolution of the setup is thus determined by the duration of the laser pulses.

At high pumping intensity a fraction of the molecules dissociates, and the probe laser can induce a fluorescence from the dissociation fragments. This laser induced fluorescence is much more intense than the spontaneous Raman scattering. One can discriminate between fluorescence and Raman scattering either spectrally or temporally. The fluorescence generally has a broad continuous spectrum and a long decay, while the spectrally discrete Raman signals coincide with the 20 ns probe pulse. Since the present measurements are carried out with the monochromator at fixed wavelengths, only temporal discrimination can be applied. The coincidence of the Raman signals with the probe pulse is therefore monitored throughout the experiment to ensure that no fluorescence contributes to the observed signals. In addition, the infrared and ultraviolet laser energy, the time delay between pump and probe, and the signal intensity are recorded for each laser pulse.

Owing to the small Raman cross sections and the low sample pressure required to satisfy collisionless conditions, the signals are in the single photon regime. Consequently, a large amount of data has to be collected and averaged to obtain a satisfactory signal-to-noise ratio. A microcomputer collects the data, sorts out the data points according to infrared pump intensity and time delay between pump and probe and averages the data.

3. Results

Experiments were done at room temperature on SF_6, CF_2HCl, CF_2Cl_2 and CH_3CHF_2 at pressures ranging from 33 Pa to 400 Pa. All gases were obtained commercially and have a reported purity better than 99.99%. Relevant spectroscopic data are given in Table I.

CF_2Cl_2. The infrared active ν_8-mode of CF_2Cl_2, which has been assigned to the CCl_2 asymmetric stretch, was pumped with 15 ns full-width at half-maximum pulses from the P(32) line of the 10.6 μm CO_2 laser branch. The 15 ns truncated pulses have a 10-90% rise time of 10 ns and a short sub-nanosecond fall time. Raman signals were obtained for the 1098 cm^{-1} CF_2 symmetric stretch ν_1-mode (A_1), the 923 cm^{-1} CCl_2 asymmetric stretch ν_8-mode (B_1), and the 667 cm^{-1} CCl_2 symmetric stretch ν_2-mode (A_1). The signals from all these modes change after infrared multiphoton excitation, allowing one to compare the intensity ratio with the thermal one. Another interesting feature of this molecule is that the ν_8 pump mode is both infrared and Raman active, allowing a direct view of the excitation in the pump mode.

SF_6. Results on this molecule, which are presented here for comparison, were published previously.[22] The data were obtained at CO_2 laser frequencies between the P(12) and P(28) lines of the 10.6 μm CO_2 laser branch, which are resonant with the triply degenerate infrared active ν_3-mode (F_{1u}) of SF_6. Two different pulse durations were employed: short 0.5 ns and truncated 15 ns pulses with fluences up to 7×10^4 J/m^2. The Raman signals were obtained at a shift of 775 cm^{-1} from the frequency-doubled ruby laser, corresponding to the totally symmetric breathing mode ν_1-mode (A_{1g}) of SF_6.

CF_2HCl. The peak absorption of this molecule coincides with the 9.4 μm R(32) CO_2 laser line at 1086 cm^{-1}. Although five Raman active modes of CF_2HCl are accessible to our apparatus, none of them shows any change

Molecule	CO_2 line	Wavenumber	Mode	Activity	Remarks
SF_6[25]			$\nu_1 = 775$	R (s)	changes
			$\nu_2 = 644$	R (w)	not probed
	10.6 μm P(20)	944	$\nu_3 = 965$	IR	pumped
			$\nu_4 = 617$	IR	
			$\nu_5 = 524$	R (w)	not probed
			$\nu_6 = 363$	inactive	
CF_2Cl_2[26,27]			$\nu_1 = 1101$	IR(s)	
			$\nu_1 = 1098$	R (m)	changes
			$\nu_2 = 667$	IR (s)	
			$\nu_2 = 667.2$	R (s)	changes
			$\nu_3 = 457.5$	R (s)	not probed
			$\nu_4 = 261.5$	R (s)	not probed
			$\nu_5 = 322$	R (w)	not probed
			$\nu_6 = 1159$	IR (s)	
			$\nu_6 = 1167$	R (w)	not probed
			$\nu_7 = 446$	IR (w)	not probed
	10.6 μm P(32)	933	$\nu_8 = 922$	IR (vs)	pumped
			$\nu_8 = 923$	R (w)	changes
			$\nu_9 = 437$	IR (w)	
			$\nu_9 = 433$	R (m)	not probed
CH_3CHF_2			870	R	changes
	10.6 μm P(20)	944		IR	pumped
			1140	R	no change
			1460	R	no change
			2980	R	no change
CF_2HCl			590	R	no change
			800	R	no change
	9.4 μm R(32)	1086		IR	pumped
			1130	R	no change
			1330	R	no change
			3030	R	no change

Table I. Spectroscopic data for the molecules studied in this paper. The vibrational data for SF_6 and CF_2Cl_2 are from literature. All data are in cm^{-1}, vs = very strong, s = strong, m = medium, and w = weak.

after infrared multiphoton excitation with 0.5 ns pulses, even at fluences up to 2×10^4 J/m^2, when the average number of photons absorbed per molecule is reported to be about ten.[24]

CH_3CHF_2. The largest of the molecules studied, CH_3CHF_2, has four accessible Raman active modes. Only one of these modes, at 870 cm^{-1}, shows a small anti-Stokes signal after infrared multiphoton excitation. The molecules were pumped with 0.5 ns pulses at the P(20) line of the 10.6 μm branch.

Some of the experimental results are shown in Figs. 3 through 13 and listed in Tables I, II and III. The results are arranged so as to emphasize the similarities and the differences in behavior between the molecules. The points shown in each of the figures are obtained by dividing the x-axis into a number of intervals (usually 10 to 20), and averaging the data that lie within each of the intervals. Since the signal fluctuations in the single photon regime are large and since the error bars are inversely proportional to the square root of the number of points, the average is taken over a large number of data points. The low repetition rate of 0.3 Hz and the stability of the alignment, however, limit the total number of pulses for a single experimental run to 10^4. This means that there is a trade-off between the number of points in each figure and the length of the error bars. In all measurements presented here the error bars are about 10% of the absolute value of the data points for SF_6 and, because of the smaller Raman cross-sections, 20% for CF_2Cl_2 and CH_3CHF_2.

The Raman spectra of infrared multiphoton excited SF_6 and CF_2Cl_2 at a pressure of 400 Pa are shown in Figs. 3 and 4. The large central peak in the spectrum corresponds to Rayleigh scattering at the probe laser wavelength. The single Raman peak at each side of the Rayleigh peak in Fig. 3 corresponds to the ν_1-mode of SF_6. At room temperature without infrared excitation only Stokes signals are observable (open circles). If the molecules are excited before the Raman probing (closed circles) anti-Stokes signals appear in the spectrum. Of the nine vibrational modes of CF_2Cl_2, three, at 667 cm^{-1}, 923 cm^{-1} and 1098 cm^{-1} respectively, are visible in the (low pressure, low resolution) spectrum in Fig. 4. Since the ν_3 mode at 923 cm^{-1} is both Raman and infrared active, CF_2Cl_2 allows direct monitoring of the pumped mode. Within the spectral resolution, the Raman shifts of the anti-Stokes signals that appear after excitation correspond to the ones reported in the literature. Note that for each of the detectable Raman peaks a corresponding anti-Stokes peak appears after excitation, both at an energy smaller than the excitation energy (667 cm^{-1}) and also at higher en-

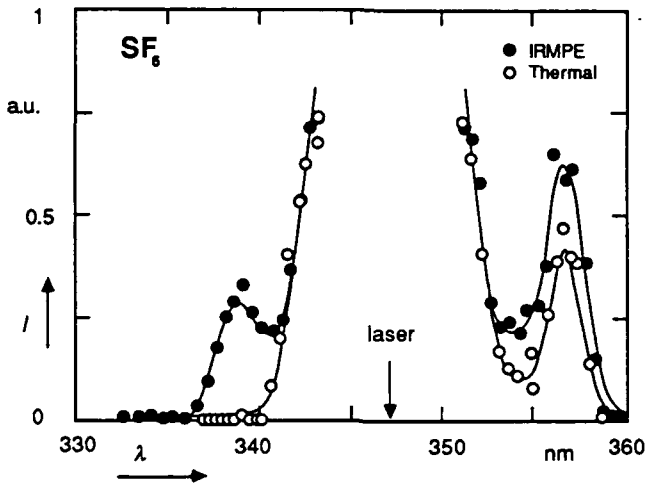

Fig. 3. Raman spectrum of SF_6, with (closed circles) and without (open circles) infrared multiphoton excitation. Infrared excitation: 10.6 μm P(20) line, 0.5 ns pulse duration, and average fluence 0.6×10^4 J/m^2. The small arrow marks the position of the probe laser radiation at 347.15 nm.

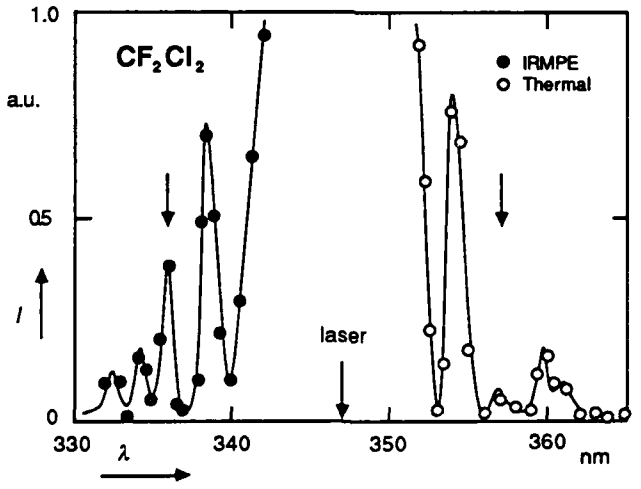

Fig. 4. Raman spectrum of CF_2Cl_2, with (closed circles) and without (open circles) infrared multiphoton excitation. Infrared excitation with 15 ns pulses at the 10.6 μm P(32) line. The arrows mark the position of the probe laser and the infrared pump mode.

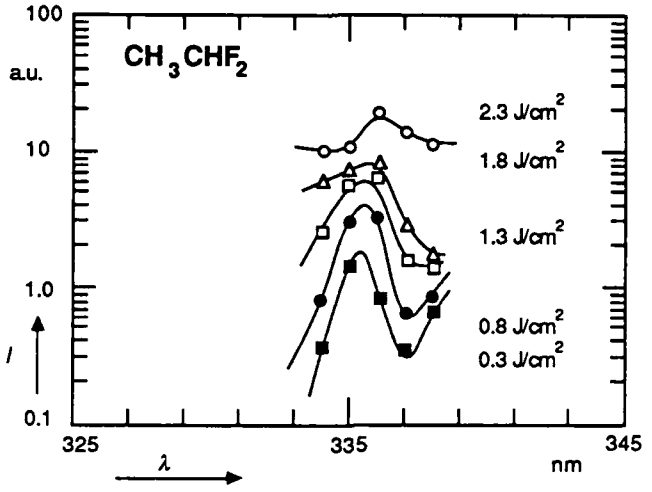

Fig. 5. Anti-Stokes signal of the 870 cm^{-1} mode of infrared multiphoton excited CH_3CHF_2 at various fluences. Infrared excitation: 10.6 μm P(20) line, 0.5 ns pulse duration. At high fluence laser induced fluorescence from the dissociation fragments replaces the Raman signal.

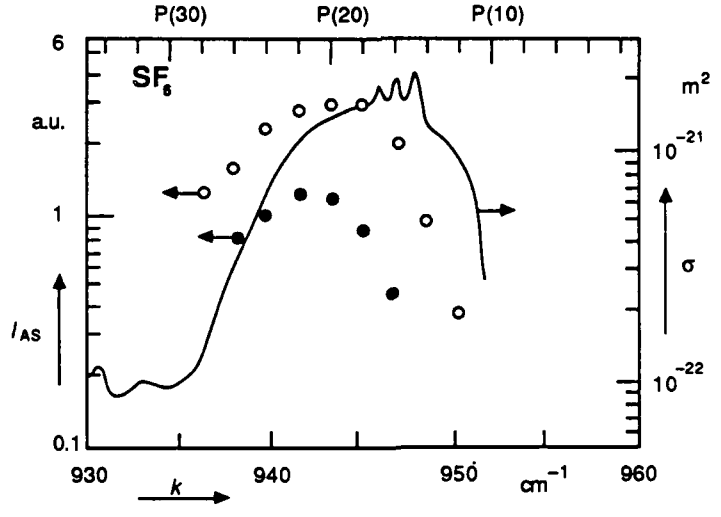

Fig. 6. Anti-Stokes signal of SF_6 for excitations at different CO_2-lines. Data for two different pulse durations at an average fluence of 10^4 J/m^2 are shown: 0.5 ns (open circles) and 15 ns (closed circles). The curve shows the one photon absorption cross section.

ergy (1098 cm^{-1}). At fluences above 3×10^4 J/m^2 a broadband laser induced fluorescence gradually replaces the Raman spectrum. This fluorescence is induced by the probe laser in the fragments of infrared multiphoton dissociated molecules.

Figure 5 shows the anti-Stokes signal of the 870 cm^{-1} mode of CH_3CHF_2 for different fluences. As the fluence is increased, the anti-Stokes peak is gradually replaced by a broadband laser induced fluorescence just as for CF_2Cl_2.

Figure 6 shows the anti-Stokes signal of SF_6 for excitation at different CO_2-lines. Each point shown represents a separate experimental run in which the anti-Stokes signal of infrared multiphoton excited SF_6 was measured for a particular CO_2-line. This graph shows the intensity of the anti-Stokes signal at a fluence of 10^4 J/m^2 for each of the CO_2-lines. As a reference the low signal absorption cross-section for SF_6 is also plotted. Apart from a red shift of about 3 cm^{-1} from the center of the one photon absorption band, the absorption spectrum is not much different from the one at low excitation.

Figure 7 shows the time dependence of the Raman signal intensities for SF_6 at 400 Pa for two infrared pulse durations, 0.5 ns and 15 ns. The vertical axis shows the *relative* intensity, I_{rel}, obtained by normalizing the anti-Stokes signal after excitation with the room temperature equilibrium Stokes signal. The horizontal axis shows the time delay between pump and probe pulses. For negative time delay the molecules are probed before the infrared multiphoton excitation (*i.e.* at room temperature equilibrium) and only a Stokes signal, which serves as calibration for the intensity scale, is detectable. The rise time of the signals reflects the 30 ns instrumental time resolution, which in turn is determined by the temporal width of the laser pulses. Within the 30 ns time resolution a *collisionless* (see discussion) increase of both Stokes and anti-Stokes signals is observed. The signal remains constant up to 800 ns after the infrared excitation. The signals revert to their original values only after a much longer time (10 μs) because of a combination of collisional relaxation and diffusion of the excited molecules out of the excitation region.[22]

A different behavior is observed for the other two molecules that exhibit changes in Raman spectrum. Figure 8 shows the time dependence of the three accessible Raman active modes of CF_2Cl_2 for infrared excitation with 15 ns pulses. Each of the anti-Stokes signals is normalized with its corresponding Stokes signal at room temperature. Just as for SF_6, anti-Stokes signals appear for all three modes after excitation at $t = 0$, but the signals decay much more rapidly, and although the time dependences are similar for the various modes, the maximum relative intensities differ. As can be seen

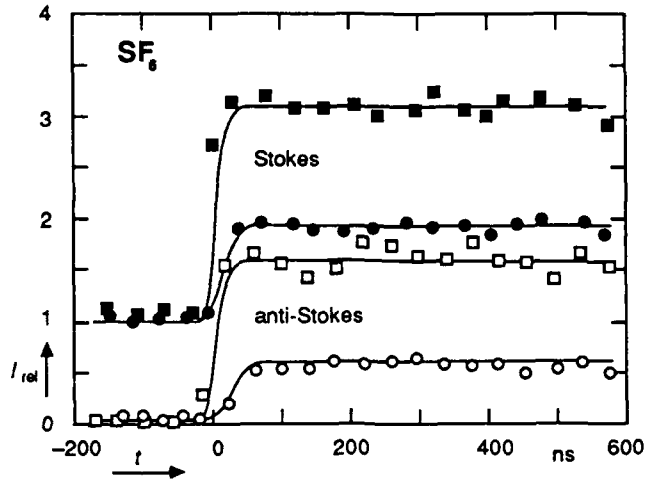

Fig. 7. Intensity of Stokes (closed symbols) and anti-Stokes (open symbols) signal as a function of the time delay between pump and probe pulses at a pressure of 67 Pa for SF_6. Infrared excitation with 0.5 ns (squares) and 15 ns (circles) pulses at the 10.6 μm P(20) line. Average fluence: 0.8×10^4 J/m^2.

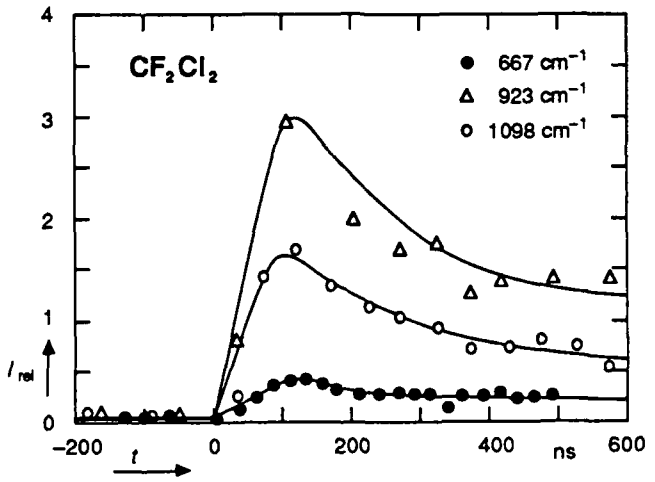

Fig. 8. Intensity of the anti-Stokes signals as a function of the time delay between pump and probe pulse for CF_2Cl_2 at 400 Pa. Infrared excitation: 10.6 μm P(32) line, 15 ns pulse with average fluence 1.8×10^4 J/m^2.

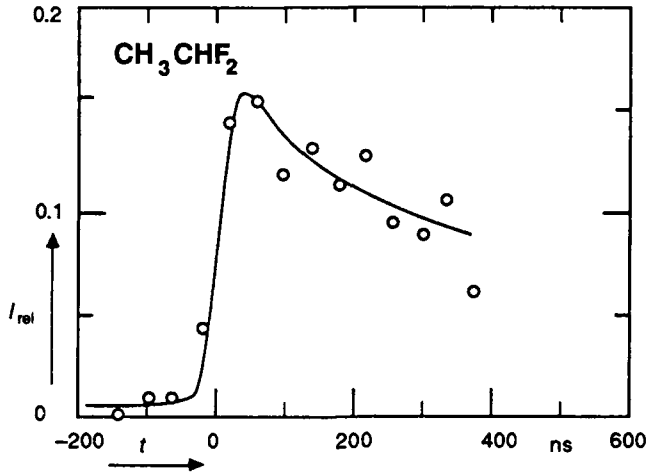

Fig. 9. Intensity of the anti-Stokes signals as a function of the time delay between pump and probe pulse for CH_3CHF_2 at 660 Pa. Infrared excitation: 10.6 μm P(20) line, 0.5 ns pulse with average fluence 1.5×10^4 J/m^2.

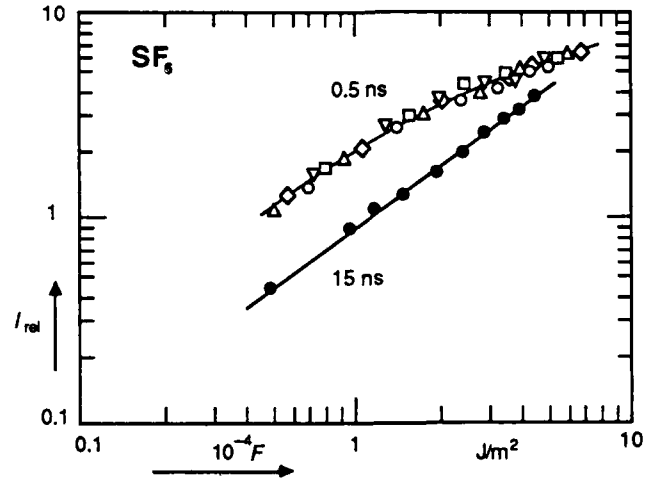

Fig. 10. Relative anti-Stokes signal of SF_6 as a function of the infrared pumping fluence for various pressures. Excitation at the 10.6 μm P(20) line with two pulse durations: 0.5 ns (open symbols) and 15 ns (closed symbols).
□ : 33 Pa; ○: 67 Pa; △: 133 Pa; ▽: 200 Pa; ◇: 267 Pa; ● : 133 Pa

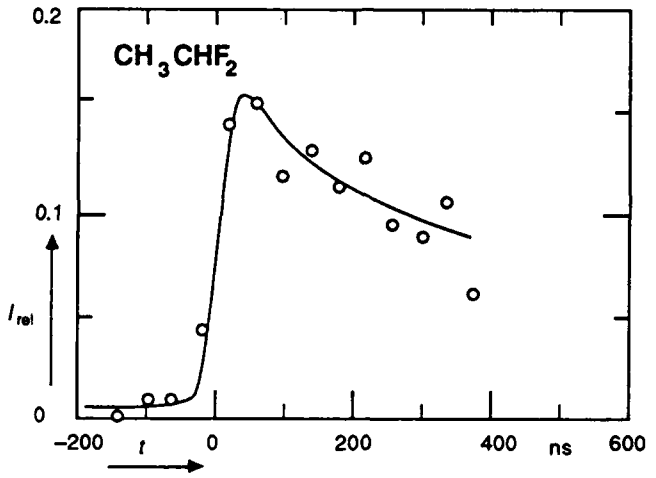

Fig. 9. Intensity of the anti-Stokes signals as a function of the time delay between pump and probe pulse for CH_3CHF_2 at 660 Pa. Infrared excitation: 10.6 μm P(20) line, 0.5 ns pulse with average fluence 1.5×10^4 J/m^2.

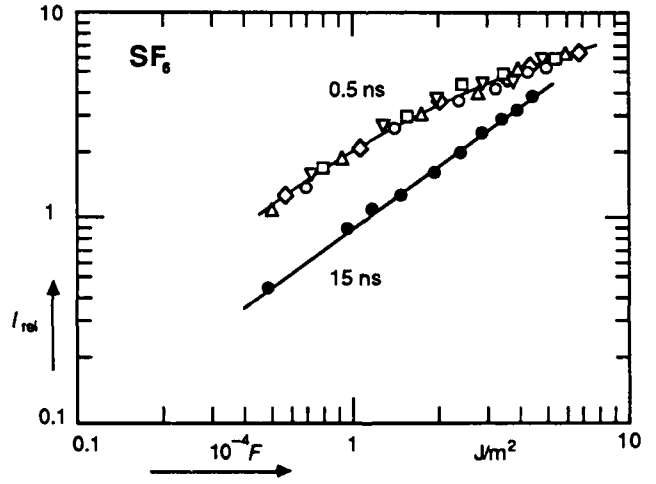

Fig. 10. Relative anti-Stokes signal of SF_6 as a function of the infrared pumping fluence for various pressures. Excitation at the 10.6 μm P(20) line with two pulse durations: 0.5 ns (open symbols) and 15 ns (closed symbols).
□ : 33 Pa; ○: 67 Pa; △: 133 Pa; ▽: 200 Pa; ◇: 267 Pa; ● : 133 Pa

in Fig. 9, a similar behavior is observed for CH_3CHF_2. Note that for this molecule the change in I_{rel} is ten times smaller than the one for the other two molecules.

The dependence of the normalized anti-Stokes signals on the infrared pumping fluence is shown in Figs. 10 and 11. The results for SF_6, shown in Fig. 10, were obtained in different measurements, each one calibrated individually, at different pressures and puise durations. The spread in data therefore shows the absolute accuracy and the reproducibility of the experimental data. As can be seen the dependence is nearly linear, except for some saturation effects at high fluence for the shorter (more intense) pulses. Also, the normalized anti-Stokes signals are independent of the sample gas pressure, as one would expect for collisionless effects.

Again, the results for CF_2Cl_2 and CH_3CHF_2 show a different behavior. Figure 11 shows the fluence dependence of the anti-Stokes signals for CF_2Cl_2. The data were obtained in a single measurement by changing the monochromator wavelength every two thousand laser shots (corresponds to about two hours in time) and averaging the data in the 0 to 500 ns range. In contrast to the linear fluence dependence of SF_6, all three modes have an exponential fluence dependence. The graph also shows clearly that the rate of increase is drastically different for the three modes. A similar exponential fluence dependence was observed for CH_3CHF_2.

The normalized anti-Stokes signals of CF_2Cl_2 were also studied in the presence of N_2 buffer gas. Figure 12 shows the intensity ratio of the anti-Stokes signals with and without buffer gas. Each of the anti-Stokes signals rapidly decreases with increasing buffer gas pressure, while at the same time the differences between them become smaller. No data are available for the anti-Stokes signal at 923 cm^{-1} at 26 kPa buffer gas pressure. Since the Raman cross-section of the 923 cm^{-1} Raman transition is much smaller than that of the other two modes, this peak falls below the noise level at high buffer gas pressure.

Figure 13 shows the spectrum of the laser induced fluorescence from the infrared multiphoton dissociated CF_2Cl_2 at three different fluences ranging from 4 to 6×10^4 J/m^2. The fluorescence signal was recorded in 10 nm increments from 290 nm to 340 nm. Although the intensity increases with increasing fluence, the spectral shape of the broadband emission does not change. In addition it should be noted that the fluorescence extends into the blue side of the incident laser field at 347.15 nm. The cut-off wavelength of the fluorescence is about 290 nm, which means that the dissociation fragments carry as much as 5000 cm^{-1}, or about 5 infrared photons, of internal energy.

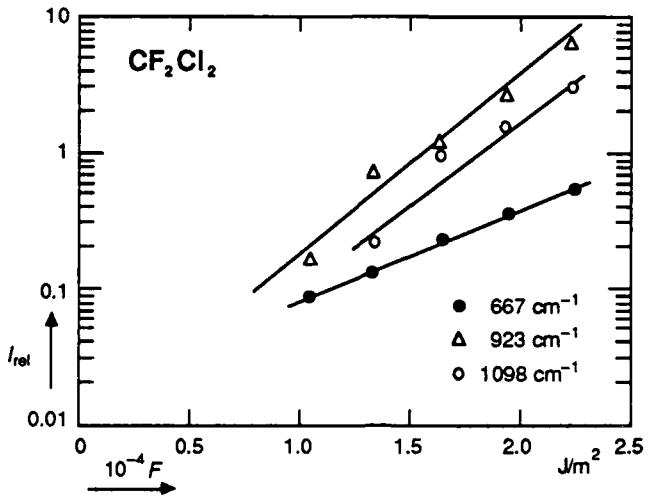

Fig. 11. Semilogarithmic plot of the fluence dependence of the anti-Stokes signals of CF_2Cl_2 at 400 Pa. The dependence is exponential for all three modes. Infrared excitation with 15 ns pulses at the 10.6 μm P(32) line.

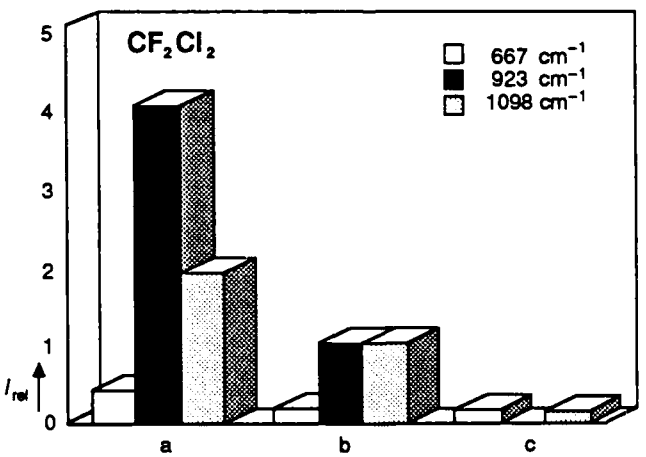

Fig. 12. Comparison of anti-Stokes intensities for CF_2Cl_2 at an average fluence of 2.1×10^4 J/m^2 and a pressure of 400 Pa, without buffer gas (*a*), and with 13 kPa (*b*), and 26 kPa (*c*) of N_2 buffer gas.

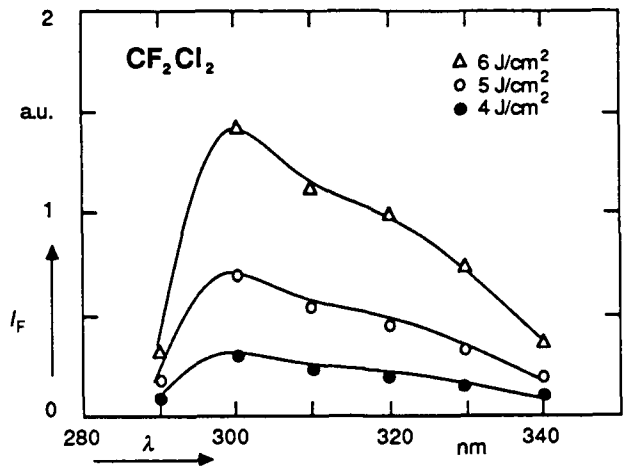

Fig. 13. Laser induced fluorescence spectrum from the dissociation fragments of CF_2Cl_2. Note that only the intensity of the fluorescence increases with increasing fluence; the spectral shape does not change.

4. Discussion

The results in the previous sections show that infrared multiphoton excitation induces significant changes in the Raman signal intensities of the molecules. In this section we will analyze these changes and interpret the results in terms of a simple picture. This will allow us to obtain information on the distribution of energy among the various modes of the multiphoton excited molecules.

In the approximation that the vibrational mode is harmonic it can readily be shown that the transition probabilities W of the Raman transitions depend on the vibrational quantum number n. For Stokes and anti-Stokes transitions, respectively, one has[22]

$$W_{n\to n+1} \sim n+1, \text{ and } W_{n\to n-1} \sim n. \tag{1}$$

The *total* intensity of the spontaneous Stokes and anti-Stokes Raman signals (summed over *all* vibrational levels of the vibrational mode considered), I_S and I_{aS} respectively, are given by

$$I_S \sim \sum_{n=0}^{\infty} P(n)\, W_{n\to n+1} \sim 1 + \sum_{n=0}^{\infty} P(n)\, n\ , \tag{2}$$

$$I_{aS} \sim \sum_{n=0}^{\infty} P(n)\, W_{n\to n-1} \sim \sum_{n=0}^{\infty} P(n)\, n\ , \tag{3}$$

with $P(n)$ the population of level n. Substituting the average energy in the mode per molecule, $E_R = h\nu_R \sum P(n)n$, with ν_R the frequency of the Raman active mode, one finds

$$I_S \sim 1 + \frac{E_R}{h\nu_R}\ , \tag{3}$$

$$I_{aS} \sim \frac{E_R}{h\nu_R}\ . \tag{4}$$

Note that the result obtained does not depend on the energy distribution $P(n)$, but only on the *average* energy E_R.

The proportionality constant between the intensities I_S and I_{aS}, and energy E_R, is related to the Raman scattering cross-section and is mode dependent. To eliminate this mode dependent quantity, the signals are normalized with the corresponding Stokes signal at room temperature, I_S^o,

$$I_{rel} \equiv \frac{I_{aS}}{I_S^o} = b^{-1} \sum_{n=0}^{\infty} n\, P(n) \ = b^{-1}\, \frac{E_R}{h\nu_R}\ , \tag{5}$$

$$\text{with} \quad b \equiv \sum_{n=0}^{\infty} (n+1)\, P_o(n), \tag{6}$$

where $P_o(n)$ is the population distribution at room temperature. If at room temperature $h\nu_R >> kT$, then the Boltzmann factor $e^{-h\nu/kT}$ is small, and $b \approx 1$. Under these circumstances the relative intensity of each mode is a direct measure of the average number of vibrational quanta, $\langle n \rangle = E_R/h\nu_R$, in that mode. The intensity ratio of the different Raman signals will therefore reflect the distribution of energy among the modes.

Questions have been raised about the influence of possible Fermi resonances on the interpretation of the Raman spectra of highly vibrationally

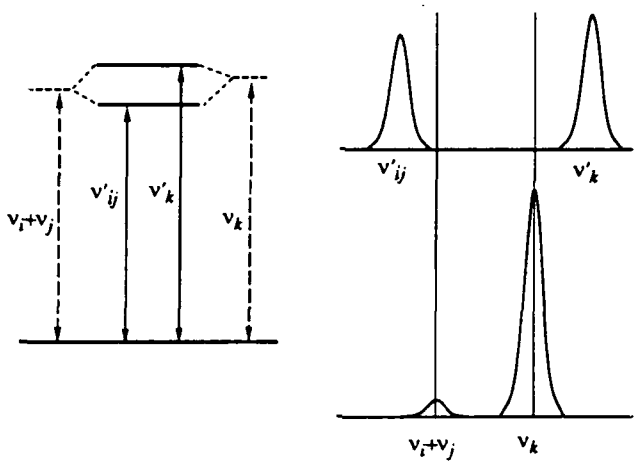

Fig. 14. The effect of a Fermi resonance on the molecular energy levels and spectrum. The interaction between the $\nu_i+\nu_j$ combination and the ν_k fundamental transitions shifts the energy levels and redistributes the spectral intensity. The bottom spectrum is the expected one without Fermi resonance, the top one shows the actual spectrum.

excited molecules.[28] The interaction of a fundamental with an overtone or with a combination mode may cause Fermi resonances when certain symmetry requirements are satisfied.[29] Basically, if the frequency of an overtone or a combination mode happens to lie close to the frequency of a fundamental mode, and if the interaction between the two is strong enough, the nature of the two processes mix and the energy levels are displaced. As a result the vibrational spectrum can be misinterpreted. One well known example is the mixing of the 1300 cm^{-1} vibrational mode and the overtone of the 667 cm^{-1} vibrational mode of CO_2, which causes *two* peaks, instead of one single peak, to appear in the Raman spectrum of CO_2 around 1300 cm^{-1}. Since this problem is related to the interpretation of the anti-Stokes signals of highly excited molecules in our experiment, the possible effect of Fermi resonances on our experimental data must be examined.

Let us consider an anti-Stokes transition in the kth vibrational mode of a certain molecule. For simplicity we assume that the initial state ψ_k corresponds to the first excited state of the kth vibrational mode, and that the final state of the Raman transition is the ground state ψ_0. We further assume that the frequency ν_k of this Raman active vibrational mode lies close to the sum of the frequencies of two other fundamental modes, $\nu_k \approx \nu_i + \nu_j$, where i, j represent the ith and jth vibrational modes respectively (see Fig. 14). In

addition we assume that the interaction matrix element between the doubly excited combination state ψ_{ij} and ψ_k

$$W_{ij,k} = \int \psi_{ij}^* \, W \, \psi_k \, d^3x \,, \tag{7}$$

with W the interaction operator, is nonzero. The actual energy levels $E' = h\nu'$, with $\nu' = \nu'_{ij}$, ν'_k, of these interacting states will then be determined by the secular equation

$$\begin{vmatrix} (\nu_i+\nu_j)-\nu' & W_{ij,k} \\ W_{ij,k} & \nu_k-\nu' \end{vmatrix} = 0. \tag{8}$$

The wavefunctions of the interacting states will be superpositions of the original wavefunctions,

$$\psi'_{ij} = a\psi_k + b\psi_{ij} \tag{9}$$

$$\psi'_k = c\psi_k + d\psi_{ij} \,, \tag{10}$$

where the transformation matrix with coefficients a, b, c and d is unitary. These two equations show the effect of Fermi resonances on the intensities of the two transitions: the peak corresponding to the inherently weak combination mode ψ_{ij} grows considerably because it 'borrows' intensity from the wavefunction of the fundamental mode ψ_k, while at the same time the intensity of the fundamental is reduced. Clearly, in high resolution spectroscopy the displacement of the line positions and the redistribution of line intensities between interacting combination and fundamental modes can be misleading.

In the present experiment, however, the situation is quite different. To accommodate the change in level spacing due to the anharmonicity of the vibrational mode, the measurements are done at low spectral resolution. Thus all Raman photons scattered from different excitation levels will be collected and integrated. If the displacements due to Fermi resonances are smaller than the resolution of the monochromator (1.5 nm) this means that one measures the *spectrally integrated* signal,

$$|\langle \psi'_{ij} | \mathcal{R}_{ij} + \mathcal{R}_k | \psi_0 \rangle|^2 + |\langle \psi'_k | \mathcal{R}_{ij} + \mathcal{R}_k | \psi_0 \rangle|^2 =$$

$$| a^*\langle\psi_k|\mathcal{R}_k|\psi_0\rangle + b^*\langle\psi_{ij}|\mathcal{R}_{ij}|\psi_0\rangle|^2 + |c^*\langle\psi_k|\mathcal{R}_k|\psi_0\rangle + d^*\langle\psi_{ij}|\mathcal{R}_{ij}|\psi_0\rangle|^2 =$$

$$|\langle\psi_k|\mathcal{R}_k|\psi_0\rangle|^2 + |\langle\psi_{ij}|\mathcal{R}_{ij}|\psi_0\rangle|^2 \approx |\langle\psi_k|\mathcal{R}_k|\psi_0\rangle|^2, \quad (11)$$

with $\mathcal{R}_{ij}$ and $\mathcal{R}_k$ the combination mode and Raman scattering operators, respectively, and where we have used the unitary properties of the transformation matrix. Equation (11) demonstrates that the spectrally integrated signal is *identical* to the one without Fermi resonance. Therefore the measured signal is the sum of the 'real' Raman signal $|\langle\psi_k|\mathcal{R}_k|\psi_0\rangle|^2$ plus a much smaller quantity $|\langle\psi_{ij}|\mathcal{R}_{ij}|\psi_0\rangle|^2$, whether or not Fermi resonances occur.

In addition to this general observation, a closer look at the available spectroscopic data for SF_6 and CF_2Cl_2 further reveals that there are no Fermi resonances with the Raman modes studied here. The only candidate for a Fermi resonance with the 775 cm^{-1} mode of SF_6 is the overtone of the 363 cm^{-1} vibrational mode. However the 363 cm^{-1} vibrational mode is spectroscopically inactive because of its F_{2u} symmetry. For CF_2Cl_2, the only reported Fermi resonance is due to the combination mode $\nu_3+\nu_9$ (882 cm^{-1}), which is infrared, not Raman active.

Summarizing the above remarks, we may conclude that Fermi resonances cannot affect our experimental data. In what follows the observed anti-Stokes signals are therefore assumed to be correctly assigned and the intensity is used as a measure of the average number of vibrational quanta in each of the modes.

Time dependence. The signal increase in Fig. 7 is consistent with the result obtained in Eq. (3–4), *i.e.* for each pulse duration both Stokes and anti-Stokes signal increase by the same amount. Surprisingly, after the initial increase the signals remain constant, even on a time scale on which collisional vibrational energy relaxation is known to play a role.[30] Clearly, collisions do not affect the total intensity of the anti-Stokes signal. Since the intensity of the signal is determined by the *average* energy in the mode only, *intermolecular* vibrational energy relaxation will not affect the Raman signals once *intramolecular* equilibrium is reached. This suggests that intramolecular equilibrium is reached on a time scale shorter than the time resolution.

The time dependence of the Raman signals for CF_2Cl_2 shown in Fig. 8 is quite different. The signals do not remain constant as for SF_6, especially for the two highly excited modes (923 cm^{-1} and 1098 cm^{-1}). This decay is most likely due to collisional transfer of energy to other, initially 'cold',

vibrational modes. Because of the limited sensitivity and spectral range, however, this cannot be verified in the present experimental setup.

Pressure dependence. Although the increase in Raman signals takes place on a time scale small compared to the mean free time of the sample molecules, collisions cannot be completely eliminated. To verify the absence of collisional effects, the dependence of the Raman signal on sample gas pressure was measured. It was indeed found that the normalized Raman signals do not depend on pressure.[22] This can also be seen in Fig. 10 which shows that the normalized anti-Stokes signals are essentially independent of the sample gas pressure. This confirms that collisions play no role in the observed increase in Raman signal.

Fluence dependence. The intramolecular vibrational energy distribution after infrared multiphoton excitation depends on the excitation region, which in turn is determined by the infrared pumping intensity. At low fluence the energy is essentially confined to the pumping mode, just as in ordinary one photon spectroscopy (region I). In this case the energy of other modes does not change after excitation, and the Raman signals from these modes simply reflect the thermal population of these modes. At higher fluences the molecule may absorb many infrared photons. In this high excitation region the vibrational modes are strongly coupled, and the nonresonant modes also acquire energy during the excitation (region II). At even higher pumping fluence, dissociation of the molecules occurs (region III). Dissociation fragments, which also contain information on the intramolecular vibrational energy distribution, have been studied by many groups.[11,31–33] Except for the fluorescence spectrum of infrared multiphoton dissociated CF_2Cl_2 all the experiments discussed in this paper were done in region II.

Figure 10 shows the infrared fluence dependence of infrared multiphoton excited SF_6 for two pulse durations. Larger signals are obtained for the shorter (higher intensity) pulses, in particular in the low fluence region. At low excitation, a high intensity is needed to overcome the anharmonic shifts, while in the high excitation region, when other nonresonant modes participate in the excitation process, intensity effects become less pronounced. This is consistent with the observation of a 'bottleneck effect' in other experiments.[18]

In contrast to the nearly linear fluence dependence of SF_6, CF_2Cl_2 shows an exponential dependence. As shown in Fig. 11, the excitation is a steep function of the pumping fluence. Above 1×10^4 J/m^2, the signals double roughly every 0.3×10^4 J/m^2 increment. Since CF_2Cl_2 is smaller than SF_6, fewer vibrational modes are available and one expects a stronger bottleneck effect in CF_2Cl_2. The observed slow rise of the signals at low

fluence, which is in sharp contrast with the linear fluence dependence of SF_6, indeed suggests that this is the case. Measurements of the Raman signal for shorter pulses would provide a better understanding of the role of intensity effects.

Raman intensities. We will now use the normalized anti-Stokes signals as a measure of the average number of quanta in the Raman active modes, and evaluate the distribution of energy in the vibrational modes. Clearly, the CF_2Cl_2 results provide the most detailed information, since the anti-Stokes signals of three Raman active modes were measured. In equilibrium the intensities of the normalized signals are given by

$$I_{\text{rel}} = \frac{1}{e^{h\nu/kT} - 1} \quad , \tag{12}$$

and the mode with lowest frequency will have the largest anti-Stokes signal. The results in Figs. 4, 8, and 11, which are tabulated in Table II, however, show that the signal intensities after infrared multiphoton excitation cannot be described by the above expression. Especially the normalized intensity of the pumped vibrational mode at 923 cm^{-1} is considerably higher than the corresponding intensities of the other two modes: at all fluences most of the energy remains in the pumped mode. In addition, as is clear from Fig. 11 the rate of increase is different for the three modes. From this figure and the data in Table II, it appears that there is a stronger coupling of the pump mode with the 1098 cm^{-1} mode than with the less energetic 667 cm^{-1} mode, notably at the high fluence end. Note also that although the intensities of the anti-Stokes signals increase significantly between 1.5 and 2.4×10^4 J/m^2, the intensity *ratio* does not change much. This rules out the possibility that the observed nonequilibrium distribution is a result of averaging a 'hot' equilibrium ensemble and a 'cold' bottlenecked ensemble, since the ratio would change as the fraction of molecules in the hot ensemble becomes larger with increasing fluence. Adding up the energy content of the three modes for CF_2Cl_2 from Table II, it appears that a complete randomization of energy only occurs above 10,000 cm^{-1} of excitation.

One expects collisions to relax the nonequilibrium energy distribution induced by the infrared multiphoton excitation. Even though the decay times of the anti-Stokes signals shown in Fig. 8 are unequal, it is not possible to draw any quantitative conclusions from these data because the signals drop below the noise level before equilibrium is reached. When buffer gas is added, the collision rate increases and the energy distribution should reach equilibrium more quickly. The intensity ratios shown in Fig. 12 indeed tend toward equilibrium with increasing buffer gas pressure.

F (10^4 J/m^2)	p_{N_2} (kPa)	I_{rel} ratio	E_{667} (cm^{-1})	E_{923} (cm^{-1})	E_{1098} (cm^{-1})
0	–	3.4 : 1 : 0.45	28	11	6
1.2	–	0.21 : 1 : 0.23	70	480	130
1.5	–	0.15 : 1 : 0.41	120	1140	560
1.8	–	0.12 : 1 : 0.48	180	2160	1240
2.1	–	0.10 : 1 : 0.48	280	3800	2190
2.4	–	0.10 : 1 : 0.48	440	6300	3620
2.1	13	0.20 : 1 : 1	130	920	1100
2.1	26	0.17 : – : 0.15	110	< 450	160

TABLE II. Average vibrational energy and relative intensity ratio for three Raman active modes at 667, 923 and 1098 cm^{-1} for CH_2Cl_2 after infrared multiphoton excitation. The top line gives the (calculated) room temperature equilibrium values. At a N_2 buffer gas pressure of 26 kPa the anti-Stokes signal of the 923 cm^{-1} mode drops below the noise level.

At a buffer gas pressure of 13 kPa the relative intensities of the 923 cm^{-1} and the 1098 cm^{-1} mode become nearly identical. At 26 kPa, equilibrium is established between the 667 cm^{-1} and the 1098 cm^{-1} modes. At this pressure, however, the overall signal has decreased so much because of vibration-translation relaxation that the anti-Stokes signal from the pump mode becomes too small to be detected.

Since SF_6 has only one Raman active mode, it is not possible to compare the energy content of different modes as for CF_2Cl_2. One can nonetheless obtain qualitative information from a comparison of the anti-Stokes Raman intensity with the result of photoacoustic experiments, which measure the total energy absorbed per molecule.[8] The comparison is done as follows. First the energy content of the Raman active mode is determined from the magnitude of the normalized anti-Stokes signals. Next the total energy content of all the modes is determined assuming all vibrational modes of SF_6 are in equilibrium. As can be seen in Fig. 15 and Table III, the results thus obtained closely match the values obtained from photoacoustic measurements. In other words, the Raman signal corresponds to what one would expect after equipartitioning the absorbed energy among all

F (10^4 J/m^2)	I_{rel}	E_{775} (cm^{-1})	E_{total} (cm^{-1})	E_{PA} (cm^{-1})
0	–	28	11	6
0.5	1.1	850	13000	15000
1.0	2.0	1600	23000	23000
2.0	3.3	2700	39000	39000
4.0	5.0	3900	57000	57000
7.0	6.8	5300	78000	78000
0.5	0.44	340	5000	–
1.0	0.9	700	10300	–
2.0	1.8	1400	20600	–
4.0	3.6	2800	41300	–

TABLE III. Relative intensity and vibrational energy of the 775 cm^{-1} vibrational mode of SF_6 after infrared multiphoton excitation with 0.5 ns (top) and 15 ns (bottom) pulses. The total vibrational energy of the molecules, calculated assuming intramolecular energy, is compared with the result obtained from photoacoustic measurement (E_{PA}).

vibrational modes. This suggest that for SF_6 the intramolecular vibrational energy distribution after collisionless infrared multiphoton excitation is in equilibrium. For a more detailed discussion the reader is referred to a previously published paper.[22]

The other two molecules studied, CF_2Cl_2 and CH_3CHF_2, show no or almost no changes in Raman spectrum, even though they absorb a significant amount of energy. This indicates that the excitation energy remains mostly in the modes that were not probed, most likely in the pumped mode, just as for the CF_2Cl_2.

Fluorescence. As can be seen in Fig. 13, the laser induced fluorescence from the dissociation fragments of infrared multiphoton dissociated CF_2Cl_2 extends far into the blue side of the Raman probe. This indicates that the dissociation fragments carry up to 5000 cm^{-1} of excitation energy, corresponding to five infrared photons. It should also be noted that the shape of the spectrum does not change with increasing fluence. This implies that an increase in fluence does not change the energy distribution of the dissociation fragments, but only increases the *number* of dissociated

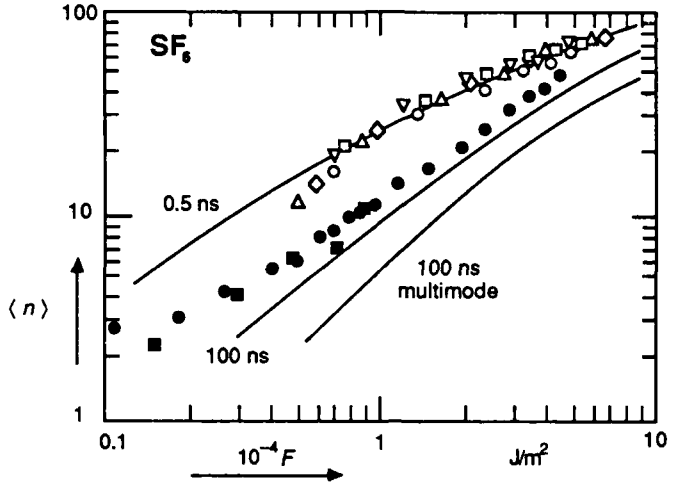

Fig. 15. Average number of infrared photons absorbed per molecule as a function of infrared fluence. The data points shown were obtained from the ones shown in Fig. 10, assuming thermal equilibrium between all vibrational modes immediately after the infrared multiphoton excitation. The solid lines are the average number of infrared photons obtained from photoacoustic measurements.

molecules. Therefore the unimolecular dissociation rate of infrared multiphoton excited CF_2Cl_2 must be much smaller than the excitation rate.

5. Conclusion

This paper presents time-resolved Raman spectra of infrared multiphoton excited molecules. After excitation, collisionless changes in signal intensities are observed for SF_6, CF_2Cl_2 and CH_3CHF_2. Information on the intramolecular distribution of energy after infrared multiphoton excitation is obtained by using the anti-Stokes Raman intensities as a measure of the energy content of the Raman active vibrational modes. For the molecules studied here, both equilibrium and nonequilibrium energy distributions were observed. Since the signals are averaged over the ensemble of all molecules in the interaction volume, whether highly excited or not, the results presented here are a convolution of the behavior at high excitation with that at low excitation. Still, for CF_2Cl_2 the anti-Stokes intensity ratio does not change as the fraction of highly excited molecules is enlarged by increasing the pumping fluence. This leads to the conclusion that even at high excitation the intramolecular vibrational distribution is still

nonequilibrium, with an excess of energy in the pumped mode. It should be emphasized, however, that these conclusions hold for molecules in region II, and not for dissociating molecules since the signal from those molecules is rejected. Therefore the above conclusions do not contradict the observation[11] that the infrared multiphoton *dissociation* of molecules is consistent with RRKM theory.[34]

Acknowledgments

We are pleased to acknowledge stimulating discussions with Professors N. Bloembergen and M. Quack and Dr. L.A. Lompré. This work was supported by Army Research Office and the Joint Services Electronics Program under contracts with Harvard University.[35]

References

1 V.S. Letokhov, *Physics Today* **11**, 34 (1980)
2 N. Bloembergen and E. Yablonovitch, *Physics Today* **5**, 23 (1978)
3 V.N. Bagratashvili, V.S. Letokhov, A.A. Makarov, E.A. Ryabov, *Multiphoton Infrared Laser Photophysics and Photochemistry* (Harwood Academic Publishers, New York, 1985)
4 D.S. King, *Dynamics of the Excited State*, Ed. K.P. Lawley (Wiley, New York, 1982)
5 W. Fuss and K.L. Kompa, *Prog. Quant. Electr.* **7**, 117 (1981)
6 P.A. Schulz, Aa. S Sudbø, D.J. Krajnovitch, H.S. Kwok, Y.R. Shen, and Y.T. Lee, *Ann. Rev. Phys. Chem.* **30**, 379 (1979)
7 C. D. Cantrell, S. M. Freund, J. L. Lyman, *Laser Handbook*, Vol. 3, Ed. M.L. Stitch (North-Holland, Amsterdam, 1979)
8 J.G. Black, P. Kolodner, M.J. Schultz, E. Yablonovitch, and N. Bloembergen, *Phys. Rev.* **A19**, 704 (1979)
9 Y.T. Lee, and Y.R. Shen, *Physics Today* **33**, 52 (1980)
10 J.D. Campbell, G. Hancock, J.B. Halpern, and K.H. Welge, *Chem. Phys. Lett.* **44**, 404 (1976)
11 David S. King and John C. Stephenson, *Chem. Phys. Lett.* **51**, 48 (1977)
12 D.S. Frankel and T.J. Manuccia, *Chem. Phys. Lett.* **54**, 451 (1978)
13 R.C. Sharp, E. Yablonovitch and N. Bloembergen, *J. Chem. Phys.* **74**, 5357 (1981)
14 P. Mukherjee and H.S. Kwok, *J. Chem. Phys.* **84**, 1285 (1986)

15 V.N. Bagratashvili, Yu.G. Vainer, V.S. Doljikov, S.F. Koliakov, A.A. Makarov, L.P. Malyavkin, E.A. Ryabov, E.G. Silkis, and V.D. Titov, *Appl. Phys.* **22**, 101 (1980)

16 V.N. Bagratashvili, Yu.G. Vainer, V.S. Dolzhikov, S.F. Kol'yakov, V.S. Letokhov, A.A. Makarov, L.P. Malyavkin, E.A. Ryabov, E.G. Sil'kis, and V.D. Titov, *Sov. Phys. JETP* **53**, 512 (1981)

17 V.N. Bagratashvili, V.S. Doljikov, V.S. Letokhov, A.A. Makarov, L.P. Maljavkin, E.A. Ryabov, E.G. Silkis, and Yu.G. Vainer, *Opt. Comm.* **38**, 31 (1981)

18 V.N. Bagratashvili, Yu.G. Vainer, V.S. Doljikov, V.S. Letokhov, A.A. Makarov, L.P. Malyavkin, E.A. Ryabov, and E.G. Sil'kis, *Opt. Lett.* **6**, 148 (1981)

19 Yu.S. Doljikov, V.S. Letokhov, A.A. Makarov, A.L. Malinovsky and E.A. Ryabov, *Chem. Phys. Lett.* **124**, 304 (1986)

20 V.S. Doljikov, Yu.S. Doljikov, V.S. Letokhov, A.A. Makarov, A.L. Malinovsky and E.A. Ryabov, *Chem. Phys.* **102**, 155 (1986)

21 E. Mazur, I. Burak, and N. Bloembergen, *Chem. Phys. Lett.* **105**, 258 (1984)

22 Jyhpyng Wang, Kuei-Hsien Chen, and Eric Mazur, *Phys. Rev. A* **34**, 3892 (1986)

23 Eric Mazur, *Rev. Sci. Instrum.* **57**, 2507 (1986)

24 T.B. Simpson, J.G. Black, I. Burak, E. Yablonovitch and N. Bloembergen, *J. Chem. Phys.* **83**, 628 (1985)

25 G. Herzberg, *Molecular spectra and molecular structure*, Vol. 2 (Van Nostrand Reinhold, New York, 1979)

26 Charles A. Bradley, Jr., *Phys. Rev.* **40**, 908 (1932)

27 T. Shimanouchi, *J. Phys. Chem. Ref. Data* **6**, 993 (1977)

28 D.W. Lupo, and M. Quack, *Chem. Rev.* **87**, 181 (1987)

29 F. Albert Cotton, *Chemical Applications of Group Theory* (Wiley-Interscience, New York, 1971)

30 R.D. Bates Jr., J.T. Knudtson, G.W. Flynn and A.M. Ronn, *Chem. Phys. Lett.* **8**, 103 (1971)

31 J.W. Hudgens, *J. Chem. Phys.* **68**, 777 (1978)

32 R.J.S. Morrison and E.R. Grant, *J. Chem. Phys.* **71**, 3573 (1979)

33 Aa.S. Sudbø, P.A. Schulz, E.R. Grant, Y.R. Shen, and Y.T. Lee, *J. Chem. Phys.* **70**, 912 (1979)

34 Benson S.W. *Chem. Rev.* **78** 23(1978)

35 Contract numbers: DAAG29-85-K-0600 and N00014-84-K-0465.

Highly Nonthermal Intramolecular Energy Distribution in Isolated Infrared Multiphoton Excited CF_2Cl_2 Molecules

Eric Mazur, Kuei-Hsien Chen and Jyhpyng Wang

Department of Physics and Division of Applied Sciences, Harvard University, Cambridge, MA 02138, USA

When a polyatomic molecule with a strong vibrational absorption band is irradiated with an intense resonant infrared laser pulse it can absorb many (10 to 40) infrared photons.[1] If some initial energy deposition is 'localized'—preferably in one vibrational mode or in a subset of modes—it may become possible to induce 'mode-selective' reactions by infrared multiphoton excitation. The intramolecular dynamics of infrared multiphoton excited molecules has been studied by a variety of spectroscopic techniques.[2] One of these techniques is spontaneous Raman spectroscopy. In the past five years this technique has been successfully applied to monitor the vibrational energy in infrared multiphoton excited molecules.[3,4]

In this work we present experimental results of recent time-resolved spontaneous Raman experiments on collisionless infrared multiphoton excited CF_2Cl_2 molecules. The experiments show that the intramolecular energy distribution is highly nonthermal, and that a large part of the vibrational energy remains localized in the pump mode for a period of time long compared to the mean free time of the molecules.

The experimental procedure is described in detail in previous papers.[5] Briefly, a 15 ns CO_2-laser pulse excites the 919 cm^{-1} band of the CF_2Cl_2 molecules. After a short time delay a second 20 ns laser pulse from a frequency-doubled ruby laser probes the excited molecules. Raman scattered light is analyzed with a double monochromator and a high-gain photomultiplier. The time delay between the two laser pulses can be varied from 10 ns to 10 μs. The present measurements were carried out at a pressure of 400 Pa.

Fig. 1 shows the anti-Stokes spectrum of the multiphoton excited CF_2Cl_2. Signals from three Raman active modes, at 664, 919 and 1082 cm^{-1} are visible. The room temperature Stokes side of the Raman spectrum is shown in the same graph. At room temperature the intensity of the anti-Stokes peaks is too small to be measured at a pressure of 400 Pa. The intensity of the Raman peaks is a measure of the vibrational energy in each of the Raman-active modes.[4] Therefore, by measuring the time dependence of the anti-Stokes intensity, one can study the evolution of the vibrational energy distribution in multiphoton excited molecules.

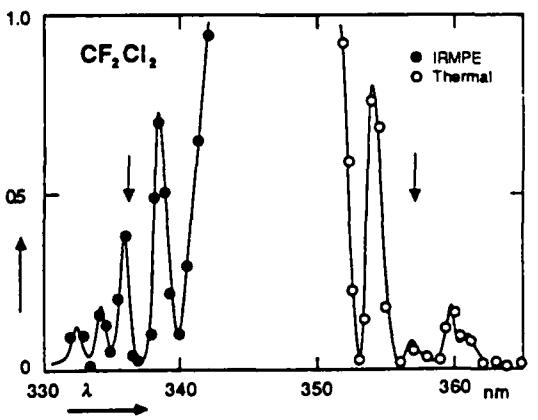

Fig. 1. Raman spectrum of infrared multiphoton excited CF_2Cl_2 at 400 Pa. The arrows show the position of the pump line.

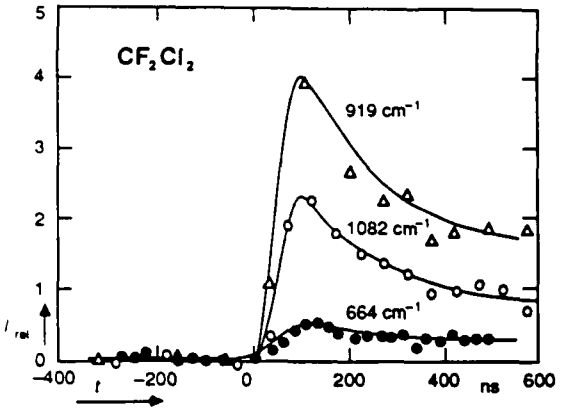

Fig. 2. Intensity of the normalized anti-Stokes signals as a function of the time delay between pump and probe pulse for CF_2Cl_2.

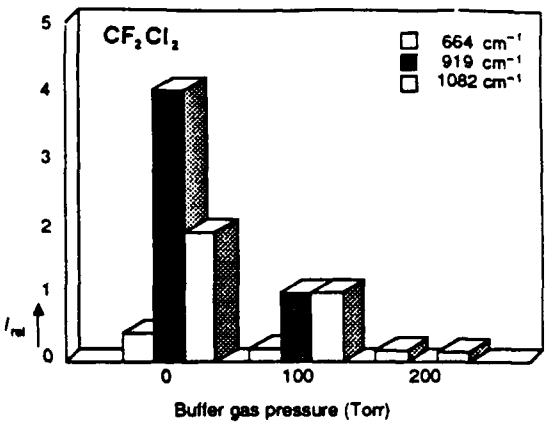

Fig. 3. Normalized anti-Stokes intensites for 3 modes of CF_2Cl_2 at 2 J/cm^2 for different N_2 buffer gas pressures.

The time dependence of the anti-Stokes Raman signals is shown in Fig. 2. The signals are normalized with their corresponding room temperature Stokes counterparts to correct for the different Raman cross sections. The rise time of the signals corresponds to the pulse duration of the laser pulses. The decay of the signals is due to a combination of collisional vibrational relaxation and diffusion of the excited molecules out of the excitation region. By comparing the intensity of the signals one can determine the distribution of energy in the vibrational modes. Fig. 3 shows the normalized intensity distribution 100 ns after excitation. From this graph it is clear that most of the excitation energy remains in the pump mode at 919 cm^{-1} for collisionless excitation without buffer gas. As an increasing amount of N_2 buffer gas is added the distribution tends toward thermal equilibrium, but the overall signal strengths decrease because of vibration-translation relaxation.

Summarizing, we present here time-resolved spontaneous Raman scattering measurements of infrared multiphoton excited CF_2Cl_2 at low pressure. The results show a highly nonthermal energy distribution among different modes, which persists even on time scales long compared to the mean free time of the molecules. A more detailed discussion of these results will be published elsewhere.[6] This work was supported by the Army Research Office and the Joint Services Electronics Program under contracts with Harvard University.[7]

References

1. See for instance the following publications and references therein: W. Fuss and K. L. Kompa, Prog. Quant. Electr. 7, 117 (1981); D.S. King, *Dynamics of the Excited State*, Ed. K. P. Lawley (Wiley, New York, 1982)
2. V.N. Bagratashvili, V.S. Letokhov, A.A. Makarov, E.A. Ryabov, *Multiple Photon Infrared Laser Photophysics and Photochemistry* (Harwood, New York, 1985)
3. V.N. Bagratashvili, Yu.G. Vainer, V.S. Doljikov, S.F. Koliakov, A.A. Makarov, L.P. Malyavkin, E.A. Ryabov, E.G. Silkis, And V.D. Titov, Appl. Phys. 22, 101 (1980)
4. Jyhpyng Wang, Kuei-Hsien Chen and Eric Mazur, Phys. Rev. A 34, 3892 (1986)
5. Eric Mazur, Rev. Sci. Instrum. 57, 2507 (1986)
6. Kuei-Hsien Chen, Jyhpyng Wang and Eric Mazur, submitted to Phys. Rev. Lett.
7. Contract numbers: DAAG29-85-K-0600 and N00014-84-K-0465, respectively

Nonthermal Intramolecular Vibrational Energy Distribution in Infrared-Multiphoton-Excited CF_2Cl_2

Kuei-Hsien Chen, Jyhpyng Wang, and Eric Mazur

Department of Physics and Division of Applied Sciences, Harvard University, Cambridge, Massachusetts 02138

(Received 24 August 1987)

The intramolecular vibrational energy distribution of infrared-multiphoton-excited CF_2Cl_2 molecules is studied with time-resolved spontaneous Raman scattering. The time evolution of the signals from three vibrational modes is studied up to 600 ns after excitation, and in the presence of N_2 buffer gas. Following collisionless infrared multiphoton excitation a nonthermal distribution of vibrational energy is observed. This nonequilibrium distribution persists up to high levels of vibrational excitation, with at least 10000 cm^{-1} in three out of the nine vibrational modes.

PACS numbers: 33.80.−b, 33.20.Fb, 82.50.Jy

In 1973 it was discovered that isolated molecules in the ground electronic state can be dissociated by a short, intense pulse from a CO_2 laser.[1] Since then, the absorption of large numbers of monochromatic infrared photons by single molecules has been studied extensively.[2-7] Because of the selectivity of vibrational excitation, infrared multiphoton excitation has received much attention. Initially it was hoped that a "bond-selective" or "mode-selective" photochemistry based on infrared multiphoton excitation could be developed.[8]

Information on the intramolecular vibrational energy distribution in infrared-multiphoton-excited molecules has been obtained experimentally in a number of ways.[9-16] It was shown that the infrared-multiphoton-dissociation branching ratios and the energy distributions of the dissociation fragments are consistent[5,16] with Rice-Ramsberger-Kassel-Marcus theory.[17] This means that when molecules are excited above or close to the dissociation threshold, equilibration of the intramolecular vibrational energy distribution occurs. Whether this holds true for highly excited molecules below the dissociation threshold remains an open question. Spontaneous Raman scattering was used to study various infrared-multiphoton-excited molecules, and the results provided information on the vibrational energy distribution after excitation.[11,12,14,18] This paper presents time-resolved Raman-scattering measurements on infrared-multiphoton-excited CF_2Cl_2, a molecule which allows direct comparison of the Raman signal intensities of different modes after excitation. Since the Raman signal intensity is directly proportional to the energy in the mode, the results provide direct information on the intramolecular vibrational energy distribution of CF_2Cl_2 at various levels of excitation. The present experimental data fill the gap in the transition regime between the well-known low-excitation (single vibrational mode) and high-excitation (dissociation) regions.

In simple harmonic approximation, the total, spectrally integrated, intensity of the Raman signal of a particular vibrational mode is proportional to the average energy in that mode, $\langle E_{\text{total}} \rangle$. This follows from the fact that the transition probability is proportional to the vibrational quantum number n.[18] For an anti-Stokes transition $n \rightarrow n-1$, with transition probability $W_{n \rightarrow n-1}$, one therefore obtains for the total anti-Stokes Raman signal intensity

$$I_{\text{total}}^{\text{AS}} = \sum_{n=0}^{\infty} P_n W_{n \rightarrow n-1} = a \sum_{n=0}^{\infty} P_n n, \tag{1}$$

where P_n is the population of vibrational state n, and a a mode-dependent quantity related to the Raman-scattering cross section. To eliminate the proportionality constant a, the anti-Stokes signal is normalized with the corresponding Stokes signal at room temperature, I_0^{S}. The resulting normalized anti-Stokes signal, I_{norm}, is therefore proportional to the average energy in that mode,

$$I_{\text{norm}} \equiv \frac{I_{\text{total}}^{\text{AS}}}{I_0^{\text{S}}} = b^{-1} \sum_{n=0}^{\infty} P_n n = b^{-1} \frac{\langle E_{\text{total}} \rangle}{h\nu}, \tag{2}$$

with

$$b \equiv \sum_{n=0}^{\infty} P_n^0 (n+1), \tag{3}$$

where P_n^0 is the population distribution at room temperature, h Planck's constant, and ν the frequency of the mode. If, as is usually the case, the energy of vibrational quanta is much larger than kT at room temperature, the Boltzmann factor $e^{-h\nu/kT}$ is small, and $b \approx 1$. Under these conditions I_{norm} is a *direct* measure of the average number, $\langle n \rangle = \langle E_{\text{total}} \rangle / h\nu$, of vibrational quanta in each vibrational mode. This allows one to compare the average energy from mode to mode after excitation of the molecules and determine the vibrational energy distribution.

The experimental setup[18,19] consists of a low-pressure gas cell, an infrared pump laser, and an ultraviolet probe laser. To isolate intramolecular from (collisional) intermolecular effects, the signals are measured at pressures low enough to ensure that no significant collisional relax-

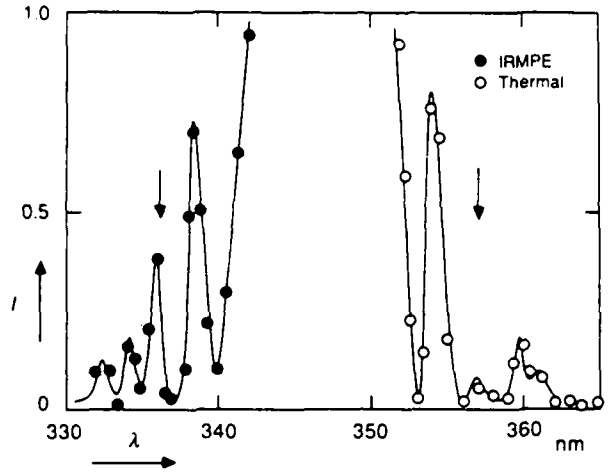

FIG. 1. Raman spectrum of CF_2Cl_2, with (filled circles) and without (open circles) infrared multiphoton excitation.

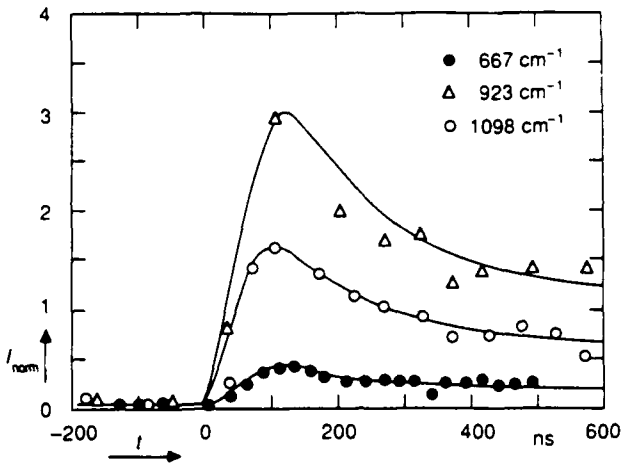

FIG. 2. Normalized anti-Stokes signals as functions of the time delay between pump and probe pulse.

ation of vibrational energy occurs on the time scale of the excitation. The infrared radiation is generated by a high-power, short-pulse, tunable CO_2 laser.[20,21] The infrared pulses of 15 ns duration have a maximum energy of 200 mJ at the $P(32)$ line of the 10.6-μm branch. A 30-ns frequency-doubled ruby laser pulse of 3 mJ serves as Raman probe. The Raman signals are detected with a low-resolution (1.5 nm) double monochromator and a high-gain fast photomultiplier tube. A complete description of the experimental setup can be found in previous papers.[18,19]

The experimental results on CF_2Cl_2 presented here were obtained at a pressure of 400 Pa (3 Torr). The reported purity of the commercially obtained gas is better than 99.995%. Of the nine vibrational modes of CF_2Cl_2,[22,23] three, at 667, 923, and 1098 cm^{-1}, are accessible to our apparatus. The CCl_2 asymmetric stretch mode at 923 cm^{-1} is resonant with the 10.6-μm $P(32)$ line of the CO_2 laser. Since this mode is both Raman and infrared active, one can directly monitor the excitation in the pumped mode.

The Raman spectrum of CF_2Cl_2, obtained with and without infrared multiphoton excitation, is shown in Fig. 1. The large central peak in the spectrum corresponds to Rayleigh scattering. Because of the low population of excited levels at room temperature, only Stokes signals can be detected in the absence of infrared pumping. These room-temperature data are shown in the right-hand side of the graph; the corresponding anti-Stokes side of the spectrum has been omitted. After the excitation, large anti-Stokes signals appear. The Stokes and anti-Stokes peaks at 356.5 and 336 nm (see arrows) correspond to the 923-cm^{-1} pump mode. One can obtain an indication of the average excitation in each mode by comparing the intensities of the anti-Stokes peaks with the intensities of the corresponding Stokes peaks in this graph, as in Eq. (2). From such a simple comparison, it becomes immediately clear that the pump mode is much more highly excited than the other modes.

Figure 2 shows the normalized anti-Stokes signal from Eq. (2), I_{norm}, versus the time delay between pump and probe pulses at an average fluence of 1.8×10^4 J/m^2. For $t<0$, the molecules are probed before the excitation, i.e., at room temperature. The rise time of all three vibrational modes is limited by the 30-ns instrumental time resolution, which in turn is determined by the temporal width of the laser pulses. The decay of the signals is most likely due to the collisional transfer of energy to other initially "cold" vibrational modes. Such a collisional relaxation should result in a growth of energy content of the initially unexcited modes. Because it is not possible to observe all nine vibrational modes, however, this could not be verified.

For an equilibrium distribution of energy among the

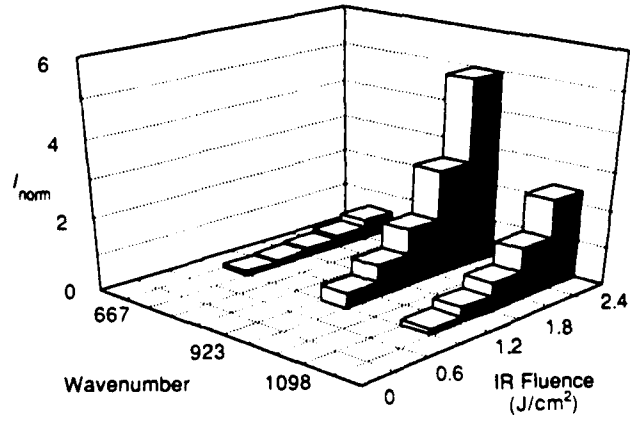

FIG. 3. Infrared fluence dependence of the normalized anti-Stokes signals for CF_2Cl_2 at 400 Pa.

vibrational modes, the intensities of the normalized signals are given by

$$I_{\text{norm}} = (e^{h\nu/kT} - 1)^{-1}. \quad (4)$$

Figure 2, however, shows that after excitation the signal intensities cannot be described by Eq. (4) for any temperature T. The normalized intensity of the pumped vibrational mode at 923 cm^{-1} is considerably higher than the corresponding intensities of the other two modes.

Figure 3 shows the normalized anti-Stokes signals as functions of infrared fluence. The normalized intensity ratios as well as values of $\langle E_{\text{total}} \rangle$ for each mode obtained from Eq. (2) are displayed in Table I. The normalized anti-Stokes intensities of all three modes increase exponentially with increasing fluence, with the pumped mode at 923 cm^{-1} containing the largest amount of energy for all infrared fluences. The ratios of normalized anti-Stokes signals clearly indicate a nonequilibrium intramolecular vibrational energy distribution among the three observed vibrational modes. As the fluence is increased from (1.8 to 2.4)$\times 10^4$ J/m^2, the energy in the pumped mode triples and the total vibrational energy in the three probed modes is at least 10000 cm^{-1}, yet the nonequilibrium ratio of intensities remains unchanged. This implies that the observed nonequilibrium distribution *cannot* be the result of averaging a "hot" equilibrium ensemble and a "cold" bottlenecked[12] ensemble. If that were the case, the intensity ratios in Table I would change as the fraction of molecules in the hot ensemble increases with increasing fluence. Since more than one mode is highly excited, the behavior is distinctly different from the low-excitation behavior. On the other hand, the nonthermal distribution at this relatively high excitation contrasts with the well established equilibrium distribution of vibrational energy in the infrared multiphoton dissociation of CF_2Cl_2 molecules.[5,16] It is therefore interesting to compare the 10000 cm^{-1} of internal energy in the three probed modes with the 24000-cm^{-1} (74 kcal/mol) thermal dissociation energy of CF_2Cl_2. At the highest fluence used, two of the probed modes contain about twice the energy that would result from a statistical distribution of the 24000-cm^{-1} dissociation energy over all the modes. One must therefore conclude that reported equilibration of vibrational energy occurs only at still higher fluences, when the energy in the pumped mode is well above its thermal-dissociation value. It is not possible, however, to probe the molecules at higher excitation because of laser-induced fluorescence from dissociation fragments.

Collisions relax the nonequilibrium intramolecular vibrational energy distribution of the excited molecules, and the normalized anti-Stokes signals should therefore approach their thermal equilibrium values as collisions occur. Unfortunately it is not possible to draw any quantitative conclusions from the decay of the anti-Stokes signals in Fig. 2, because the signals drop below the noise level before equilibrium is reached. The relaxation rate was therefore increased by addition of N_2 buffer gas. Figure 4 shows the normalized anti-Stokes signals at various buffer-gas pressures. The same graph also shows the equilibrium values of the Raman signals, calculated under the assumption of the same amount of total internal energy in the three modes as in the left graph. The observed signals decrease quickly with increasing buffer-gas pressure, but at the same time the differences between them become smaller. Within the experimental accuracy, equilibrium is reached between the 923- and 1098-cm^{-1} modes at 13 kPa buffer-gas pressure. At 26 kPa, equilibrium between the 667- and 1098-cm^{-1} modes is also established. Because of the small Raman

TABLE I. Average vibrational energy and relative intensity ratio for three Raman-active modes of CF_2Cl_2, at 667, 923, and 1098 cm^{-1}, after infrared multiphoton excitation. The top row gives the (calculated) room-temperature equilibrium values.

F (10^4 J/m^2)	p_{N_2} (kPa)	I_{rel} ratio	E_{667} (cm^{-1})	E_{923} (cm^{-1})	E_{1098} (cm^{-1})
0	···	3.4:1:0.45	28	11	6
1.2	···	0.21:1:0.23	70	480	130
1.5	···	0.15:1:0.41	120	1140	560
1.8	···	0.12:1:0.48	180	2160	1240
2.1	···	0.10:1:0.48	280	3800	2190
2.4	···	0.10:1:0.48	440	6300	3620
2.1	13	0.20:1:1	130	920	1100
2.1	26	0.17:···:0.15	110	<450	160

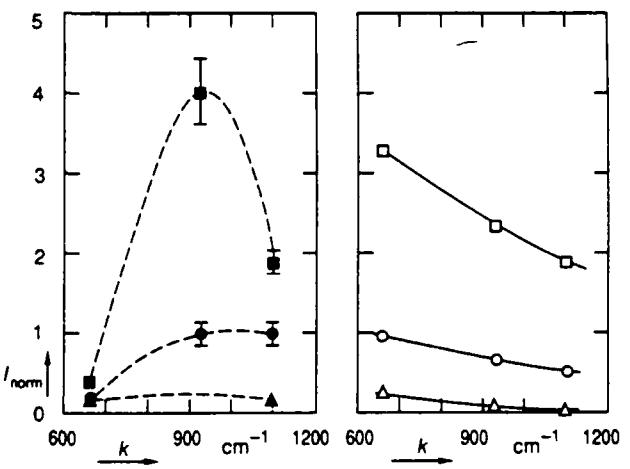

FIG. 4. Comparison of the observed normalized anti-Stokes signals with calculated equilibrium values. On the left, signals after infrared multiphoton excitation for three different N_2 buffer-gas pressures: 0 Pa (squares), 13 kPa (circles), and 26 kPa (triangles). On the right, calculated equilibrium values at three different temperatures: 3900 K (squares), 1500 K (circles), and 600 K (triangles).

cross section of the 923-cm^{-1} mode, data are not available for this mode at 26 kPa buffer-gas pressure. At this pressure the vibrational energy of the highly excited CF_2Cl_2 is rapidly transferred to the buffer gas, and the anti-Stokes signal of the 923-cm^{-1} pump mode drops below the noise level. A comparison with the calculated equilibrium values on the other side of the graph shows that as the buffer-gas pressure is increased, the intramolecular vibrational energy distribution tends to equilibrate.

In conclusion, we have employed time-resolved spontaneous Raman scattering to study the infrared multiphoton excitation of CF_2Cl_2. The observed anti-Stokes signals show a nonthermal energy distribution among the observed Raman-active modes of infrared-multiphoton-excited CF_2Cl_2 which tends toward equilibrium as an increasing amount of buffer gas is added. Even though at high excitation two of the observed modes already contain about twice their "statistical share" of the dissociation energy, the distribution of energy is still far from the well established equilibrium at dissociation.

This work is supported by the Army Research Office, the Joint Services Electronics Program under Grants No. DAAG29-85-K0060 and No. N00014-84-K-0465, and Hamamatsu Photonics K.K.

[1]N. R. Isenor, V. Merchant, R. S. Hallsworth, and M. C. Richardson, Can. J. Phys. **51**, 1281 (1973).

[2]V. B. Bagratashvili, V. S. Letokhov, A. A. Makarov, and E. A. Ryabov, *Multiple Photon Infrared Laser Photophysics and Photochemistry* (Harwood Academic, New York, 1985).

[3]N. Bloembergen and E. Yablonovitch, Phys. Today **31**, No. 5, 23 (1978).

[4]C. D. Cantrell, S. M. Freund, and J. L. Lyman, in *Laser Handbook*, edited by M. L. Stitch (North-Holland, Amsterdam, 1979), Vol. 3.

[5]P. A. Schultz, Aa. S. Sudbø, D. J. Krajnovitch, H. S. Kwok, Y. R. Shen, and Y. T. Lee, Annu. Rev. Phys. Chem. **30**, 379 (1979).

[6]W. Fuss and K. L. Kompa, Prog. Quantum Electron. **7**, 117 (1981).

[7]D. S. King, in *Dynamics of the Excited State*, edited by K. P. Lawley (Wiley, New York, 1982).

[8]V. S. Letokhov, Phys. Today **33**, No. 11, 34 (1980).

[9]D. S. Frankel and T. J. Manuccia, Chem. Phys. Lett. **54**, 451 (1978).

[10]J. G. Black, P. Kolodner, M. J. Schultz, E. Yablonovitch, and N. Bloembergen, Phys. Rev. A **19**, 704 (1979).

[11]V. B. Bagratashvili, Yu. G. Vainer, V. S. Dolzhikov, S. F. Kol'yakov, A. A. Makarov, L. P. Malyavkin, E. A. Ryabov, E. G. Silkis, and V. D. Titov, Appl. Phys. **22**, 101 (1980).

[12]V. B. Bagratashvili, Yu. G. Vainer, V. S. Dolzhikov, S. F. Kol'yakov, V. S. Letokhov, A. A. Makarov, L. P. Malyavkin, E. A. Ryabov, E. G. Sil'kis, and V. D. Titov, Zh. Eksp. Teor. Fiz. **80**, 1008 (1981) [Sov. Phys. JETP **53**, 512 (1981)].

[13]R. C. Sharp, E. Yablonovitch, and N. Bloembergen, J. Chem. Phys. **74**, 5357 (1981).

[14]E. Mazur, I. Burak, and N. Bloembergen, Chem. Phys. Lett. **105**, 258 (1984).

[15]Yu. S. Doljikov, V. S. Letokhov, A. A. Makarov, A. L. Malinovksy, and E. A. Ryabov, Chem. Phys. Lett. **124**, 304 (1986).

[16]D. S. King and J. C. Stephenson, Chem. Phys. Lett. **51**, 48 (1977).

[17]P. J. Robinson and K. A. Holbrook, *Unimolecular Reactions* (Wiley-Interscience, New York, 1972).

[18]Jyhpyng Wang, Kuei-Hsien Chen, and Eric Mazur, Phys. Rev. A **34**, 3892 (1986).

[19]Eric Mazur, Rev. Sci. Instrum. **57**, 2507 (1986).

[20]E. Yablonovitch and J. Goldhar, Appl. Phys. Lett. **25**, 580 (1974).

[21]H. S. Kowk and E. Yablonovitch, Opt. Commun. **21**, 252 (1977).

[22]Charles A. Bradley, Jr., Phys. Rev. **40**, 908 (1932).

[23]T. Shimanouchi, J. Phys. Chem. Ref. Data **6**, 993 (1977).

THE INTERACTION OF INTENSE PICOSECOND INFRARED PULSES WITH ISOLATED MOLECULES

Eric Mazur

Division of Applied Sciences and Department of Physics
Harvard University
Cambridge, MA 02138, USA

Introduction

In the past decade there has been much interest in the dynamics of highly vibrationally excited and dissociating molecules. Selectivity at high levels of excitation may eventually lead to the realization of laser-controlled photochemistry, with broad applications in such diverse areas as laser-assisted chemical vapor deposition, isotope separation, and photosynthesis. Polyatomic molecules in the ground electronic state can reach levels of excitation up to the dissociation threshold by absorbing a large number of photons from a resonant high-power infrared laser. Despite the selectivity of infrared excitation at low energy, however, at high excitation the excitation energy is no longer confined to one 'mode'. It has been shown experimentally that for molecules excited close to or above the dissociation threshold equilibration of energy occurs, in agreement with theoretical predictions. There is no agreement, however, as to the validity of theoretical models that presuppose equipartitioning of energy in the region *below* the dissociation threshold. Recent spontaneous Raman spectroscopy experiments on infrared multiphoton excited molecules in our laboratory provide information on the intramolecular vibrational energy distributions of highly vibrationally excited molecules in this region. The experimental results show that an excess of energy can remain in the pumped mode up to levels of excitation close to the dissociation threshold. This paper provides a review of the results that were obtained in the past three years, part of which were published previously.

Background

In 1973 it was discovered that isolated molecules in the ground electronic state can be dissociated by a short, intense pulse from a CO_2 laser.[1] Since then the absorption of large numbers of monochromatic infrared photons by isolated molecules has been studied extensively.[2–8] The early work in this field was motivated by the hope of driving chemical reactions in either a bond-specific or isotopically selective fashion by 'localized' deposition of energy in a small subset of modes.

In the past ten years many experimental techniques have been applied to study infrared multiphoton excitation. Photoacoustic measurements were applied to determine the energy absorbed by the molecules,[9] and to study the excitation as a function of various pa-

rameters, such as pumping fluence, intensity, and wavelength, pressure, etc. Photoacoustic spectroscopy was also used at high intensities to study dissociation yields as a function of absorbed energy. More detailed information on infrared multiphoton dissociation, such as the species of the dissociation fragments, branching ratios of different dissociation channels, and the translational energy distribution of the fragments, was obtained by mass and time-of-flight spectrometry.[10] Pump-and-probe experiments have also provided more detailed knowledge of the infrared multiphoton excitation and dissociation. For example, laser induced fluorescence[11,12] was used to measure the vibrational energy distribution of the infrared multiphoton dissociation fragments. Infrared double-resonance experiments[13–15] were done to determine the rotational relaxation rate and the population depletion of the vibrational ground state. Spontaneous and coherent anti-Stokes Raman scattering were used to probe the distribution of vibrational energy over the different modes of infrared multiphoton excited molecules.[16–24]

The following qualitative picture has emerged from the experimental results. Basically, one can distinguish between three different regions in the molecular vibrational spectrum depending on the level of excitation. At low excitation the energy is essentially confined to the pumping mode, just as in ordinary one-photon spectroscopy: the first few photons absorbed by a 'cold' molecule produce transitions between separate discrete vibrational states located in the resonant mode (region I). At higher levels of excitation, the spacing between individual vibrational states becomes increasingly smaller due to molecular anharmonicities, and other nonresonant modes also acquire energy during the excitation (region II, often referred to as the 'quasicontinuum'). Molecular excitation in this region is thought to occur through stepwise incoherent transitions between homogeneously broadened states that are superpositions of various normal mode states. Once in region II, many polyatomic molecules easily absorb large numbers of infrared photons and reach the continuum above the dissociation threshold (region III). Clearly the excitation process is very different in each of these three regions, and experimental results often reflect a combination of the spectroscopies of different regions.

Most of the experiments carried out to date have centered around characterizing the gross features of infrared multiphoton excitation by relatively large molecules. The parameters that have been measured, such as average number of photons absorbed per molecule, dissociation rates and branching ratios, are the product of a number of mechanical and kinetic processes and, hence, are incapable of probing the detailed dynamics of the excitation process. It has been established, however, that the infrared multiphoton dissociation branching ratios and the energy distributions of the dissociation fragments are generally consistent with statistical theories, such as the RRKM theory. This means that when molecules are excited into region III, equilibration of the intramolecular vibrational energy distribution occurs, and dissociation takes place along a thermodynamically favored path, resulting in a loss of the initial 'selectivity'. Whether equilibration occurs for highly excited molecules *below* the dissociation threshold (region II) remains an open question.

Direct information on the intramolecular energy distribution in highly excited molecules was obtained experimentally with pump-probe type experiments, in particular by Raman probing. Raman spectroscopy was first employed by Bagratashvili and coworkers[16] and later by our group[19] as a tool for studying infrared multiple photon excitation. In the Raman experiments, the population in various vibrational modes is probed after excitation of the molecules into region II with an intense infrared pulse. Since the Raman signal intensities are a measure for the amount of energy in each mode,[19] this type of experiment provides direct experimental information on the intramolecular energy distribution.

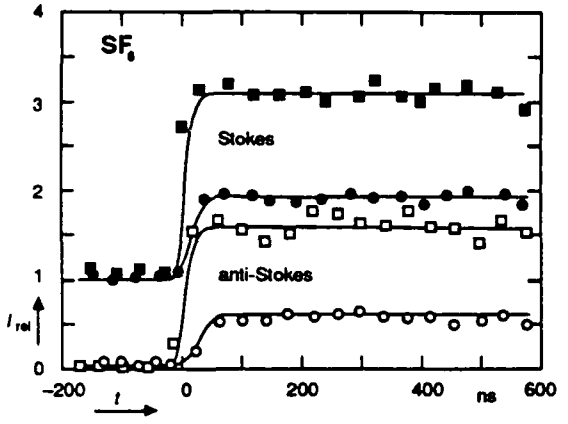

Fig. 1. Intensity of Stokes (closed symbols) and anti-Stokes (open symbols) signal as a function of the time delay between pump and probe pulses at a pressure of 67 Pa for SF_6. Infrared excitation with 0.5 ns (squares) and 15 ns (circles) pulses at the 10.6 μm P(20) line. Average fluence: 0.8×10^4 J/m^2. Data from Ref. 20.

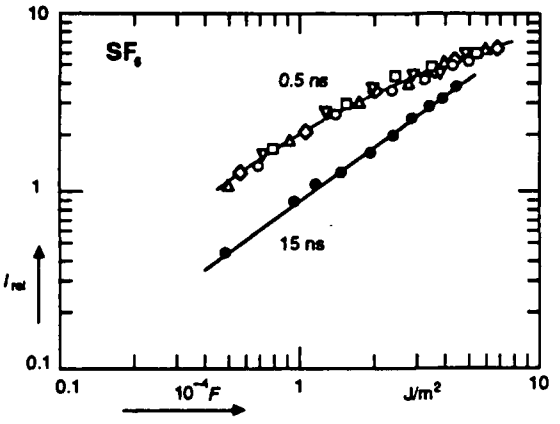

Fig. 2. Relative anti-Stokes signal of SF_6 as a function of the infrared pumping fluence for various pressures. Excitation at the 10.6 μm P(20) line with two pulse durations: 0.5 ns (open symbols) and 15 ns (closed symbols). Data from Ref. 20.

□ : 33 Pa; ○: 67 Pa; △: 133 Pa; ▽: 200 Pa; ◇: 267 Pa; ● : 133 Pa

Intramolecular energy distributions

The experimental technique and apparatus have been described previously.[20,21] Four different molecules, CF_2HCl, CF_2Cl_2, SF_6 and CH_3CHF_2, varying in size from five to eight atoms, were studied with the present apparatus.[20,22–24] An overview of experimental results is presented in Table I. All measurements were carried out at room temperature, with gas pressures ranging from 14 to 500 Pa and with infrared fluences up to 8 $\times 10^4$ J/m^2. The commercially obtained gases have a reported purity better than 99.99%.

The first molecule studied, SF_6, has only one accessible Raman active mode, ν_1, with a Raman shift of 775 cm^{-1}. Data were obtained for CO_2-laser frequencies between the P(12) and the P(28) lines of the 10.6 μm branch, which are resonant with the triply degenerate infrared active ν_3-mode (944 cm^{-1}). Two different infrared pulse durations were employed: 0.5 and 15 ns full-width at half-maximum pulses.

Fig. 1 shows the increase in Stokes and anti-Stokes signals, measured at 356.7 and 338 nm respectively, as a function of the time delay between the pump and the probe pulse for two infrared pulse durations. The signals are normalized with the room temperature Stokes signal (for $t < 0$, room temperature equilibrium data are automatically obtained). At $t = 0$ infrared excitation takes place and both Stokes and anti-Stokes signals increase. The rise time of the signals is determined by the 20 ns pulse duration of the second harmonic of the probe laser. However, although not resolved in these measurements, the increase in signal clearly occurs on a time-scale that is much shorter than the mean free time between collisions (about 200 ns at a pressure of 67 Pa). The pressure dependence of the signals further shows that the increase in signal is not due to collisions, but is truly a *collisionless* phenomenon.[20] Interestingly enough the signals remain constant, even on a time scale on which collisional vibrational energy relaxation occurs.[20] For longer delay times ($t > 2$ μs), diffusion of the excited molecules out of the probing region causes the signals to revert to their original values.[20]

Molecule	CO_2 line	Wavenumber	Mode	Activity	Remarks[20,22–24]
SF_6[25]			$\nu_1 = 775$	R (s)	changes after excitation
			$\nu_2 = 644$	R (w)	not probed
	10.6 μm P(20)	944	$\nu_3 = 965$	IR	pumped
			$\nu_4 = 617$	IR	
			$\nu_5 = 524$	R (w)	not probed
			$\nu_6 = 363$	inactive	
CF_2Cl_2[26,27]			$\nu_1 = 1101$	IR(s)	
			$\nu_1 = 1098$	R (m)	changes after excitation
			$\nu_2 = 667$	IR (s)	
			$\nu_2 = 667.2$	R (s)	changes after excitation
			$\nu_3 = 457.5$	R (s)	not probed
			$\nu_4 = 261.5$	R (s)	not probed
			$\nu_5 = 322$	R (w)	not probed
			$\nu_6 = 1159$	IR (s)	
			$\nu_6 = 1167$	R (w)	not probed
			$\nu_7 = 446$	IR (w)	not probed
	10.6 μm P(32)	933	$\nu_8 = 922$	IR (vs)	pumped
			$\nu_8 = 923$	R (w)	changes after excitation
			$\nu_9 = 437$	IR (w)	
			$\nu_9 = 433$	R (m)	not probed
CH_3CHF_2			870	R	changes after excitation
	10.6 μm P(20)		944	IR	pumped
			1140	R	no change
			1460	R	no change
			2980	R	no change
CF_2HCl			590	R	no change
			800	R	no change
	9.4 μm R(32)		1086	IR	pumped
			1130	R	no change
			1330	R	no change
			3030	R	no change

Table I. Spectroscopic data for the molecules studied in this paper. The vibrational data for SF_6 and CF_2Cl_2 are from literature. All data are in cm^{-1}, vs = very strong, s = strong, m = medium, and w = weak.

The dependence of the anti-Stokes signal intensity on the infrared laser fluence (energy per unit area) is shown in Fig. 2 for different pressures and pulse durations. The data obtained for the two pulse durations show that at low fluence the signals depend on the exciting laser pulse intensity: a larger increase in Raman signal occurs at the shorter, higher intensity, pulses. At low excitation one needs a high intensity for *coherent* multiphoton excitation through the lower part of the vibrational ladder. At the higher fluences, once the

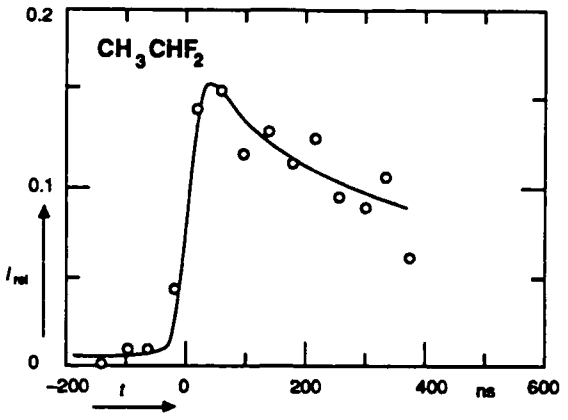

Fig. 3. Intensity of the anti-Stokes signals versus time delay between pump and probe pulse for CH_3CHF_2 at 660 Pa. Infrared excitation: 10.6 μm P(20) line, 0.5 ns pulse with average fluence 1.5×10^4 J/m^2. Data from Ref. 22.

molecules are highly excited, the curves for the 0.5 and 15 ns pulse durations approach each other, and the dependence of the signal intensity on laser pulse intensity vanishes in agreement with the behavior observed in photoacoustic measurements.[9]

The observed collisionless changes in Raman signals provide clear and direct evidence that some of the nonresonant modes do indeed participate in the excitation process. The main purpose of this research is to obtain information on the role of nonresonant modes in the multiphoton excitation of polyatomic molecules. Since the intensity of the signals is proportional to the average energy in the mode, E_R, one can determine E_R from the ratio of the anti-Stokes intensity to the thermal room temperature value of the Stokes signal, I_{rel}. Unfortunately SF_6 has only one accessible Raman active mode, so that it is not possible to compare the values of E_R for different Raman active modes. This limits us therefore to a comparison of energy in the ν_1 mode with the average total energy absorbed per molecule, $\langle E\rangle$, known from photoacoustic measurements. If one assumes an equilibrium distribution of the excitation energy $\langle E\rangle$, the amount of energy in the ν_1 mode agrees remarkably well with the value for E_R that one obtains from the Raman measurements,[19,20] suggesting that for SF_6 the intramolecular energy distribution indeed equilibrates. The absence of a decay of the Raman signals in Fig. 1 further supports this suggestion. Even though the initially nonequilibrium *intermolecular* distribution of energy equilibrates,[18] E_R remains constant once intramolecular equilibrium is achieved. In the absence of intramolecular equilibrium, one would expect E_R, and consequently the signal intensities, to change on a much shorter time scale because of a rearrangement of energy over the various vibrational modes.

The asymmetric CF_2HCl molecule has five accessible Raman active modes of widely different energy (600–3000 cm^{-1}). The peak absorption of this molecule coincides with the 9.4 μm R(32) CO_2 laser line at 1086 cm^{-1}. Even at the maximum fluence at this line (2×10^4 J/m^2), *none* of the five Raman lines show a detectable change in intensity.[22] Photoacoustic studies[23] of the infrared multiphoton excitation of this molecule have shown that at such a fluence the molecules absorb about ten infrared photons (10,000 cm^{-1}). The absence of anti-Stokes scattering from low lying levels, such as the Raman active mode at 587 cm^{-1}, suggests that not all modes participate in the excitation process, and that the energy distribution for this molecule does not equilibrate without collisions.

The asymmetric isomer CH_3CHF_2 has four accessible Raman modes. Data were obtained for 0.5 ns long pulses at the P(20) line of the 10.6 μm branch, which is resonant with the infrared active C—F stretch mode at 942 cm^{-1}. Only one of the Raman active modes, at 870 cm^{-1}, shows an increase in signal after excitation.[22] Fig. 3 shows the time-

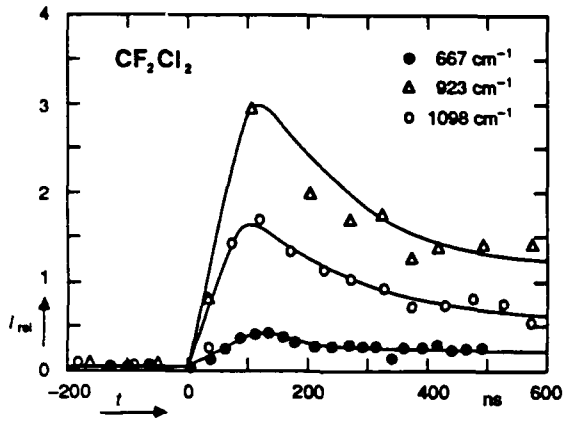

Fig. 4. Intensity of the anti-Stokes signals as a function of the time delay between pump and probe pulse for CF_2Cl_2 at 400 Pa. Infrared excitation: 10.6 μm P(32) line, 15 ns pulse with average fluence 1.8×10^4 J/m^2. Data from Ref. 23.

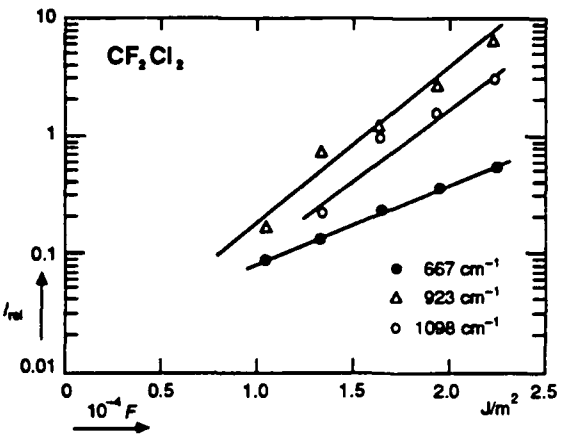

Fig. 5. Semilogarithmic plot of the fluence dependence of the anti-Stokes signals of CF_2Cl_2 at 400 Pa. The dependence is exponential for all three modes. Excitation with 15 ns pulses at the 10.6 μm P(32) line. Data from Ref. 23.

dependence of this signal at a pressure of 660 Pa and a fluence of 1.5×10^4 J/m^2. Again a short collisionless increase in signal occurs, but in contrast to SF_6 the signal now decays on a time scale of the order of collisional relaxation times. This, combined with the fact that no other Raman active mode exhibits any change, leads to the conclusion that for this particular molecule too, the excitation energy does not equilibrate.

The most complete set of data was obtained for CF_2Cl_2.[23,24] This five atom molecule has four accessible Raman active modes, three of which (at 667, 923, and 1098 cm^{-1} respectively) were measured after infrared multiphoton excitation. The C—Cl stretch mode at 923 cm^{-1} is both infrared and Raman active and can be pumped with the P(32) line of the 10.6 μm branch of the CO_2 laser. This allows one to directly observe the energy in the pump mode and compare it with the energy in other modes. The measurements presented here were all carried out at a gas pressure of 400 Pa.

Fig. 4 shows the time-dependence of the anti-Stokes signals, each normalized with its corresponding room temperature Stokes signals. The signals rise in 20 ns and show a clear decay, especially for the two highly excited modes (923 cm^{-1} and 1098 cm^{-1}). This decay is most likely attributed to collisional transfer of energy to other, initially 'cold' vibrational modes. The fluence dependence of the anti-Stokes signals of CF_2Cl_2 is nearly exponential (Fig. 5): above 1×10^4 J/m^2, the signals double roughly every 0.3×10^4 J/m^2 increment. Since CF_2Cl_2 is smaller than SF_6, fewer vibrational modes are available and one expects a stronger bottleneck effect in CF_2Cl_2. The observed slow rise of the signals at low fluence, which is in sharp contrast with the linear fluence dependence of SF_6 (*cf.* Figs. 2 and 5), indeed suggests that this is the case. Measurements of the Raman signal with shorter infrared pulses would provide a better understanding of the role of intensity effects.

Since more than one Raman active mode was measured for this molecule, one can directly compare the intensities from the various modes. In equilibrium, the intensities of the normalized signals are given by a Maxwell-Boltzmann distribution. The results in Figs. 4, and 5, however, show that the signal intensities after infrared multiphoton excitation cannot be described by such a distribution. Especially the normalized intensity of the pumped vibrational mode at 923 cm^{-1} is considerably higher than the corresponding intensities of the other two modes: at all fluences most of the energy remains in the pumped mode. In addition, as is clear from Fig. 5 the rate of increase is different for the three modes. It appears that there is a stronger coupling of the pump mode with the 1098 cm^{-1} mode than with the less energetic 667 cm^{-1} mode, notably at the high fluence end. Note also that

although the intensities of the anti-Stokes signals increase significantly between 1.5 and 2.4×10^4 J/m^2, the intensity *ratio* does not change much. This rules out the possibility that the observed nonequilibrium distribution is a result of averaging a 'hot' equilibrium ensemble and a 'cold' bottlenecked ensemble, since the ratio would change as the fraction of molecules in the hot ensemble becomes larger with increasing fluence. Adding up the energy content of the three modes for CF_2Cl_2 calculated from the signal intensities in Fig. 5, it follows that a complete equilibration of energy does not occur below 10,000 cm^{-1} of excitation. Preliminary measurements show that after pumping the 1098 cm^{-1} mode an excess of energy is found in both the 923 and the 1089 cm^{-1} cm mode.

Conclusion

This paper presents an overview of the results of measurements on various collisionless infrared multiphoton excited molecules ranging in size from 5 to 8 atoms. The amount of energy in various modes of these molecules is determined from the spontaneous Raman scattering signals from each of these modes. Most of these molecules have more than one Raman active mode and thus allow *direct* observation of the intramolecular distribution of vibrational energy among these modes after the infrared multiphoton excitation. The experiments unambiguously show: (1) that collisionless intramolecular transfer of energy to Raman active modes takes place within the 20 ns time resolution, and (2) that for highly excited molecules below the dissociation threshold the final distribution of energy—after excitation, before collisional relaxation—*is not necessarily in equilibrium.* For CF_2Cl_2 in particular it was found that the pumped mode contains an excess of energy up to *at least* 10,000 cm^{-1} of excitation energy. This implies a certain degree of 'localization' of excitation energy in the pump mode up to fairly high levels of excitation. Although this is at variance with observations made in the Soviet Union, that claim complete equilibration at about 7,000 cm^{-1}, it agrees with recent theoretical studies of the intramolecular dynamics of model systems, that show that for some molecules equilibration occurs only for energies very close to the dissociation limit.[25] To the best of our knowledge this is the first direct experimental evidence that region II may indeed extend quite close to the dissociation threshold.

Acknowledgments

We are pleased to acknowledge financial support by the Army Research Office, the Joint Services Electronics Program and by the Hamamatsu Corporation.

References

1 N.R. Isenor, V. Merchant, R.S. Hallsworth and M.C. Richardson, *Can. J. Phys.* **51**, 1281 (1973)

2 V.N. Bagratashvili, V.S. Letokhov, A.A. Makarov, E.A. Ryabov, *Multiple Photon Infrared Laser Photophysics and Photochemistry* (Harwood Academic Publishers, New York, 1985)

3 N. Bloembergen and E. Yablonovitch, *Physics Today* **5**, 23 (1978)

4 C.D. Cantrell, S.M. Freund, J.L. Lyman, *Laser Handbook*, Vol. 3, Ed. M.L. Stitch (North-Holland, Amsterdam, 1979)

5 P.A. Schultz, Aa. S. Sudbø, D.J. Krajnovitch, H.S. Kwok, Y.R. Shen, and Y.T. Lee, *Ann. Rev. Phys. Chem.* **30**, 379 (1979)

6 V.S. Letokhov, *Physics Today* **11**, 34 (1980)

7 W. Fuss and K.L. Kompa, *Prog. Quant. Electr.* **7**, 117 (1981)

8 D.S. King, *Dynamics of the Excited State*, Ed. K.P. Lawley (Wiley, New York, 1982)

9 J.G. Black, P. Kolodner, M.J. Schultz, E. Yablonovitch, N. Bloembergen, *Phys. Rev.* **A19**, 704 (1979)

10 Y.T. Lee and Y.R. Shen, *Physics Today* **33**, 52 (1980)

11 J.D. Campbell, G. Hancock, J.B. Halpern, and K.H. Welge, *Chem. Phys. Lett.* **44**, 404 (1976)

12 D.S. King and J.C. Stephenson, *Chem. Phys. Lett.* **51**, 48 (1977)

13 D.S. Frankel and T.J. Manuccia, *Chem. Phys. Lett.* **54**, 451 (1978)

14 R.C. Sharp, E. Yablonovitch and N. Bloembergen, *J. Chem. Phys.* **74**, 5357 (1981)

15 P. Mukherjee and H.S. Kwok, *J. Chem. Phys.* **84**, 1285 (1986)

16 V.N. Bagratashvili, Yu.G. Vainer, V.S. Dolzhikov, S.F. Kol'yakov, A.A. Makarov, L.P. Malyavkin, E.A. Ryabov, E.G. Silkis, and V.D. Titov, *Appl. Phys.* **22**, 101 (1980)

17 V.N. Bagratashvili, Yu.G. Vainer, V.S. Dolzhikov, S.F. Kol'yakov, V.S. Letokhov, A.A. Makarov, L.P. Malyavkin, E.A. Ryabov, E.G. Sil'kis, and V.D. Titov, *Sov. Phys. JETP* **53**, 512 (1981)

18 V.N. Bagratashvili, Yu.G. Vainer, V.S. Doljikov, V.S. Letokhov, A.A. Makarov, L.P. Malyavkin, E.A. Ryabov, and E.G. Sil'kis, *Opt. Lett.* **6**, 148 (1981)

19 E. Mazur, I. Burak, and N. Bloembergen, *Chem. Phys. Lett.* **105**, 258 (1984)

20 Jyhpyng Wang, Kuei-Hsien Chen, and Eric Mazur, *Phys. Rev. A* **34**, 3892 (1986)

21 Eric Mazur, *Rev. Sci. Instrum.* **57**, 2507 (1986)

22 Eric Mazur, Kuei-Hsien Chen, Eric Mazur, *Proc. Int. Conf. on Lasers '86*, 359 (1986)

23 Jyhpyng Wang, Kuei-Hsien Chen and Eric Mazur, *Laser Chemistry*, in press

24 Kuei-Hsien Chen , Jyhpyng Wang and Eric Mazur, to be published

25 G. Herzberg, *Molecular spectra and molecular structure*, Vol. 2 (Van Nostrand Reinhold, New York, 1979)

26 Charles A. Bradley, Jr., *Phys. Rev.* **40**, 908 (1932)

27 T. Shimanouchi, *J. Phys. Chem. Ref. Data* **6**, 993 (1977)

28 B.G. Sumpter and D.L. Thompson, J. Chem. Phys. **86**, 2805 (1987)

ENERGY LOCALIZATION IN INFRARED MULTIPHOTON EXCITED CF_2Cl_2 STUDIED BY TIME RESOLVED RAMAN SPECTROSCOPY

Jyhpyng Wang, Kuei-Hsien Chen and Eric Mazur
Division of Applied Sciences and Department of Physics
Harvard University, Cambridge, MA 02138, USA

Introduction

Since the discovery of infrared multiphoton excitation in 1973,[1] there has been much interest in the dynamics of highly vibrational excited and dissociating molecules. Selectivity at high levels of excitation may eventually lead to the realization of laser-controlled photochemistry. In 1980 time-resolved Raman spectroscopy was used to obtain mode-specific information of infrared multiphoton excited molecules.[2] During the past five years we have employed this technique to study the intramolecular vibrational energy distribution of several collisionless infrared multiphoton excited molecules.[3,4] In this paper new results on highly excited CF_2Cl_2 molecules are reported. In contrast to the well established equilibrium intramolecular vibrational energy distribution in molecules excited above dissociation threshold,[5,6] we found that excitation of the ν_1 and ν_8 mode of CF_2Cl_2 below the dissociation threshold give rise to different, highly non-equilibrium vibrational energy distributions.

Results

A complete description of the experimental setup can be found in previous papers.[3,4] The Raman signals from the ν_1, ν_2, and ν_8 mode (ν_1 = 1098, ν_2 = 667, and ν_8 = 923 cm^{-1}) of CF_2Cl_2 were measured after multiphoton excitation of either the ν_1 or the ν_8 mode, which are both Raman and infrared active, and are resonant with CO_2 laser lines.

It can be shown that the average number of vibrational quanta in the Raman mode, $\langle n \rangle$, is proportional to the spectrally integrated anti-Stokes Raman signal, I_{aS},

$$I_{norm} \equiv \frac{I_{aS}}{I_S^o} = \langle n \rangle, \tag{1}$$

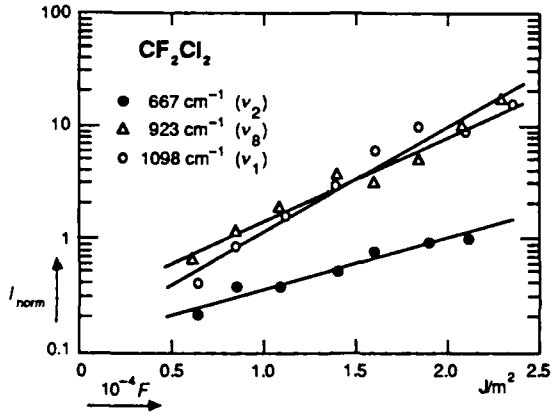

Fig. 1. Infrared fluence dependence of the normalized anti-Stokes signals after ν_1 excitation.

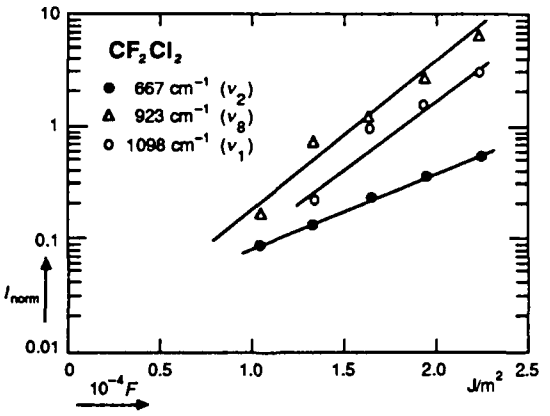

Fig. 2. Infrared fluence dependence of the normalized anti-Stokes signals after ν_8 excitation.

with I_S^0 the room temperature Stokes signal.[3] The total vibrational energy of the Raman mode is then

$$E_R = h\nu_R I_{norm}, \tag{2}$$

with h Plank's constant, and ν_R the Raman shift.

Figs. 1 and 2 show the normalized Raman signals, defined in Eq. (1), as a function of infrared fluence, after excitation of the ν_1 and ν_8 mode, respectively. The energy of all the probed Raman modes increases exponentially with increasing fluence.

For both excitation of the ν_1 and ν_8 mode, the vibrational energy distribution is distinctly different from an equilibrium, Boltzmann distribution,

$$I_{norm} = (e^{h\nu/kT} - 1)^{-1}, \tag{3}$$

In both cases too, the pumped mode reaches the highest excitation, while the energy of ν_2 mode is almost an order of magnitude smaller. The nonequilibrium nature of the vibrational energy distribution is visible more clearly in Figs. 3 and 4, which compare the measured energy distributions with calculated equilibrium distributions.

Note also, that although the intensities of the anti-Stokes signals increase by more than a factor ten when the infrared fluence is increased, the intensity *ratios* do not change considerably. This rules out the possibility that the observed nonequilibrium distribution is a result of averaging a 'hot' equilibrium ensemble and a 'cold' bottlenecked ensemble. If this were so, the ratios would tend toward equilibrium as the fraction of molecules in the hot ensemble becomes larger when the fluence is increased.

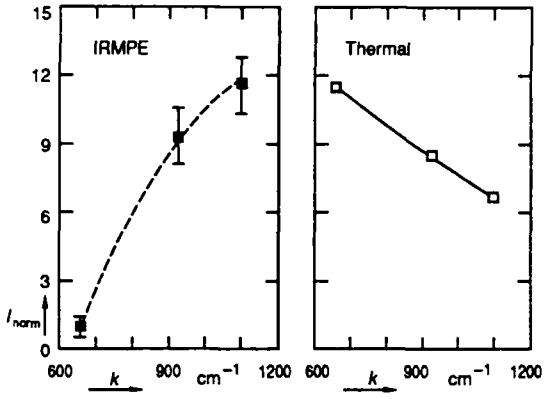

Fig. 3. Comparison of the observed normalized anti-Stokes signals with calculated equilibrium values after after ν_1 excitation.

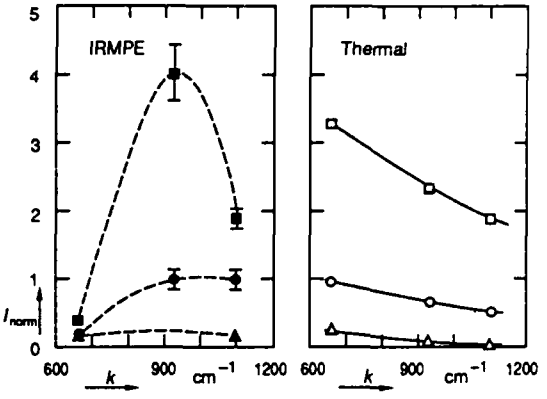

Fig. 4. Comparison of the observed normalized anti-Stokes signals with calculated equilibrium values after ν_8 excitation. The lower data points show the effect of collisional relaxation N_2 buffer gas pressure: 13 kPa (circles), and 26 kPa (triangles).

From Eq. (2) one obtains that the total energy content of the three modes for CF_2Cl_2 at the highest fluence is 21,000 cm^{-1}, so that for the molecule as a whole $E_{internal} > 21{,}000\,cm^{-1}$. The observed nonequilibrium distributions therefore imply that complete equilibration only occurs above this level of excitation.

Collisions relax the nonequilibrium intramolecular vibrational energy distribution of the excited molecules, and the normalized anti-Stokes signals should therefore approach their thermal equilibrium values as collisions occur. Fig. 4 shows the effect of collisional relaxation of the non-equilibrium vibrational energy distribution, induced by adding N_2 buffer gas. Because of the collisional relaxation, the observed signals decrease quickly with increasing buffer gas pressure, but at the same time the differences in signal intensity become smaller. Within the experimental accuracy, equilibrium is reached between the ν_1 and ν_8 modes at a 13 kPa buffer gas pressure. At 26 kPa, equilibrium is also established between the ν_1 and ν_2 modes. Because of the small Raman cross section of the ν_8 mode, data are not available for this mode at 26 kPa. At this buffer gas pressure the anti-Stokes signal of the ν_8 mode drops below the noise level. A comparison with the calculated equilibrium distributions on the other side of the graph shows indeed, that, as the buffer gas pressure is increased, the intramolecular vibrational energy distribution tends towards equilibrium.

Conclusion

We have employed time-resolved spontaneous Raman scattering to measure the intramolecular vibrational energy distribution of infrared multiphoton excited CF_2Cl_2. The results show a distinct nonequilibrium energy distribution among the observed Raman active modes even at excitations as high as 21,000 cm^{-1}. The nonequilibrium vibrational energy distribution tends toward equilibrium as an increasing amount of buffer gas is added. The measurements also show that excitation of the ν_1 and the ν_8 mode give rise to different energy distributions.

References

1 N.R. Isenor, V. Merchant, R.S. Hallsworth and M.C. Richardson, *Can. J. Phys.* **51**, 1281 (1973)

2 V.N. Bagratashvili, Yu.G. Vainer, V.S. Dolzhikov, S.F. Kol'yakov, A.A. Makarov, L.P. Malyavkin, E.A. Ryabov, E.G. Silkis, and V.D. Titov, *Appl. Phys.* **22**, 101 (1980)

3 Jyhpyng Wang, Kuei-Hsien Chen, and Eric Mazur, *Phys. Rev. A* **34**, 3892 (1986)

4 Kuei-Hsien Chen, Jyhpyng Wang, and Eric Mazur, *Phys. Rev. Lett.* **59**, 2728 (1987)

5 Aa.S. Sudbø, P.A. Schulz, E.R. Grant, Y.R. Shen, and Y.T. Lee, *J. Chem. Phys.* **70**, 912 (1979)

6 David S. King and John C. Stephenson, *Chem. Phys. Lett.* **51**, 48 (1977)

END

DATE

FILMED

8-88

DTIC